

1 Inter-comparison of multiple two-way coupled meteorology and air quality models (WRF  
2 v4.1.1-CMAQ v5.3.1, WRF-Chem v4.1.1, and WRF v3.7.1-CHIMERE v2020r1) in  
3 eastern China

4  
5 Chao Gao<sup>1,2</sup>, Xuelei Zhang<sup>1,2,\*</sup>, Aijun Xiu<sup>1,2,\*</sup>, Qingqing Tong<sup>1,2</sup>, Hongmei Zhao<sup>1,2</sup>, Shichun Zhang<sup>1,2</sup>,  
6 Guangyi Yang<sup>1,2,3</sup>, Mengduo Zhang<sup>1,2,3</sup>, and Shengjin Xie<sup>1,2,4</sup>

7  
8 <sup>1</sup>Key Laboratory of Wetland Ecology and Environment, Northeast Institute of Geography and Agroecology, Chinese  
9 Academy of Sciences, Changchun, 130102, China

10 <sup>2</sup>Key Laboratory of Wetland Ecology and Environment, State Key Laboratory of Black Soils Conservation and  
11 Utilization, Northeast Institute of Geography and Agroecology, Chinese Academy of Sciences, Changchun, 130102,  
12 China

13 <sup>3</sup>University of Chinese Academy of Sciences, Beijing, 100049, China

14 <sup>4</sup>School of Environment, Harbin Institute of Technology, 150000, Harbin, China

15 Correspondence to: X.L. Zhang (zhangxuelei@iga.ac.cn) & A.J. Xiu (xiuaijun@iga.ac.cn)

16

17 Abstract

18 Two-way coupled meteorology and air quality models, which account for aerosol-  
19 radiation-cloud interactions, have been employed to simulate meteorology and air quality  
20 more realistically. Although numerous related studies have been conducted, none  
21 compared the performances of multiple two-way coupled models in simulating  
22 meteorology and air quality over eastern China. Thus, we systematically evaluated annual  
23 and seasonal meteorological and air quality variables simulated by three open-sourced,  
24 widely utilized two-way coupled models (Weather Research and Forecasting (WRF)-  
25 Community Multiscale Air Quality (WRF-CMAQ), WRF coupled with chemistry  
26 (WRF-Chem), and WRF coupled with a regional chemistry-transport model named  
27 CHIMERE (WRF-CHIMERE)) by validating their results with surface and satellite  
28 observations for eastern China in 2017. Although we have made every effort to evaluate  
29 these three coupled models under configurations as consistent as possible, there are still  
30 unavoidable differences in the treatments of physical and chemical processes in them.  
31 Our thorough evaluations revealed that all three two-way coupled models reasonably  
32 captured the annual and seasonal spatiotemporal characteristics of meteorology and air  
33 quality. Notably, the roles of aerosol-cloud interaction (ACI) in improving the models'  
34 performances were limited compared to those of aerosol-radiation interaction (ARI). The  
35 sources of uncertainties and bias among the different ACI schemes in the two-way  
36 coupled models were identified. With sufficient computational resources, these models  
37 can provide more accurate air quality forecasting to support atmospheric environment  
38 management and deliver timely warning of heavy air pollution events. Finally, we  
39 proposed potential improvements of two-way coupled models for future research.  
40

Deleted: AbstractIn the eastern China region, two

Deleted: -

Deleted: quality models, which account for aerosol-

Deleted: performsimulate a more realistically simulate

Deleted: beinghave been conducted, but

Deleted: the

Deleted: have not been compared in

Deleted: of this region

Deleted: In this study

Deleted: the...annual and seasonal meteorological and air

Deleted:

Deleted: that were

Deleted: source and sourced, widely used...tilized two-way

Commented [Editor1]: Tip: Abbreviation: Usually, an

Deleted: (CHIMERE) ...designed for regional atmospheric

Deleted: the modeltheir results with surface and satellite

Deleted: E

Deleted: duringin 2017. Note that although

Deleted: Although we have done our best to keep ensured

Deleted: showedrevealed that all

Deleted: the

Deleted: well

Deleted: simulatedcaptured the annual and seasonal

Deleted:

Commented [Editor2]: Tip: En dash: An en dash is used in

Deleted: -quality variables

Deleted: The impacts

Deleted: Notably, tthe roles of the

Deleted: -

Deleted: onin improving the models' performances'

Commented [Editor3]: Tip: Abbreviation: Usually, an

Deleted: withto those of the

Deleted: --radiation interaction (ARI) (ARI),

Deleted: and several possible improvements on ACI

Deleted: Thus, we discussed and proposed. When several

Deleted: become available, two-way coupled, these models

Deleted: achieve

Deleted:

164 1 Introduction

165 Aerosols in the atmosphere due to anthropogenic and nature emissions not only  
166 cause air pollution but also induce climate and meteorological impacts through  
167 aerosol-radiation interaction and aerosol-cloud interaction (Carslaw et al., 2010;  
168 Rosenfeld et al., 2014; Fan et al., 2016; IPCC, 2021). The feedbacks of aerosols to  
169 meteorology have been widely investigated by two-way coupled meteorology and air  
170 quality models in the past two decades (Jacobson, 1994, 1997, 1998, 2001, 2002; Grell et  
171 al., 2005; Wong et al., 2012; Wang et al., 2014; Zhou et al., 2016; Briant et al., 2017;  
172 Feng et al., 2021). In these models, two-way interactions between meteorology and  
173 aerosols are enabled by including all the processes involving ARI or/and ACI (Grell and  
174 Baklanov, 2011; Wang et al., 2014; Briant et al., 2017; Wang et al., 2021). The  
175 fundamental theories, modeling techniques, developments, and applications of two-way  
176 coupled meteorology and air quality models in North America, Europe and Asia have  
177 been systemically reviewed (Zhang, 2008; Baklanov et al., 2014; Gao et al., 2022).

178 As pointed out by these review papers, the treatments and parameterization schemes  
179 of all the physiochemical processes involving ARI and ACI can be very different in  
180 two-way coupled models, so that the simulation results from these models could vary in  
181 many aspects. At the same time, the configurations of coupled models, such as  
182 meteorological and chemical initial and boundary conditions (ICs and BCs), horizontal  
183 and vertical resolutions, and emission inventories and processing tools, etc., play  
184 important roles in models' simulations. In the past, model inter-comparison projects have  
185 been carried out targeting various two-way coupled meteorology and air quality models.  
186 For example, the Air Quality Model Evaluation International Initiative Phase II focused  
187 on the performance of multiple two-way coupled models and the effects of aerosol  
188 feedbacks in Europe and the United States (Brunner et al., 2015; Im et al., 2015a, b;  
189 Makar et al., 2015a, b). In Asia, the Model Inter-Comparison Study for Asia Phase III  
190 was conducted to evaluate ozone (O<sub>3</sub>) and other gaseous pollutants, fine particulate matter  
191 (PM<sub>2.5</sub>), and acid and reactive nitrogen deposition with various models with/out ARI  
192 or/and ACI (Li et al., 2019; Chen et al., 2019; Itahashi et al., 2020; Ge et al. al., 2020;  
193 Kong et al., 2020). With respect to this project, Gao et al. (2018, 2020) have reviewed in  
194 detail the model performance of seven two-way coupled models from different research  
195 groups in simulating a heavy air pollution episode during January 2010 in North China  
196 Plain and how aerosol feedbacks affected simulations of meteorological variables and  
197 PM<sub>2.5</sub> concentrations. Targeting the heavy polluted India region, Govardhan et al. (2016)  
198 compared aerosol optical depth (AOD) and various aerosol species (black carbon,  
199 mineral dust, and sea salt) modeled by WRF-Chem (with ARI) and Spectral  
200 Radiation-Transport Model for Aerosol Species (with both ARI and ACI), but under  
201 different model configurations.

202 So far, there is no comprehensive comparisons of multiple coupled models under the  
203 same model configuration with respect to the high aerosol loading region over eastern  
204 China, where has experienced rapid growth of economy, urbanization, population, as well

Deleted: (ARI)

Deleted: (ACI)

207 as severe air quality problems in the past decades (He et al., 2002; Wang and Hao, 2012;  
 208 Gao et al., 2017; Geng et al., 2021). In the eastern China region (ECR), several  
 209 open-source and proprietary two-way coupled models have been applied to investigate  
 210 the ARI and/or ACI effects, yet most studies have focused on certain short-term episodes  
 211 of heavy air pollution without any year-long simulations (Xing et al., 2017; Ding et al.,  
 212 2019; Ma et al., 2021). The commonly used open-source models in ECR are WRF-Chem  
 213 and WRF-CMAQ (Grell et al., 2005; Wong et al., 2012), but there is no any application  
 214 of the two-way coupled WRF-CHIMERE model that has been applied to examine  
 215 aerosol-radiation-cloud interactions in Europe and Africa (Briant et al., 2017; Tuccella et  
 216 al., 2019). At the same time, model simulations should be compared not only against  
 217 surface measurement data but also satellite data (Zhao et al., 2017; Hong et al., 2017;  
 218 Campbell et al., 2017; Wang et al., 2018). Even though the running time of an individual  
 219 modeling system (e.g., WRF-CMAQ and WRF-CHIMERE) was evaluated by  
 220 considering its online and offline versions and under various computing configurations  
 221 (Wong et al., 2012; Briant et al., 2017), the computational efficiencies of multiple  
 222 two-way coupled models need to be accessed under the same computing conditions as  
 223 well.

224 In this paper, a comparative evaluation of three open-sourced two-way coupled  
 225 meteorology and air quality models (WRF-CMAQ, WRF-Chem and WRF-CHIMERE) in  
 226 ECR is conducted. The remainder of the paper is organized as follows: Section 2  
 227 describes the study methods including model configurations and evaluation protocols.  
 228 Sections 3 and 4 presents the analyses and intercomparisons of simulations from these  
 229 three two-way coupled models with regard to meteorology and air quality, respectively.  
 230 The major findings of this work are summarized in Section 5.

## 231 232 2 Data and methods

### 233 2.1 Model configurations and data sources

234 One-year simulations of meteorology and air quality in eastern China were  
 235 examined using the two-way coupled WRF-CMAQ, WRF-Chem, and WRF-CHIMERE  
 236 models with and without enabling ARI and/or ACI, as well as with a 27 km horizontal  
 237 grid resolution (the east-west direction comprised 110, 120, and 120 grid cells, and the  
 238 north-south direction 150, 160, and 170 grid cells for the WRF-CMAQ, WRF-Chem,  
 239 and WRF-CHIMERE models, respectively). All the three coupled models used in this  
 240 study have 30 levels (i.e., 29 layers) from the surface to 100 hPa with 11 layers in the  
 241 bottom 1 km and the bottom-layer thickness being 23.2 m. The anthropogenic emissions  
 242 of Multi-resolution Emission Inventory for China (MEIC) (Li et al., 2017) and the Fire  
 243 INventory from NCAR, version 1.5 (FINN v1.5), biomass burning emissions  
 244 (Wiedinmyer et al., 2011) were considered in our simulations, and their spatial, temporal,  
 245 and species allocations were performed using Python (Wang et al., 2023). Biogenic  
 246 emissions were calculated using the Model of Emissions of Gases and Aerosols from

Deleted: (long-term)

Deleted: in eastern

Deleted: the

Deleted: of

Deleted: E

Deleted: -

Deleted: -

Deleted: -

Deleted: ,

Deleted: and

Deleted: -

Deleted: spacing

Deleted: there were

Deleted: in the east-west direction

Deleted: 150, 160, and 170 in

Deleted: -

Deleted: comprised

Deleted: -

Deleted: -

Deleted: -

Deleted: All the

Deleted: The three coupled models used in this study have exhibited 30 levels (i.e., 29 layers) from the surface to 100 hPa, with 11 layers in the bottom 1 km and; the bottom-layer exhibited a thickness being of 23.2 m...

Deleted: the

Deleted: -

Deleted: version

Deleted: )

Deleted: applied

Deleted: language

278 Nature, version 3.0 (MEGAN v3.0; Gao et al., 2019). Dust and sea salt emissions were  
 279 used in the calculations of the inline modules (Table 1). The meteorological ICs and  
 280 lateral BCs were derived from the National Center for Environmental Prediction Final  
 281 Analysis (NCEP-FNL) datasets (<http://rda.ucar.edu/datasets/ds083.2>), with a horizontal  
 282 resolution of  $1^\circ \times 1^\circ$  at 6-hour intervals for each of the three coupled models, and the flux  
 283 in the model-top boundary was set to zero. To improve the long-term accuracy of the  
 284 meteorological variables when utilizing the WRF model, we turned on the options of  
 285 observational and grid four-dimensional data assimilation (FDDA), and pressure, station  
 286 height, relative humidity, wind speed (WS), and wind direction were observed four times  
 287 per day at 00:00, 06:00, 12:00, and 18:00 UTC from 2,168 stations  
 288 (<https://doi.org/10.5281/zenodo.6975602>, Gao et al., 2022). Notably, turning on FDDA in  
 289 two-way coupled models could dampen the simulated aerosol feedback (Wong et al.,  
 290 2012; Forkel et al., 2012; Hogrefe et al., 2015; Zhang et al., 2016). To mitigate the effects  
 291 of turning on FDDA on aerosol feedback in long-term simulations, we set the nudging  
 292 coefficients of the u/v wind, temperature, and water vapor mixing ratio above the  
 293 planetary boundary layer to 0.0001, 0.0001, and  $0.00001 \text{ s}^{-1}$ , respectively. The chemical  
 294 ICs/lateral BCs were downscaled from the whole atmosphere community climate model  
 295 (WACCM) for WRF-CMAQ and WRF-Chem using the moztart2camx and mozbc tools,  
 296 respectively. WRF-CHIMERE employed the climatology from a general circulation  
 297 model developed at the Laboratoire de Météorologie Dynamique (LMDz) coupling a  
 298 global chemistry and aerosol model INTERactions between Chemistry and Aerosols (INCA;  
 299 Mailler et al., 2017). For chemical model-top BCs, the WRF-CMAQ and WRF-Chem  
 300 models consider the impacts of stratosphere-troposphere  $\text{O}_3$  exchange using  $\text{O}_3$ -potential  
 301 vorticity parameterization (Safieddine et al., 2014; Xing et al., 2016). The related options  
 302 of both models were used in this study. WRF-CHIMERE employs the climatology from  
 303 the LMDz-INCA data (Mailler et al., 2017).

304 Table 1 lists the options of parameterization schemes of aerosol-radiation-cloud  
 305 interactions. To maintain the consistency of physical schemes, the same Rapid Radiative  
 306 Transfer Model for General Circulation Models Applications (RRTMG) short-wave (SW)  
 307 and long-wave (LW) radiation schemes and the Morrison microphysics scheme were  
 308 adopted in the WRF-Chem and WRF-CMAQ models. WRF-CHIMERE applies the  
 309 same radiation schemes, as well as the Thompson microphysics scheme. The other  
 310 different schemes (cumulus, surface, and land surface) in the WRF-CMAQ and WRF-  
 311 Chem models were selected, following Gao et al.'s (2022) widely utilized options  
 312 outlined in Table S1. The other schemes employed in WRF-CHIMERE are the same as  
 313 those in WRF-Chem. To consider the effects of clouds on radiative transfer calculations,  
 314 the fractional cloud cover and cloud optical properties were included in the RRTMG  
 315 SW/LW radiation schemes employed in the three coupled models (Xu and Randall, 1996;  
 316 Iacono et al., 2008). The coupled WRF-CMAQ model with the Kain-Fritsch cumulus  
 317 scheme included the impacts of cumulus cloud fraction (CF) on RRTMG radiation  
 318 (Alapaty et al., 2012), whereas the WRF-Chem and WRF-CHIMERE models with the

Deleted: ) (; Gao et al., 2019). Dust and sea...salt emissions

Commented [Editor4]: Remark: Units of measure that accompany numerical values must be appropriately abbreviated. The appropriate abbreviations for the SI units of time, hour, minute, and second, are h, min, and s, respectively.

Deleted:

Deleted: iswas set to zero. To improve the long-term

Commented [Editor5]: Remark: In American English, commas are used every 3 digit positions for numbers larger

Deleted: Turing

Deleted: feedbacksfeedback (Wong et al., 2012; Forkel et al.

Commented [Editor6]: Remark: Please note, units except

Deleted:  $\text{s}^{-1}$ ... 0.0001  $\text{s}^{-1}$

Commented [Editor7]: Remark: Although an

Deleted: Whole Atmosphere Community Climate Model

Deleted: -CMAQ and WRF-...Chem via

Deleted: -CHIMERE used...employed the climatology from

Deleted: WRF

Deleted: -Chem models both take into account...consider the

Deleted: alternatives

Deleted: In WRF-...CHIMERE,...employs the climatology

Deleted: The options

Deleted: alternativesoptions of the

Deleted: -radiation-...cloud interactions are listed in Table

Deleted: keep

Deleted: the physical schemes, the same Rapid Radiative

Deleted: shortwave) short-wave (SW) and longwave

Deleted: s

Deleted: arewere adopted in both...he WRF-...Chem and

Deleted: the

Deleted: impacts(CF) on RRTMG radiation (Alapaty et al



428 Grell-Freitas cumulus scheme **did not**. In the Fast-JX photolysis scheme **employed** by the  
429 three coupled models, the impacts of clouds **were** included by considering **the** cloud  
430 cover and cloud optical properties. However, the calculations of **the** cloud cover and  
431 cloud optical properties **differed** in these models, and **Table S1 presents** the relevant  
432 information. **Regarding the aerosol-size distribution**, we used **the** modal approach with  
433 Aitken, accumulation, and coarse modes in WRF-CMAQ, **as well as** the 4, and 10 bin  
434 sectional approaches in **the** WRF-Chem and WRF-CHIMERE models, respectively  
435 (Binkowski and Roselle, 2003; Zaveri et al., 2008; Nicholls et al., 2014; Menut et al.,  
436 2013, 2016).

437 To demonstrate the capabilities of the three two-way coupled models with/without  
438 aerosol **feedbacks** in simulating meteorology and air quality, we **comprehensively**  
439 **evaluated** the strengths and weaknesses **of** each coupled model **and validated them**  
440 against extensive ground-based and satellite measurements. **The ground-based data**  
441 included 572 hourly ground-based meteorological observations (air temperature (T2) and  
442 relative humidity (RH2) at **2 m** above the surface, **WS** at **10 m** above the surface (WS10),  
443 and precipitation (PREC)) (<http://data.cma.cn>); 327 hourly national environmental  
444 observations [fine particulate matter (PM<sub>2.5</sub>), ozone (O<sub>3</sub>), nitrogen dioxide (NO<sub>2</sub>), sulfur  
445 dioxide (SO<sub>2</sub>), and carbon monoxide (CO)] (<http://106.37.208.233:20035>); 109 hourly  
446 surface **SW** radiation (SSR) measurements (Tang et al., 2019); and 74 radiosonde **data**  
447 retrieved **two times** per day, **which used to calculate planetary boundary layer height at**  
448 **08:00 and 20:00 local time (PBLH08 and PBLH12)** (Guo et al., 2019). **Figure 1 shows**  
449 the locations of these data. Because there were no observed water vapor mixing ratio (w)  
450 data, this parameter was calculated **by**  $w = \frac{rh}{w_s}$ , where rh is the relative humidity and w<sub>s</sub>  
451 is the saturation mixing ratio (Wallace and Hobbs, 2006).

452 **The satellite** data included the following: monthly average downwelling **SW/LW**  
453 flux at the surface and **SW/LW** flux at the top of the atmosphere (TOA) **obtained** from the  
454 **clouds** and the Earth's **radiant energy system** (CERES) (<https://ceres.larc.nasa.gov>);  
455 **PREC** from the Tropical Rainfall Measuring Mission (TRMM); **CF**, liquid-water path  
456 (LWP), and **AOD** from the Moderate Resolution Imaging Spectroradiometer (MODIS);  
457 tropospheric NO<sub>2</sub> and SO<sub>2</sub> **columns** in the planetary boundary layer (PBL) from the  
458 Ozone Monitoring Instrument; total CO column from the Measurements of Pollution in  
459 the Troposphere (<https://giovanni.gsfc.nasa.gov/giovanni>); total column ozone (TCO)  
460 from the Infrared Atmospheric Sounding Interferometer-Meteorological Operational  
461 Satellite-A (IASI-METOP-A) (<https://cds.climate.copernicus.eu/cdsapp#!/dataset/satellite-ozone?tab=form>); and total  
462 ammonia (NH<sub>3</sub>) column from IASI-METOP-B  
463 (<https://cds-espri.ipsl.fr/iasib13/iasih3/V3.1.0>). These data were downloaded and  
464 interpolated to the same horizontal resolution as the model results using **the** Rasterio  
465 library (Gillies et al., 2013). **Thereafter**, the model and observed values at each grid point  
466 were extracted.  
467  
468

Deleted: --Freitas cumulus scheme did not. In the Fast-JX

Deleted: feedbacksfeedbacks in simulating meteorology

Commented [Editor8]: Remark: Please note, when parentheses are nested (one set inside another set), the outer parentheses are typically square while the inner parentheses are rounded following ( [ { ... } ] ) format.

Commented [Editor9]: Remark: An element name and the corresponding symbol are not to be treated as an abbreviation and its spelled-out form. Either the name or the symbol can be directly introduced in the text and used consistently at all instances (e.g., Si is the most commonly used element in semiconductors, or Silicon is the most commonly used element in semiconductors, but not Silicon (Si) is the most commonly used element in semiconductors).

Deleted: )

Deleted: ); 109 hourly surface shortwave...W radiation

Deleted: sites

Deleted: twice

Moved (insertion) [1]

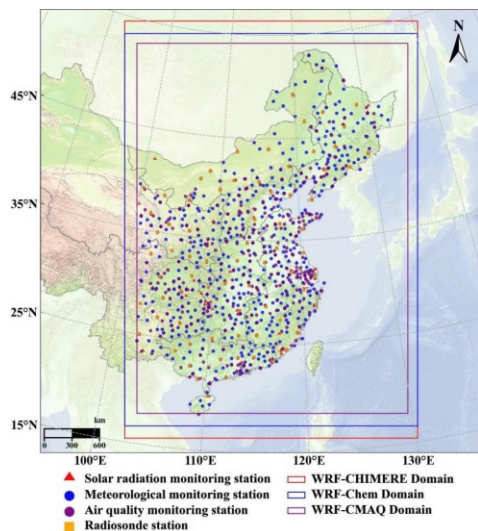
Deleted: .

Deleted: ); 1 shows the locations of these data are depicted

Moved up [1]: Fig.

Deleted: 1. Because there were no observed water vapor

Deleted: SatelliteThe satellite data included the following



531

532 Figure 1. Modeling domains (WRF-CMAQ, WRF-Chem, and WRF-CHIMERE) and solar radiation,  
 533 meteorology, air quality, and radiosonde stations.

534

535 Table 1. Model setups and inputs for the two-way coupled models (WRF-CMAQ, WRF-  
 536 Chem, and WRF-CHIMERE).

		WRF-CMAQ	WRF-Chem	WRF-CHIMERE
Domain	Horizontal grid spacing	27 km (110 × 150)	27 km (120 × 160)	27 km (120 × 170)
configuration	Vertical resolution	30 levels	30 levels	30 levels
Physics parameterization	Shortwave radiation	RRTMG	RRTMG	RRTMG
	Longwave radiation	RRTMG	RRTMG	RRTMG
	Cloud microphysics	Morrison	Morrison	Thompson
	PBL	ACM2	YSU	YSU
	Cumulus	Kain-Fritsch	Grell-Freitas	Grell-Freitas
	Surface	Pleim-Xiu	Monin-Obukhov	Monin-Obukhov
	Land surface	Pleim-Xiu LSM	Noah LSM	Noah LSM
Chemistry scheme	Icloud	Xu-Randall method	Xu-Randall method	Xu-Randall method
	Aerosol mechanism	AERO6	MOSAIC	SAM
	Aerosol size distribution	Modal (3 modes)	Sectional (4 bins)	Sectional (10 bins)
	Aerosol mixing state	Core-Shell	Core-Shell	Core-Shell
	Gas-phase chemistry	CB6	CBMZ	MELCHIOR2
Emission	Photolysis	Fast-JX with cloud effects	Fast-JX with cloud effects	Fast-JX with cloud effects
	Anthropogenic emission	MEIC 2017	MEIC 2017	MEIC 2017
	Biogenic emission	MEGAN v3.0	MEGAN v3.0	MEGAN v3.0

Deleted:

Commented [Editor10]: Remark: Abbreviations are typically re-explained in the figure legends. Please check your target journal with respect to this, if they need to be defined or not in the figure legends.

Deleted: -

Deleted: -

Deleted: -

Deleted: ),

Deleted: .

Deleted: -

Deleted: -

Deleted: -

Deleted: ).

	Biomass burning emission	FINN v1.5	FINN v1.5	FINN v1.5
	Dust emission	Foroutan	GOCART	Menuet
	Sea-salt emission	Gong	Gong	Monahan
Input data	Meteorological ICs and BCs	FNL	FNL	FNL
	Chemical ICs and BCs	MOZART	MOZART	LMDZ-INCA

547

548 2.2 Scenario ~~setup~~

549 To ~~comprehensively~~ assess the ~~performances~~ of WRF v4.1.1-CMAQ v5.3.1, WRF-  
550 Chem v4.1.1, and WRF v3.7.1-CHIMERE v2020r1 and ~~performances affected by~~  
551 aerosol ~~feedbacks~~ over ~~eastern China~~ in 2017, eight sets of annual hindcast simulations  
552 with/without ARI and/or ACI were ~~performed~~ (Table 2). Compared ~~with~~ WRF v4.1.1-  
553 CMAQ v5.3.1 and WRF-Chem v4.1.1, this WRF v3.7.1-CHIMERE v2020r1 ~~version~~ can  
554 be officially obtained, and a higher version of WRF-CHIMERE has not been developed.  
555 ~~Notably, the official~~ WRF-Chem and WRF-CHIMERE ~~can execute the simulation of~~  
556 ARI and ACI, ~~whereas~~ WRF-CMAQ ~~cannot~~. In all of the simulations performed in this  
557 study, a ~~spin-up time of one month~~ was set up to reduce the influence of the initial  
558 conditions. Multiple statistical metrics, including the correlation coefficient (R), mean  
559 bias (MB), normalized mean bias (NMB), normalized gross error (NGE), and root mean  
560 square error (RMSE), ~~were used between each scenario simulation and~~  
561 ~~ground-based/satellite-borne observations~~. The mathematical definitions of these metrics  
562 are provided in ~~Supplementary Information (SI) S1~~. To compare ~~the simulations by the~~  
563 three coupled models, the respective model configurations of ~~the~~ physics and chemistry  
564 routines ~~were~~ set as ~~consistent~~, as possible. We systemically analyzed the annual and  
565 seasonal statistical metrics of ~~the~~ meteorological and air ~~quality~~ variables, including  
566 simulations by ~~the~~ three two-way coupled models with/without ~~the~~ ARI and/or ACI  
567 effects. ~~Thereafter, we~~ quantified the respective contributions of the ARI and ACI effects  
568 to ~~model~~ performance.

569 Table 2. Summary of ~~scenario settings~~ in ~~the~~ three coupled models.

Model	Scenario	Configuration option	Description
WRF-CMAQ	(1) WRF-CMAQ_NO	DO_SW_CAL=F	Without aerosol feedbacks
	(2) WRF-CMAQ_ARI	DO_SW_CAL=T	ARI
WRF-Chem	(3) WRF-Chem_NO	aer_ra_feedback=0 wetscav_onoff=0 cldchem_onoff=0	Without aerosol feedbacks
	(4) WRF-Chem_ARI	aer_ra_feedback=1 wetscav_onoff=0 cldchem_onoff=0	ARI
	(5) WRF-Chem_BOTH	aer_ra_feedback=1 wetscav_onoff=1	ARI and ACI

- Deleted: set up
- Deleted: thoroughlycomprehensively assess the ...
- Commented [Editor11]: Remark: Journals often require both the manufacturer's name and location (e.g., city or town, state [if from the USA], and country names) for specialized equipment, materials, software, and reagents at first mention in the main text. Please consider adding this information to equipment used in the methodology based on the journal's guidelines.
- Deleted: its affected by
- Deleted: their effects on
- Deleted: feedbacksfeedbacks over eastern during ...
- Deleted: Eeastern Europe ...
- Deleted: conducted, as presented in performed (Table 2. ...
- Deleted: ), were used between each scenario simulation and ...
- Deleted: arewere set as consistent ...
- Deleted: ly as possible. We systemically analyzed the annual ...
- Deleted: quality variables, including simulations by all, be ...
- Deleted: the
- Deleted: scenarios setting
- Deleted: the
- Deleted: .
- Formatted: Justified

WRF-CHIMERE	(6) WRF-CHIMERE_NO	cldchem_onoff=1 direct_feed_chimere=0 indirect_feed_chimere=0	Without aerosol feedbacks
	(7) WRF-CHIMERE_ARI	direct_feed_chimere=1 indirect_feed_chimere=0	ARI
	(8) WRF-CHIMERE_BOTH	direct_feed_chimere=1 indirect_feed_chimere=1	ARI and ACI

631

632 3 ~~Multimodel~~ meteorological evaluations

633 This section presents ~~the~~ annual and seasonal (March–May, Spring; June–August,  
634 Summer; September–November, Autumn; and December–February, Winter) statistical  
635 metrics of ~~the~~ simulated meteorological variables and air quality, ~~as well as their~~  
636 ~~comparison~~ with ~~the~~ ground-based and satellite observations. ~~The~~ running times of the  
637 eight ~~simulation scenarios are also discussed.~~

638 3.1 Ground-based observations

639 ~~Figures 2 and S1–S7 show~~ the spatial distributions of R, MB, and RMSE for hourly  
640 SSR, T2, Q2, RH2, WS10, PREC, ~~PBLH08~~, and ~~PBLH120~~ from WRF–CMAQ, WRF–  
641 Chem, and WRF–CHIMERE with/without turning on aerosol ~~feedback~~ against  
642 ground-based observations from each site ~~throughout~~ 2017. The calculated annual model  
643 evaluation metrics for all sites in ~~eastern~~ China are summarized in Table S1, and the  
644 related seasonal R and MB values are presented in Fig. 3. Here, we mainly focused on the  
645 comparisons of SSR, T2, RH2, and WS10. ~~Further, Section 1.1 of SI presents the~~  
646 ~~analyses~~ of PREC, ~~PBLH08~~, and ~~PBLH20~~.

647 The accuracy of radiation ~~prediction~~ is of great significance in ~~ARI~~ evaluation. ~~The~~  
648 ~~annual~~ and seasonal average simulated SSR data were compared with ~~the~~ ground-based  
649 observations (Figs. 3–4 and Table S3), and SSR over ~~eastern~~ China was simulated ~~very~~  
650 reasonably by ~~the~~ models, with R-values of 0.61–0.78. ~~The~~ simulated results were  
651 overestimated ~~on the~~ annual and seasonal scales (MBs in spring and summer were larger  
652 than those in autumn and winter). ~~The~~ overestimated annual SSRs were 19.98, 14.48, and  
653 9.24 W m<sup>-2</sup> for WRF–CMAQ, WRF–Chem, and WRF–CHIMERE, respectively. ~~Brunner~~  
654 ~~et al.’s (2015) comparative study also reported that~~ most two-way coupled models  
655 ~~overestimated SSR~~ for Europe and North America. Such overestimations could be ~~caused~~  
656 by multiple factors, namely, the uncertainties in cloud development owing to PBL and  
657 convection parameterizations (Alapaty et al., 2012) and the diversity in ~~the~~ treatment of  
658 land–surface processes (Brunner et al., 2015), which ~~tend~~ to play more important roles  
659 than ~~the~~ enabling of ~~the~~ two-way aerosol ~~feedbacks~~ on SSR through ~~the~~ effects of ARI  
660 and ACI. When the three models ~~incorporated the~~ ARI effects, the simulation ~~accuracies~~  
661 ~~for~~ SSR over the whole year and four seasons improved, ~~although~~ the enabling of ~~the~~ ACI  
662 effects resulted in relatively limited improvement. ~~Additionally~~, the MB variations of  
663 ~~WRF–CMAQ~~ and ~~WRF–Chem~~ simulations were higher in spring and winter than in

Deleted: Multi-model

Deleted: April–May, Spring; June–July–

Deleted:

Deleted: October–November, Autumn; and December–

Deleted: Figures

Deleted: s.

Deleted: –S7 illustrate

Deleted: PBLH00PBLH08, and PBLH12

Deleted: –CMAQ, WRF–...Chem, and WRF–...CHIMERE

Deleted: E

Deleted: e

Deleted: , and. Further, Section 1.1 of SI presents the ana

Deleted: PBLH00PBLH08, and PBLH2012

Deleted: are presented in Section 1.1 of Supplement

Deleted: predicationprediction is of great significance in

Deleted: E

Deleted: well by all...he models, with R...values in the

Deleted: –CMAQ, WRF–...Chem, and WRF–...CHIMERE

Deleted:

Deleted: effects in

Deleted: on the models

Deleted: considered incorporated the ARI effects, the

Deleted: WRF

Deleted: –Chem simulations were higher in spring and

757 summer and autumn, whereas the maximum and minimum MBs of WRF-CHIMERE  
758 simulations were obtained in summer ( $-10.33 \text{ W m}^{-2}$ ) and autumn ( $-7.64 \text{ W m}^{-2}$ ),  
759 respectively. The annual and seasonal decrease in SSR simulated by WRF-Chem and  
760 WRF-CHIMERE with enabled ACI effects were significantly smaller than those with  
761 enabled ARI effects.

762 Generally, the simulated magnitudes and temporal variations in the air temperature  
763 at 2 m above the ground exhibited high consistency with the observations ( $R = 0.88-$   
764  $0.97$ ). Considering the annual and seasonal T2, the models tended to display a negative  
765 bias, and the T2 underestimations in spring and winter were greater than those in summer  
766 and autumn (Figs. 3 and 4). Following Makar et al. (2015a), WRF-Chem and GEM-  
767 MACH produced negative MBs in summer and positive MBs in winter with enabled ACI  
768 and ARI effects; additionally, WRF-CMAQ with only the ARI effects enabled produced  
769 negative MBs in summer over North America in 2010. Notably, Makar et al.'s. (2015a)  
770 study lacked winter meteorology evaluations using WRF-CMAQ. The comparison  
771 results of MBs revealed the following order: WRF-CHIMERE > WRF-CMAQ > WRF-  
772 Chem. The annual and seasonal MBs of WRF-CMAQ and WRF-Chem were  
773 approximately  $-1^\circ\text{C}$ , whereas that of WRF-CHIMERE ranged from  $-2$  to  $-1^\circ\text{C}$ . The  
774 RMSE values of WRF-CMAQ ( $2.71-3.05^\circ\text{C}$ ) and WRF-Chem ( $2.82-3.27^\circ\text{C}$ ) were  
775 almost equal. Those of WRF-CHIMERE ( $3.39-4.53^\circ\text{C}$ ) were larger on the annual and  
776 seasonal scales. Notably, reduced underestimations of the annual and seasonal T2 by the  
777 three coupled models were observed in eastern China when the ARI effects were enabled.  
778 With the enabled ACI effects, the MBs for T2 simulated by WRF-Chem BOTH did not  
779 change significantly compared with those of WRF-Chem NO; additionally, compared  
780 with WRF-CHIMERE NO, WRF-CHIMERE\_BOTH further enhanced the  
781 underestimations of T2 in the full year ( $-1.30^\circ\text{C}$ ), spring ( $-0.12^\circ\text{C}$ ), and winter  
782 ( $-0.40^\circ\text{C}$ ).

783 Regarding RH2, the annual and seasonal simulations using WRF-CMAQ exhibited  
784 the highest correlation with the observed values, followed by WRF-Chem and WRF-  
785 CHIMERE, and the smallest correlation coefficients of the three models were observed in  
786 autumn ( $\sim 0.5$ ). The spatial MBs between the simulations using the three models and  
787 observations displayed a general converse trend compared with T2 (i.e., RH2 was  
788 overestimated where T2 was underestimated, and vice versa). This can be explained by  
789 calculating RH2 based on T2 in the models (Wang et al., 2021). The annual and seasonal  
790 MBs were  $0.65\%-71.03\%$  and  $-21.30\%$  to  $60.00\%$ , respectively (Fig. 4 and Table S3);  
791 only WRF-Chem produced negative MBs in the summer. The magnitude of RMSE  
792 exhibited an inverse pattern compared with R for the three models, with maximum  
793 ( $28.48\%-29.52\%$ ) and minimum ( $12.57\%-16.07\%$ ) values observed in autumn and  
794 summer, respectively. Figs. 3-4 and Table S3 show that WRF-CMAQ ARI further  
795 reduced the overestimations of the annual and seasonal RH2 in ECR, whereas WRF-  
796 Chem\_ARI (except for summer) and WRF-CHIMERE ARI displayed the opposite trend.  
797 Moreover, the variations in the annual and seasonal RH2 MBs simulated by WRF-

Deleted: whilewhereas the MB...aximum and minimum MBs

Deleted: WRF

Deleted: showed a maximum were obtained in summer

Commented [Editor12]: Remark: In grammar, both is considered redundant when it is followed by the two words it represents.

Deleted: reductionsdecrease in SSR simulated by

Deleted: In generalGenerally, the simulated magnitudes and

Deleted: have

Deleted: As pointed out byFollowing Makar et al. (2015a)

Commented [Editor13]: Tip: Spacing: Conventionally, a single space is inserted between a numeral and its unit except for “%” and “°” symbol.

Commented [Editor14]: Remark: Note that “while” is used to denote time, but “whereas” is used to denote contrasting facts. Therefore, “whereas” should be used here as the author

Commented [Editor15]: Remark: Ideally, the °C unit should

Deleted: while those

Deleted:

Deleted: -

Deleted: °C

Deleted: °C.

Deleted: RMSEs were approximately equal forRMSE values

Deleted: °C

Deleted: °C)°C) and WRF-

Deleted: °C

Deleted: °C), and larger for WRF-

Deleted: °C

Deleted: °C) at both°C) were larger on the annual and

Deleted: E

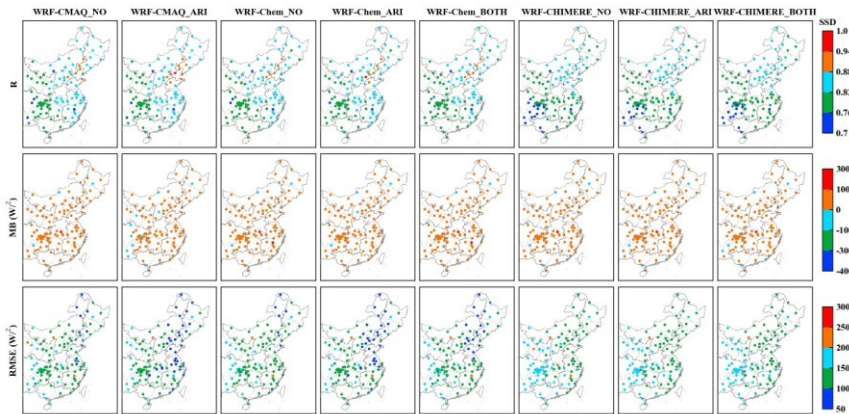
Deleted: WhenWith the enabled ACI effects were enabled

Deleted: Looking atRegarding RH2, the annual and seasonal



912 Chem\_BOTH and WRF\_CHIMERE\_BOTH were further reduced compared with those  
 913 simulated by WRF\_Chem ARI (except for summer) and WRF\_CHIMERE ARI,  
 914 respectively.  
 915 Furthermore, similar analyses were performed for WS10, and the results revealed  
 916 that WRF\_CMAQ performed better in capturing the WS10 patterns than WRF\_Chem and  
 917 WRF\_CHIMERE. The R-values for all three models ranged from 0.47 to 0.60; WRF\_  
 918 CMAQ and WRF\_Chem overestimated WS by  $\sim 0.5 \text{ m s}^{-1}$ , whereas WRF\_CHIMERE  
 919 overestimated it by  $\sim 1.0 \text{ m s}^{-1}$  (Table S3 and Figs. 3–4). The overestimation of WS10  
 920 under real-world low-wind conditions is a common phenomenon of existing weather  
 921 models, and it is mainly caused by outdated geographic data, coarse model resolution,  
 922 and a lack of good physical representation of the urban canopy (Gao et al., 2015, 2018).  
 923 The three models exhibited lower correlations (0.31–0.54) and MBs (0.20–0.86  $\text{m s}^{-1}$ ) in  
 924 summer compared with the other seasons, and the RMSEs were  $\sim 2.0 \text{ m s}^{-1}$ . Enabling the  
 925 ARI effects mitigated the overestimations of the three models, particularly WRF-  
 926 CMAQ\_ARI.

927



928

929 Figure 2. Statistical metrics (R, MB, and RMSE) for annual simulations and observations of SSR in  
 930 eastern China.

Deleted: --CHIMERE\_BOTH were further reduced

Deleted: SimilarFurthermore, similar analyses were

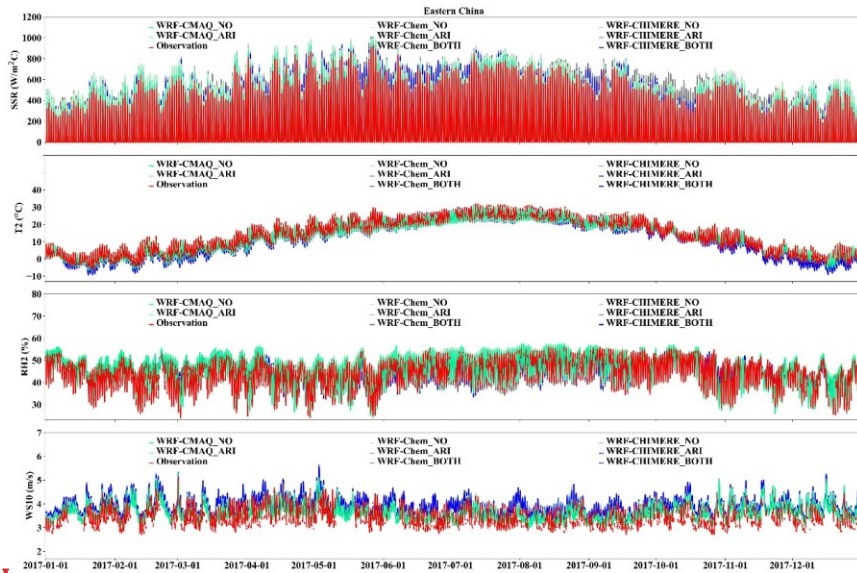
Deleted: values for all three models ranged from 0.47 to

Deleted: -wind conditions is a common phenomenon of

Deleted: betweenfor annual simulations and observations of

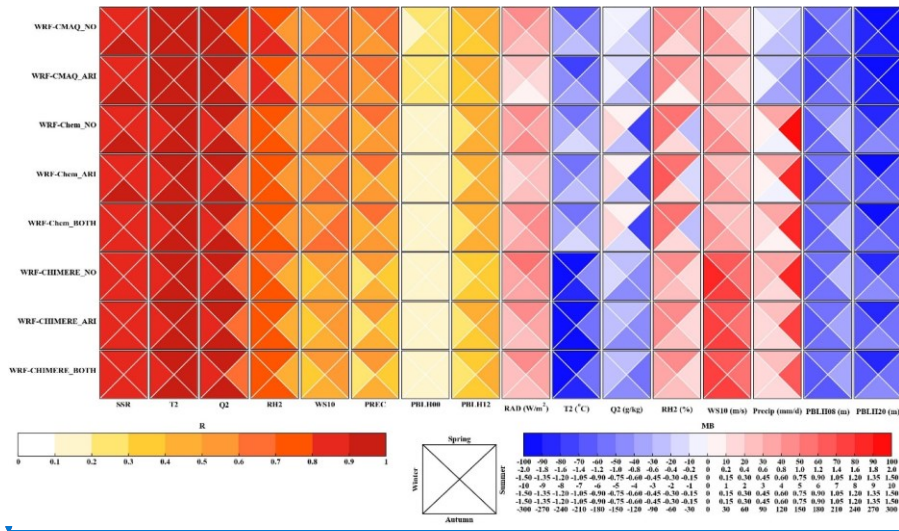
Deleted: E

Deleted: .



970  
971 Figure 3. Time series of the observed and simulated hourly SSR, T2, and WS10 by coupled  
972 WRF-CMAQ, WRF-Chem and WRF-CHIMERE with/without aerosol feedbacks over ECR in 2017.

973



974  
975 Figure 4. Portrait plots of the statistical indices (R and MB) between the seasonal simulations and  
976 surface observations of the meteorological variables (SSR, T2, Q2, RH2, WS10, PREC, and PBLH at

Deleted:

Commented [Editor16]: Tip: American-British Style: In American English, a comma is inserted before the conjunction that precedes the last element of a series (e.g., bread, eggs, and milk). This comma is called the Oxford comma and is inserted for clarity.

Deleted: -

Deleted: -

Deleted: and

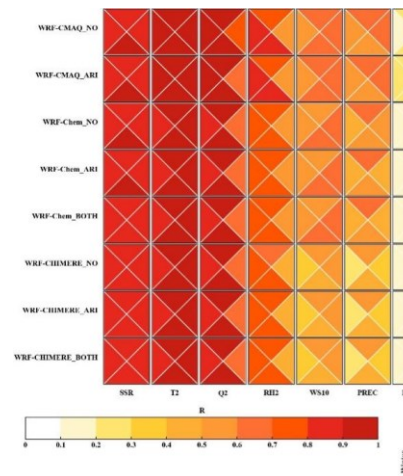
Deleted: -

Deleted: feedbacks

Deleted: Eastern China during the year of

Deleted: .

Deleted:



Deleted:

987 08:00 and 20:00 LT) in ECR.

988 To determine and quantify how well our results compared with those of the extant  
989 studies using two-way coupled models, we compared our study with previous ones in  
990 terms of the evaluation results of meteorology and air quality. We discussed meteorology  
991 and air quality in this section and Section 4.1, respectively. We employed  
992 box-and-whisker plots, and the 5<sup>th</sup>, 25<sup>th</sup>, 75<sup>th</sup>, and 95<sup>th</sup> percentiles were used as statistical  
993 indicators. In the plots, the dashed lines in the boxes represent the mean values, and the  
994 circles represent outliers. Previous studies mainly used WRF-Chem and WRF-CMAQ to  
995 evaluate meteorology and air quality, whereas the WRF-NAQPMS and GRAPES-  
996 CUACE barely had application potential. As mentioned in Section 1, previous  
997 investigations of meteorology and air quality using WRF-CHIMERE with/without  
998 aerosol feedbacks have not been conducted in ECR. Therefore, only the evaluation results  
999 involving WRF-Chem and WRF-CMAQ were analyzed to study aerosol feedbacks.

1000 Figure S8 shows the comparison between the statistical metrics T2, RH2, Q2, and  
1001 WS10, in this study and the evaluation results of previous studies. Based on the number  
1002 of samples in the statistical metrics of each meteorological variable, most previous  
1003 studies mainly involved the simulation and evaluation of T2, WS10, and RH2, with only  
1004 a relatively few studies focusing on Q2. Compared with the evaluation results of the  
1005 extant studies, the ranges of our statistical metrics were roughly similar, although there  
1006 were some notable differences. The R<sub>e</sub>-values of the WRF-CMAQ and WRF-Chem  
1007 models in our study were higher than those of the previous studies; MBs of T2 simulated  
1008 by WRF-CMAQ were smaller, whereas those of T2 simulated by WRF-Chem were  
1009 larger; and RMSEs of the WRF-CMAQ simulation were larger, whereas those of the  
1010 WRF-Chem simulation were smaller. For RH2, the R<sub>e</sub>-values for our WRF-CMAQ and  
1011 WRF-Chem were larger than the average level of the previous studies, whereas MBs and  
1012 RMSEs for WRF-CMAQ were larger. Those for WRF-Chem were smaller than the  
1013 average reported in previous studies. For Q2, the model performance of WRF-CMAQ in  
1014 this study was generally better than the average level reported in previous studies,  
1015 although the R-value between the WRF-Chem simulation results and observed values  
1016 was higher (and MB and RMSE were lower) than the average level reported in previous  
1017 studies. We also conclude that the simulation results of our WRF-CMAQ and WRF-  
1018 Chem better reproduced the variations in WS10 compared with the simulation reported  
1019 by previous studies.

### 1021 3.2 Satellite-borne observations

1022 To further evaluate the performances of WRF-CMAQ, WRF-Chem, and WRF-  
1023 CHIMERE against the satellite observations, we analyzed the annual and seasonal  
1024 statistical metrics of SW and LW radiations at the surface, PREC, cloud cover, and LWP  
1025 simulated by the three coupled models with and without aerosol feedbacks by  
1026 comparisons the simulations with the satellite-borne observations (Table 3, and Figs. 5, S9,  
1027 and S12–S14). Additionally, evaluations of SW and LW radiation at TOA are presented in

Deleted: LT

Deleted: eastern China.

Deleted: identifydetermine and quantify how well our results

Deleted: arerepresent the mean values, and the circles

Deleted: the

Deleted: --CHIMERE with/without aerosol

Moved (insertion) [2]

Deleted: .

Deleted: TheS8 shows the comparison between the statistical

Moved up [2]: Fig.

Deleted: S8. According to the number of samples (NS).. in

Deleted: performanceperformances of WRF-...CMAQ, ...

1126 Section 1.2 of SI.

1127 As shown in Table 3 and Fig. 5, the three coupled models exhibited relatively poor  
1128 performances for SSR, with annual MBs of 8.21–30.74 W m<sup>-2</sup> and correlations of 0.61–  
1129 0.78. A similar poor performance for SW radiation was also reported in the United States  
1130 using the coupled WRF-CMAQ and offline WRF models (Wang et al., 2021). The  
1131 overall seasonal characteristics of SSR were reproduced by the three coupled models (Fig.  
1132 S10). Concurrently, regardless of whether aerosol feedbacks were enabled or not, the  
1133 three models overestimated seasonal SSR (except WRF-Chem ARI in winter), obtaining  
1134 higher MBs in spring and summer than in autumn and winter. The seasonal SSR  
1135 overestimations might be directly due to the underestimation of the calculated AOD when  
1136 examining the ARI effects (Wang et al., 2021). Compared with SSR, the three coupled  
1137 models predicted the surface LW radiation variables (SLR) well (R<sub>v</sub>-values were up to  
1138 0.99), with annual domain-average MBs of -9.97 to -6.05 W m<sup>-2</sup>. Furthermore,  
1139 significant seasonal differences were observed in the simulated LW radiation by the three  
1140 coupled models; the WRF-CMAQ and WRF-CHIMERE scenarios yielded  
1141 underestimations, with maximum and minimum SLR values in winter and summer,  
1142 respectively, whereas the maximum underestimations of WRF-Chem were recorded in  
1143 autumn, particularly for WRF-Chem BOTH (Fig. S9).

1144 As the three coupled models adopted the same grid resolution (27 × 27 km) as well  
1145 as SW and LW radiation schemes (RRTMG), the above analysis demonstrated that the  
1146 configuration differences among the aerosol components, size distributions, and  
1147 mechanisms contributed to the diverse seasonal MBs (Tables 1 and S2). Moreover, the  
1148 three two-way coupled models with ARI feedbacks effectively improved the  
1149 performances of annual and seasonal SSR; however, for SLR, the performance  
1150 improvements were much more variable across the three coupled models and different  
1151 scenarios with and without ARI and/or ACI feedbacks enabled (Table S4). When the ARI  
1152 effects were enabled, the diverse refractive indices of the aerosol species groups caused  
1153 discrepancies in the online calculated aerosol optical properties in different SW and LW  
1154 bands in the RRTMG SW/LW radiation schemes of WRF-CMAQ, WRF-Chem, and  
1155 WRF-CHIMERE (Tables S5–S6). The online calculated cloud optical properties induced  
1156 by aerosol absorption in the RRTMG radiation schemes differed regarding their  
1157 treatments of the aerosol species groups in the three coupled models. With the ACI effects  
1158 enabled, the activation of cloud droplets from aerosols based on the Köhler theory was  
1159 considered in WRF-Chem and WRF-CHIMERE compared with the simulations without  
1160 aerosol feedbacks (Table S7). The treatments of prognostic ice-nucleating particles (INP)  
1161 formed via the heterogeneous nucleation of dust particles (diameters > 0.5 μm) and  
1162 homogeneous freezing of hygroscopic aerosols (diameters > 0.1 μm) were only  
1163 investigated in WRF-CHIMERE, whereas the prognostic INP were not included in  
1164 WRF-CMAQ and WRF-Chem. These discrepancies eventually contributed to the  
1165 differences in the simulated radiation changes caused by aerosols.

1166 From IPCC 2007–2021, the effects of aerosol feedbacks (particularly with the ACI

Deleted: Supplement

Deleted: showed relativeexhibited relatively poor

Deleted: was

Deleted: allthe three models overestimated seasonal SSR

Deleted: allthe three coupled models adopted the same grid

Deleted: arewere enabled, the diversities of...iverse

Deleted: s

Deleted: --CMAQ and WRF-...Chem. These discrepancie

Deleted: to IPCC –2021, the effects of aerosol feedback



1252 effects enabled) on PREC and cloud processes remained unclear. In this study, we further  
1253 assessed the annual and seasonal simulated PREC, cloud cover, and LWP in ECR with  
1254 high aerosol loadings against the satellite observations (Table 3 and Figs. S12–S14) to  
1255 provide new insights into enabling online feedbacks in two-way coupled modeling  
1256 simulations from a yearly perspective.

1257 The results indicated that PREC simulated by WRF\_CMAQ (0.51–0.89) exhibited  
1258 higher correlations than those simulated by WRF\_Chem (0.61–0.73) and WRF\_  
1259 CHIMERE (0.54–0.70). WRF\_CMAQ demonstrated the best correlation in winter,  
1260 whereas WRF\_Chem and WRF\_CHIMERE had the best correlation in spring; the three  
1261 models presented their worst correlations in summer, as the numerical models struggled  
1262 to effectively capture enhanced convective activities in summer. Huang and Gao (2018)  
1263 also revealed that the accurate representations of lateral boundaries were crucial to  
1264 improving PREC simulations in China during summer. WRF\_CMAQ underestimated  
1265 annual PREC, with MBs of –76.49 to –51.93 mm, whereas WRF\_Chem and WRF\_  
1266 CHIMERE produced large PREC overestimations ranging from +108.04 to +207.05 mm  
1267 (Table 3), particularly in southern China regions (Fig. S11). WRF\_CMAQ also produced  
1268 negative biases (–27.89 to +42.08 mm) for seasonal PREC, except for WRF\_  
1269 CMAQ\_ARI in winter. WRF\_Chem and WRF\_CHIMERE only underestimated seasonal  
1270 PREC in autumn (–31.39 to –26.89 mm) and winter (–7.12 to –4.43 mm), respectively  
1271 (Fig. S12). The variations in the annual and seasonal MBs of PREC were consistent with  
1272 the changes in CF and LWP (Zhang et al., 2016), and these changes will be discussed in  
1273 detail below.

1274 By considering aerosol feedbacks, the ARI-induced decrease in annual MBs of  
1275 PREC for WRF\_CMAQ, WRF\_Chem, and WRF\_CHIMERE were 24.56, 12.11, and  
1276 4.70 mm, respectively. WRF\_Chem BOTH (24.9 mm) and WRF\_CHIMERE BOTH  
1277 (3.41 mm) enhanced the overestimation of annual PREC compared with WRF\_  
1278 Chem\_ARI and WRF\_CHIMERE\_ARI, respectively. Significant increases (+53.15 mm)  
1279 and decreases (–6.3 to –3.41 mm) in MBs were facilitated by WRF\_CMAQ and the other  
1280 two models with ARI effects enabled compared with those without feedbacks,  
1281 respectively. WRF\_Chem and WRF\_CHIMERE with ARI and ACI effects enabled  
1282 produced larger MB enhancements (+3.54 to +7.46 mm) on the seasonal scale (Fig. S12).  
1283 Notably, the discrepancies in simulated PREC were mainly attributable to the selection of  
1284 different microphysics and cumulus schemes in WRF\_CMAQ (Morrison and Kain-  
1285 Fritsch), WRF\_Chem (Morrison and Grell-Freitas), and WRF\_CHIMERE (Thompson  
1286 and Grell-Freitas).

1287 CF and LWP can significantly influence the spatiotemporal distributions of PREC;  
1288 our simulated results of annual and seasonal CFs in ECR are presented in Table 3 and Fig.  
1289 S13. Overall, WRF\_CMAQ performed best in simulating CF. The R-values of WRF\_  
1290 Chem during summer (0.69) and winter (0.70) were larger than those of WRF\_CMAQ  
1291 (0.59 and 0.64) and WRF\_CHIMERE (0.56 and 0.66), whereas WRF\_CMAQ and WRF\_  
1292 CHIMERE obtained better simulation results in winter and autumn, with correlations of

Deleted: precipitationPREC and cloud processes remain ...

Deleted: s

Deleted: eastern China ECR with high aerosol loadings ...

Deleted: illustrated those correlations of precipitation ...

Deleted: exhibited

Deleted: whilewhereas WRF-...Chem and ...

Deleted: exhibited

Deleted: allthe three models showed ...

Deleted: exhibited

Deleted: correlationcorrelations in summer. The reason for ...

Deleted: S

Deleted: of southern China (Fig. S11). WRF-...CMAQ also ...

Deleted:

Deleted: When By considering aerosol feedbacks were ...

Deleted: the

Deleted: precipitation couldPREC were mainly be ...

Deleted: Cloud fraction (CF)...and LWP can significantly ...

Deleted: WRF

Deleted: -values for...f WRF-...Chem during summer (0.69) ...



1415 up to 0.89 and 0.67, respectively. **The** three coupled models underestimated annual and  
 1416 seasonal **CFs**, with MBs **of** -16.83% to -6.18% and -21.13% to -4.13%, respectively;  
 1417 these **results** were consistent with **those of** previous two-way coupled modeling studies  
 1418 using WRF-**CMAQ** (-19.7%) and WRF-**Chem** (-32% to -9%) in China (Hong et al.,  
 1419 2017; Zhao et al., 2017). **The** models reasonably simulated **the** annual LWP in **ECR**, with  
 1420 **R**-values **of** >0.55 and **negative** biases varying from -57.36 to -31.29 g m<sup>-2</sup>. **These**  
 1421 underestimations were closely related to missing cloud homogeneity (Wang et al., 2015;  
 1422 Dionne et al., 2020) and **the** excessive conversion of liquid **water** to ice in **the** selected  
 1423 cloud microphysics schemes (Klein et al., 2009). As shown in Fig. S14, **the** models  
 1424 **performed** best in simulating LWP in spring (R = 0.51–0.79), and **their highest**  
 1425 underestimations **were observed** in winter (MBs = -54.82 to -40.89 g m<sup>-2</sup>), except for  
 1426 WRF-**Chem**, which **obtained** its maximum bias in autumn.

1427 **To** quantitatively **determine** the **impacts** of aerosol **feedbacks** on CF and LWP, **the**  
 1428 simulated scenarios revealed that WRF-**CMAQ** ARI overwhelmingly decreased **the**  
 1429 annual and seasonal underestimations of CF (0.48%–1.05%) and LWP (3.03–4.29 g m<sup>-2</sup>),  
 1430 **whereas in WRF-Chem ARI and WRF-CHIMERE ARI** slightly increased **the**  
 1431 underestimations (CF: 0.02%–0.39%; LWP: 0.03–0.58 g m<sup>-2</sup>). **Compared with WRF-CHIMERE ARI, WRF-CHIMERE BOTH** produced larger variations in **the** annual and  
 1432 seasonal MBs of CF (0.23%–0.93%) and LWP (-2.96 to 7.38 g m<sup>-2</sup>). **WRF-Chem BOTH and WRF-Chem ARI** exhibited equivalent variations (CF: 0.03%–0.71%;  
 1433 LWP: 0.02–2.89 g m<sup>-2</sup>). This **could** be explained **by** the different parameterization  
 1434 treatments of **the** cloud droplet number concentration (CDNC) simulated by the three  
 1435 coupled models with/without enabling **the** ACI effects. The cloud condensation nuclei  
 1436 (**CCN**) activated **by the** aerosol particles can increase CDNC and impact LWP and CF.  
 1437 Without enabling any aerosol **feedbacks** or **by** enabling **only** ARI, CDNC is **by** default,  
 1438 prescribed as a constant value of 250 cm<sup>-3</sup> in the Morrison **schemes** of WRF-**CMAQ** and  
 1439 WRF-**Chem** and 300 cm<sup>-3</sup> in the Thompson **schemes** of WRF-**CHIMERE**. **With enabling**  
 1440 only ACI or **both** ARI and ACI **effects**, prognostic CDNC is **online** calculated in **the**  
 1441 **two-way coupled WRF-Chem and WRF-CHIMERE models when cloud maximum**  
 1442 **supersaturation is greater than aerosol critical supersaturation** (Abdul-Razzak and Ghan,  
 1443 2002; Chapman et al., 2009; Tuccella et al., 2019). Although we have obtained  
 1444 preliminary quantitative results of the ACI effects on regional **PREC**, CF, and LWP, **we**  
 1445 **acknowledge** that several limitations still exist **regarding the representation of the ACI**  
 1446 **effects** in state-of-the-art two-way coupled models. **These limitations** include a lack of  
 1447 consideration **for** the responses of convective clouds to ACI (Tuccella et al., 2019).  
 1448 **numerical descriptions for giant CCN** (Wang et al., 2021) and heterogeneous ice nuclei  
 1449 (Keita et al., 2020).

1450  
 1451  
 1452  
 1453 Table 3. Statistical metrics (R, MB, NMB, NGE, and RMSE) between **the** annual  
 1454 simulations and satellite retrievals of **SSR** and **SLR**, **TOA SW** and **LW** radiation, **PREC**,  
 1455 **CF**, and **LWP** in **ECR**. The best results are **captured in bold fonts, and the mean**

Deleted: AllThe three coupled models underestimated annual...

Deleted: In terms ofTo quantitatively determining...etermina...

Deleted: g m<sup>-2</sup>

Deleted: ) were produced by WRF-CHIMERE\_BOTH compared with WRF-CHIMERE\_ARI. WRF-

Deleted: maycould be explained as...by the different

Deleted: When

Deleted: both

Deleted: are enabled, the online

Deleted: calculating

Deleted: calculation of...prognostic CDNC is online

Deleted: -Chem and WRF-...CHIMERE models when

Deleted: using the

Deleted: method of

Deleted: method

Deleted: precipitationPREC, CF, and LWP, it should be kept

Deleted: and , a lack of

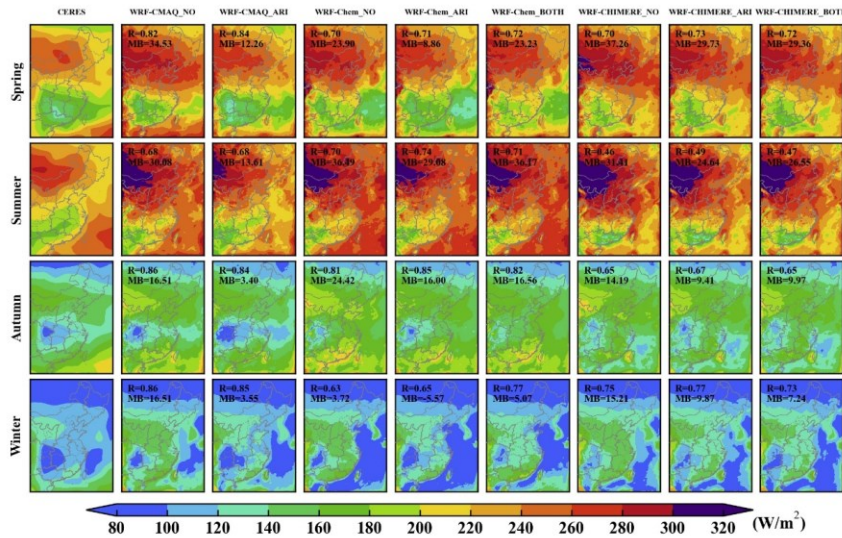
Deleted: offer giant cloud condensation nuclei

Deleted: surface shortwaveSSR and longwave...LR, TOA

1554 simulations and observations are in italics.

Variables	Statistics	WRF-CMAQ_NO	WRF-CMAQ_ARI	WRF-Chem_NO	WRF-Chem_ARI	WRF-Chem_BOTH	WRF-CHIMERE_NO	WRF-CHIMERE_ARI	WRF-CHIMERE_BOTH
Surface shortwave radiation ( <i>72.74</i> W m <sup>-2</sup> )	Mean_sim	<i>197.15</i>	<i>180.94</i>	<i>203.48</i>	<i>194.52</i>	<i>201.45</i>	<i>197.39</i>	<i>191.34</i>	<i>195.58</i>
	R	0.76	0.75	0.73	<b>0.78</b>	0.75	0.61	0.64	0.66
	MB	24.41	8.21	30.74	21.78	28.71	24.75	18.71	22.94
W m <sup>-2</sup>	NMB (%)	14.13	<b>4.75</b>	17.79	12.61	16.62	14.34	10.84	13.29
	NGE (%)	15.13	<b>8.66</b>	18.61	13.53	17.38	17.44	14.42	15.83
	RMSE	30.25	<b>20.37</b>	35.34	26.88	32.80	34.70	29.60	31.45
Surface longwave radiation ( <i>322.3</i> W m <sup>-2</sup> )	Mean_sim	<i>316.25</i>	<i>315.83</i>	<i>312.96</i>	<i>312.60</i>	<i>312.32</i>	<i>313.33</i>	<i>314.60</i>	<i>314.47</i>
	R	0.98	0.98	0.98	0.98	0.98	<b>0.99</b>	<b>0.99</b>	<b>0.99</b>
	MB	-6.05	-6.46	-9.34	-9.70	-9.97	-9.66	-8.39	-8.53
W m <sup>-2</sup>	NMB (%)	<b>-1.88</b>	-2.00	-2.90	-3.01	-3.09	-2.99	-2.60	-2.64
	NGE (%)	<b>3.22</b>	3.46	3.70	3.77	3.84	3.96	3.60	3.66
	RMSE	<b>13.65</b>	14.13	14.81	14.97	15.17	15.47	14.52	14.72
TOA shortwave radiation ( <i>111.56</i> W m <sup>-2</sup> )	Mean_sim	<i>107.76</i>	<i>112.68</i>	<i>110.38</i>	<i>110.95</i>	<i>107.16</i>	<i>114.33</i>	<i>116.62</i>	<i>113.09</i>
	R	<b>0.81</b>	0.79	0.69	0.68	0.62	0.65	0.65	0.65
	MB	-3.80	1.13	-1.18	-0.61	-4.40	3.12	5.42	1.89
W m <sup>-2</sup>	NMB (%)	-3.40	<b>1.01</b>	-1.05	-0.55	-3.94	2.81	4.87	1.70
	NGE (%)	<b>10.19</b>	10.45	11.52	10.96	11.69	14.43	14.36	12.93
	RMSE	<b>15.75</b>	16.04	17.07	16.10	17.21	20.85	20.67	18.96
TOA longwave radiation ( <i>233.68</i> W m <sup>-2</sup> )	Mean_sim	<i>231.54</i>	<i>232.26</i>	<i>234.34</i>	<i>233.96</i>	<i>234.39</i>	<i>232.52</i>	<i>232.17</i>	<i>233.18</i>
	R	0.88	0.90	0.91	0.91	<b>0.92</b>	0.74	0.74	0.76
	MB	-2.14	-1.42	0.66	0.28	0.71	-0.61	-0.96	0.05
W m <sup>-2</sup>	NMB (%)	-0.92	-0.61	0.28	<b>0.12</b>	0.30	-0.26	-0.41	0.02
	NGE (%)	2.28	2.04	1.79	1.79	<b>1.74</b>	3.02	2.98	2.92
	RMSE	6.94	6.20	6.00	5.94	<b>5.86</b>	10.10	10.07	9.70
Precipitation ( <i>948.91</i> mm y <sup>-1</sup> )	Mean_sim	<i>872.42</i>	<i>896.98</i>	<i>1069.06</i>	<i>1056.95</i>	<i>1081.84</i>	<i>1165.06</i>	<i>1160.35</i>	<i>1163.77</i>
	R	<b>0.71</b>	<b>0.71</b>	<b>0.71</b>	<b>0.71</b>	0.70	0.69	0.69	0.69
	MB	-76.49	-51.93	120.15	108.04	132.94	207.05	202.35	205.76
W m <sup>-2</sup>	NMB (%)	-9.23	<b>-8.40</b>	12.66	11.39	14.01	21.61	21.12	21.48
	NGE (%)	<b>32.46</b>	34.36	44.54	43.38	45.13	42.54	42.52	42.58
	RMSE	<b>573.14</b>	595.76	675.91	668.92	693.74	776.60	786.36	790.73
Cloud cover ( <i>64.09</i> %)	Mean_sim	<i>52.51</i>	<i>53.32</i>	<i>48.18</i>	<i>47.80</i>	<i>47.46</i>	<i>58.12</i>	<i>57.98</i>	<i>58.55</i>
	R	0.68	0.68	<b>0.69</b>	<b>0.69</b>	0.68	0.66	0.66	0.64
	MB	-11.58	-10.77	-16.12	-16.50	-16.83	-6.60	-6.74	-6.18
W m <sup>-2</sup>	NMB (%)	-18.07	-16.80	-25.07	-25.66	-26.18	-10.20	-10.41	<b>-9.54</b>
	NGE (%)	19.48	18.87	26.01	26.56	26.97	16.74	16.92	<b>16.72</b>
	RMSE	16.47	16.28	20.17	20.48	20.73	15.28	15.33	15.34
liquid water path ( <i>88.44</i> g m <sup>-2</sup> )	Mean_sim	<i>53.50</i>	<i>57.15</i>	<i>32.29</i>	<i>31.87</i>	<i>31.08</i>	<i>56.23</i>	<i>56.21</i>	<i>54.00</i>
	R	<b>0.61</b>	0.58	0.47	0.46	0.28	0.55	0.55	0.51
	MB	-34.94	-31.29	-56.16	-56.58	-57.36	-32.37	-32.40	-34.61

NMB (%)	-39.51	<b>-35.38</b>	-63.49	-63.97	-64.86	-36.54	-36.56	-39.06
NGE (%)	57.05	57.99	66.88	67.25	67.91	<b>53.15</b>	53.33	56.88
RMSE	54.35	54.31	63.54	63.92	67.21	<b>53.39</b>	53.42	55.86



- Deleted:
- Deleted:
- Deleted: from
- Deleted: -
- Deleted: -
- Deleted: -
- Deleted: feedbacks
- Deleted: eastern China.
- Deleted: Multi-model
- Deleted:
- Deleted: In a similar way
- Deleted: feedbacks
- Deleted:
- Deleted: eastern China
- Deleted: as
- Deleted: during
- Deleted: is
- Deleted: in
- Deleted: .
- Deleted: each of
- Deleted: Supplement
- Deleted:
- Deleted: for
- Deleted: -
- Deleted: -
- Deleted: ),
- Deleted: -
- Deleted: All
- Deleted: showed
- Deleted: compared with those

1555  
1556 Figure 5. Spatial distributions of seasonal SSR between CERES observations and simulations using  
1557 WRF\_CMAQ, WRF\_Chem, and WRF\_CHIMERE with and without aerosol feedbacks in ECR.

1558  
1559 4 Multimodel air-quality evaluations

1560 Similar to meteorology, to further determine the quantitative effects of enabling  
1561 aerosol feedbacks on the simulation accuracy of the air-quality variables in ECR,  
1562 ground-based and satellite-borne observations were adopted for comparisons in the  
1563 following evaluation analysis. The usage status of computing resources in each  
1564 simulation process was also assessed (Section 4.3).

1565  
1566 4.1 Ground-based observations

1567 Table 4 and Fig. 7 present the statistical metrics of the annual and seasonal air  
1568 pollutant concentrations (PM<sub>2.5</sub>, O<sub>3</sub>, NO<sub>2</sub>, SO<sub>2</sub>, and CO) simulated by the three coupled  
1569 models. The evaluations between the surface measurements and simulations of PM<sub>2.5</sub> and  
1570 O<sub>3</sub> are presented below, and the performance assessments of the other gaseous pollutants  
1571 are presented in Section 2 of SI.

1572 The R-values of the annual PM<sub>2.5</sub> concentrations simulated by WRF\_CMAQ (0.68)  
1573 were the highest, followed by those obtained by WRF\_Chem (0.65–0.68) and WRF\_  
1574 CHIMERE (0.52–0.53). The three models exhibited higher correlations in winter than in

1605 the other seasons (Fig. 7). Table 4 and Figs. 6–7 reveal that WRF\_CMAQ underestimated  
 1606 the annual and seasonal (except for autumn) PM<sub>2.5</sub> concentrations, with NMBs of –9.78%  
 1607 to –6.39% and –17.68% to +5.17%, respectively. WRF\_Chem overestimated and  
 1608 underestimated PM<sub>2.5</sub> on the annual and seasonal scales, with related NMBs varying from  
 1609 –39.11% to +24.72%. Concurrently, WRF\_CHIMERE excessively overestimated the  
 1610 annual and seasonal PM<sub>2.5</sub> concentrations (NMB: +19.51% to +75.47%). These biases  
 1611 could be related to the different aerosol and gas-phase mechanisms, dust and sea salt  
 1612 emission schemes, chemical ICs and BCs, and the aerosol-size-distribution treatments  
 1613 applied to the three two-way coupled models. Based on the NMB differences between the  
 1614 simulations with ARI and those without aerosol feedbacks, the ARI-induced annual and  
 1615 seasonal NMB variations in WRF\_CMAQ ARI and WRF\_Chem ARI ranged from  
 1616 +3.01% to +4.21% and +3.07% to +5.02%, respectively, indicating that enabling ARI  
 1617 feedbacks slightly reduced the annual and seasonal (except for autumn) underestimations  
 1618 of PM<sub>2.5</sub> concentrations. Notably, WRF\_CHIMERE ARI further overestimated the  
 1619 annual and seasonal PM<sub>2.5</sub> concentrations, with an NMB increase of up to 10.04%. The  
 1620 increases in the PM<sub>2.5</sub> concentrations due to the ARI effects were attributable to the  
 1621 synergetic decreases in SSR, T2, WS10, and PBLH, as well as increases in RH2. With  
 1622 ACI feedbacks further enabled, WRF\_Chem BOTH largely underestimated the annual  
 1623 and seasonal PM<sub>2.5</sub>, with NMBs varying from –24.15% to –14.44%, compared with  
 1624 WRF\_Chem ARI. WRF\_CHIMERE BOTH tended to decrease (–2.1% to –0.51%) the  
 1625 annual and autumn-winter NMBs and increase (+0.35% to +3.04%) the spring-summer  
 1626 ones. A further comparison of the ARI- and ACI-induced NMB variations demonstrated  
 1627 that the ARI-induced variations in the PM<sub>2.5</sub> concentrations were smaller than the  
 1628 ACI-induced ones in WRF\_Chem, and that the reversed pattern proceeded in WRF\_  
 1629 CHIMERE. This might be explained by the incorporation of dust aerosols in WRF\_  
 1630 CHIMERE serving as IN, which was not included in WRF\_Chem in this study.

1631 For O<sub>3</sub>, WRF\_CHIMERE (R = 0.62) exhibited the highest correlation, followed by  
 1632 WRF\_CMAQ (R = 0.55) and WRF\_Chem (R = 0.45) (Table 4 and Fig. S16). WRF\_  
 1633 CMAQ slightly underestimated the annual O<sub>3</sub> concentration, with NMBs and NGEs of  
 1634 –12.57% to –11.52%; conversely, WRF\_Chem and WRF\_CHIMERE significantly  
 1635 overestimated it, with NMBs of 47.82%–48.10% and 29.46%–29.75%, respectively. The  
 1636 seasonal results of the statistical metrics displayed consistent patterns with the annual  
 1637 simulations, and the O<sub>3</sub> pollution levels in summer were better simulated than in the other  
 1638 seasons (Fig. 6). The models with enabling ARI feedbacks slightly decreased the annual  
 1639 and seasonal O<sub>3</sub> NMBs and NGEs, ranging from –3.02% to +0.85% (the only positive  
 1640 value of +0.85% was produced by WRF\_CMAQ in summer) and –1.42% to –0.75%,  
 1641 respectively. Concurrently, regarding the ACI effects, WRF\_Chem and WRF\_CHIMERE  
 1642 exhibited increased annual O<sub>3</sub> NMBs and NGEs of 0.12%–0.65% and 0.40%–0.55%,  
 1643 respectively. The ACI-induced seasonal NMB variations for WRF\_Chem differed from  
 1644 those for WRF\_CHIMERE; WRF\_Chem increased and decreased in spring-summer and  
 1645 autumn-winter, respectively, whereas WRF\_CHIMERE increased in all seasons except

Deleted: As shown in

Deleted: , reveal that WRF-...CMAQ underestimated the

Deleted: -phase mechanisms, dust and sea salt emission

Deleted: -CHIMERE (R = 0.62) exhibited the highest

Deleted: -CMAQ slightly underestimated the annual O<sub>3</sub>

Deleted: ed

Deleted: resulted in slight decreases in ARI feedbacks slightly

winter (Fig. 7). Such diverse NMB and NGE variations can be explained by two aspect differences. Under the model-top BCs, the WRF-CMAQ and WRF-Chem models employed the parameterization scheme of O<sub>3</sub>-potential vorticity, and WRF-CHIMERE employed the climatological data from LMDz-INCA. Regarding the gas-phase chemistry mechanisms, the three coupled models incorporated various photolytic reactions, with a more comprehensive discussion in Section 4.2.

Knote et al. (2015) comprehensively assessed the effects of seven gas-phase chemical mechanisms (RADM2, RADMKA, RACM-ESRL, CB05Clx, CB05-TUCL, CBMZ, and MOZART-4) on O<sub>3</sub> simulations using the three two-way coupled models (WRF-Chem, WRF-CMAQ, and COSMO-ART). They concluded that the O<sub>3</sub> concentrations simulated by WRF-Chem using the CBMZ mechanism were closest to the mean values of multiple models for North America and Europe in spring and summer. However, dissimilar to North America and Europe, the two-way coupled WRF-Chem with CBMZ exhibited the lowest performance in spring for ECR. Additionally, the ARI and/or ACI effects contributed to atmospheric dynamics and stability (as mentioned in the PBLH evaluation part of Section 1.1 in SI), as well as photochemistry and heterogeneous reactions; thus, they eventually influenced O<sub>3</sub> formation (Xing et al., 2017; Qu et al., 2021; Zhu et al., 2021).

Table 4. Statistical metrics (R, MB, NMB, NGE, and RMSE) of the annual simulations and observations of surface PM<sub>2.5</sub>, O<sub>3</sub>, NO<sub>2</sub>, SO<sub>2</sub>, and CO in ECR. The best results are in bold, while the mean simulations and observations are in italics.

Variables	Statistics	WRF-CMAQ_NO	WRF-CMAQ_ARI	WRF-Chem_NO	WRF-Chem_ARI	WRF-Chem_BOTH	WRF-CHIMERE_NO	WRF-CHIMERE_ARI	WRF-CHIMERE
PM <sub>2.5</sub> (44.99 μg m <sup>-3</sup> )	Mean sim	<i>40.59</i>	<i>42.12</i>	<i>44.45</i>	<i>46.65</i>	<i>38.33</i>	<i>62.17</i>	<i>65.36</i>	<i>65.13</i>
	R	<b>0.68</b>	<b>0.68</b>	0.65	0.65	0.69	0.52	0.53	0.53
	MB	-4.40	-2.87	-0.54	1.66	-6.66	17.18	20.37	20.14
	NMB (%)	-9.78	-6.39	<b>-1.21</b>	3.69	-14.81	38.19	45.27	44.76
	NGE (%)	<b>46.41</b>	47.08	57.82	59.91	52.10	89.85	94.10	94.01
	RMSE	<b>27.62</b>	27.69	32.58	34.64	32.48	55.13	60.25	59.41
O <sub>3</sub> (62.23 μg m <sup>-3</sup> )	Mean sim	<i>55.06</i>	<i>54.41</i>	<i>88.53</i>	<i>87.81</i>	<i>87.89</i>	<i>76.92</i>	<i>76.48</i>	<i>76.89</i>
	R	0.54	0.55	0.46	0.45	0.45	<b>0.62</b>	<b>0.62</b>	<b>0.62</b>
	MB	-7.17	-7.83	26.30	25.58	25.65	14.69	14.25	14.66
	NMB (%)	<b>-11.52</b>	-12.57	42.26	41.10	41.22	23.60	22.90	23.55
	NGE (%)	<b>41.02</b>	41.40	87.02	86.17	86.57	58.17	57.63	58.18
	RMSE	<b>28.32</b>	28.68	48.10	47.99	47.82	29.65	29.46	29.75
NO <sub>2</sub> (31.2 μg m <sup>-3</sup> )	Mean sim	<i>33.94</i>	<i>34.46</i>	<i>21.17</i>	<i>21.98</i>	<i>21.40</i>	<i>21.85</i>	<i>22.20</i>	<i>22.24</i>
	R	0.59	<b>0.60</b>	0.50	0.50	0.50	0.55	0.56	0.56
	MB	2.74	3.26	-10.03	-9.22	-9.80	-9.35	-9.00	-8.96
	NMB (%)	<b>8.77</b>	10.44	-32.14	-29.55	-31.40	-29.96	-28.84	-28.73
	NGE (%)	55.04	55.74	54.57	54.37	54.43	50.56	<b>50.82</b>	50.89
	RMSE	<b>19.14</b>	19.48	21.23	21.21	21.21	18.72	18.68	18.70

Deleted: for

Deleted: diversity indiverse NMB and NGE variations can be

Deleted:

Moved (insertion) [3]

Deleted: A comprehensive assessment of(2015)

Moved up [3]: Knote et al.

Deleted: (2015); they concluded that the O<sub>3</sub> concentrations

Deleted: betweenof the annual simulations and observations

Formatted Table

Formatted: Font: 六号

Formatted: Font: Italic

Deleted: /

Formatted

Formatted: Font: 六号

Formatted: Font: 六号

Formatted: Font: Italic

Deleted: /

Formatted

Formatted

Formatted: Font: 六号

Formatted: Font: Italic

Deleted: /

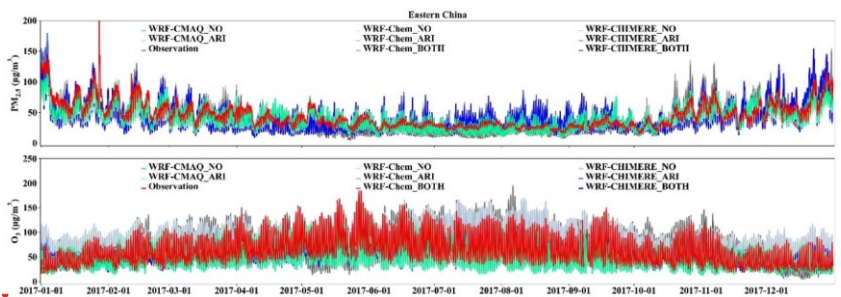
Formatted

Formatted



SO <sub>2</sub> (18.51 μg m <sup>-3</sup> )	Mean sim	14.02	14.39	8.22	8.56	7.85	8.88	9.18	9.19
	R	0.40	0.40	0.44	0.44	<b>0.46</b>	0.40	0.41	0.41
	MB	-4.49	-4.12	-10.29	-9.95	-10.66	-9.63	-9.33	-9.32
	NMB (%)	-24.25	<b>-22.24</b>	-55.61	-53.76	-57.57	-52.02	-50.39	-50.34
	NGE (%)	75.44	76.26	64.18	64.20	<b>66.09</b>	75.54	75.86	75.87
	RMSE	21.11	21.30	20.13	<b>20.02</b>	20.20	22.07	22.17	22.18
CO (0.96 mg m <sup>-3</sup> )	Mean sim	0.44	0.45	0.53	0.54	0.53	0.56	0.58	0.57
	R	0.23	0.24	0.21	0.22	0.22	0.47	<b>0.48</b>	0.47
	MB	-0.52	-0.51	-0.43	-0.42	-0.43	-0.40	-0.39	-0.39
	NMB (%)	-53.97	-52.99	-45.10	-43.94	-44.68	-41.82	<b>-40.11</b>	-40.28
	NGE (%)	65.44	65.11	53.63	53.38	53.80	47.27	<b>47.08</b>	47.09
	RMSE	0.90	0.90	0.82	0.83	0.83	<b>0.62</b>	<b>0.62</b>	<b>0.62</b>

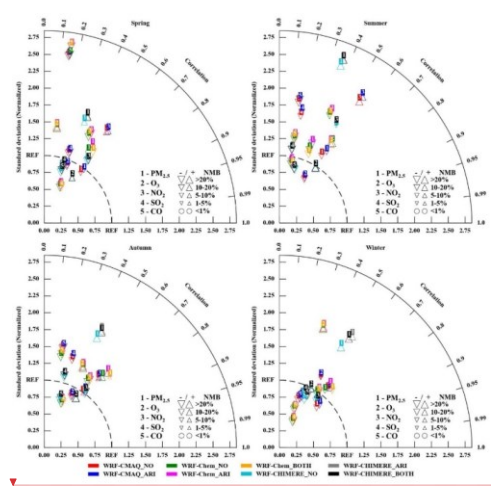
1809



1810

1811 Figure 6. Time series of the observed and simulated hourly PM<sub>2.5</sub> and O<sub>3</sub> concentrations by WRF-  
 1812 CMAQ, WRF-Chem, and WRF-CHIMERE with/without aerosol feedbacks over ECR in 2017.

1813



1814

1815 Figure 7. Taylor diagrams (R, normalized standard deviation, and NMB) of seasonal PM<sub>2.5</sub>, O<sub>3</sub>, NO<sub>2</sub>,

- Formatted: Font: 六号
- Formatted: Font: Italic
- Deleted: /
- Formatted: Font: 六号, Italic
- Formatted: Font: 六号
- Formatted: Font: 六号
- Formatted: Font: 六号
- Formatted: Font: 六号
- Formatted: Font: Italic
- Deleted: /
- Formatted: Font: 六号, Italic
- Formatted: Font: 六号
- Formatted: Font: 六号
- Deleted:

- Deleted: -
- Deleted: -
- Deleted: -
- Deleted: feedbacks over Eastern China during the year of
- Deleted: in
- Deleted: .
- Deleted:

1826 SO<sub>2</sub>, and CO using the three two-way coupled models (WRF-CMAQ, WRF-Chem, and WRF-  
1827 CHIMERE) with/without the ARI and/or ACI effects in ECR compared with the surface observations.  
1828 Similar to the meteorological variables presented above, we conducted quality  
1829 assurance for the statistical metrics via further comparisons with the PM<sub>2.5</sub> and O<sub>3</sub> results  
1830 in previous model evaluations (Fig. S20). In this study, the performances of WRF-  
1831 CMAQ and WRF-Chem in simulating PM<sub>2.5</sub> were better than the average levels reported  
1832 by the previous studies on ECR. Regarding the simulation of the O<sub>3</sub> level, WRF-Chem  
1833 performed worse compared with the average level reported by the previous studies.  
1834 Although the R<sub>c</sub>-values of O<sub>3</sub> simulated by WRF-CMAQ in this study were lower than  
1835 the average level reported in the previous studies, our RMSEs were smaller.

Deleted: viausing the three two-way coupled models

Deleted: In a similar manner...imilar to the meteorological

#### 1836 4.2 Satellite-borne observations

1837 In this section, we further investigated the discrepancies among the different models  
1838 regarding the calculated AOD and column concentrations of the gases (O<sub>3</sub>, NO<sub>2</sub>, SO<sub>2</sub>, CO,  
1839 and NH<sub>3</sub>) and compared them with various satellite observations. Regarding NH<sub>3</sub>, as the  
1840 output of simulated NH<sub>3</sub> concentrations was not set in WRF-CHIMERE, the discussion  
1841 here only includes the results from the WRF-CMAQ and WRF-Chem models.

Deleted: investigateinvestigated the discrepancies among the

Deleted:

1842 Table 5 reveals that the annual AOD at 550 nm, TCO, NO<sub>2</sub>, and CO simulated by the  
1843 three models agreed the most with the satellite observations, with R-values of 0.80–0.98;  
1844 these were followed by NH<sub>3</sub> (0.75–0.76), and SO<sub>2</sub> (0.50–0.53). WRF-CMAQ exhibited  
1845 negative biases for the annual AOD (–0.01), TCO (–5.92 Dobson Units (DU)), SO<sub>2</sub>  
1846 (–0.03 to –0.02 DU), CO (–1.25 × 10<sup>17</sup> molecules cm<sup>-2</sup>), and NH<sub>3</sub> (–2.95 × 10<sup>15</sup>  
1847 molecules cm<sup>-2</sup>). Conversely, it exhibited a positive bias for NO<sub>2</sub> (1.09–1.21  
1848 petamolecules cm<sup>-2</sup>). Regarding AOD, WRF-Chem and WRF-CHIMERE produced  
1849 positive (+0.09) and negative (–0.06) MBs. WRF-Chem and WRF-CHIMERE  
1850 overestimated NO<sub>2</sub> (0.28–0.63 petamolecules cm<sup>-2</sup>) and CO (0.93–1.21 × 10<sup>17</sup> molecules  
1851 cm<sup>-2</sup>) and underestimated O<sub>3</sub> (–10.99 to –3.63 DU) and SO<sub>2</sub> (–0.03 to –0.02 DU).  
1852 Similar to WRF-CMAQ, WRF-Chem underestimated NH<sub>3</sub> by approximately –3.14 ×  
1853 10<sup>15</sup> molecules cm<sup>-2</sup>.

Deleted: As shown in Table 5,...reveals that the annual AOD

1854 Regarding the seasonal variations, we observed relatively high correlation  
1855 relationships (0.71–0.88) regarding AOD in autumn, with lower values (0.53–0.84) in the  
1856 other seasons (Fig. 8). WRF-CMAQ and WRF-Chem tended to underestimate (MBs of  
1857 –0.1 to –0.4) and overestimate (MBs of 0.01–0.05) AOD in summer and the other  
1858 seasons, respectively. WRF-CHIMERE exhibited positive (0.03–0.04) and negative  
1859 (–0.10 to –0.01) biases in winter and the other seasons, respectively. Regarding TCO (Fig.  
1860 S24), the performances of the WRF-CMAQ and WRF-Chem models in spring and  
1861 winter were slightly better than the performances in summer and autumn; however, the  
1862 R-values of all the seasons were above 0.89. WRF-CMAQ (–9.53 to –0.72 DU) and  
1863 WRF-Chem (–24.62 to +10.57 DU) exhibited negative biases in all the seasons (except  
1864 WRF-Chem in autumn). WRF-CHIMERE better captured TCO in spring and summer  
1865 (overestimations of +9.19 to +29.20 DU) than in autumn and winter (underestimations of  
1866 –33.75 to –19.40 DU). The R<sub>c</sub>-values of the NO<sub>2</sub> columns for the three models were

Deleted: For Regarding the seasonal variations, we observed

1966 slightly higher in autumn and winter (0.82–0.91) than in spring and summer (0.76–0.84).  
 1967 Generally, WRF<sub>-CMAQ</sub> (–0.68 to –0.16 DU), WRF<sub>-Chem</sub> (–1.40 to –0.44 DU), and  
 1968 WRF-CHIMERE (–1.31 to –0.19 DU) generally underestimated the seasonal NO<sub>2</sub>  
 1969 columns (Fig. S22). All the models overestimated the SO<sub>2</sub> column concentrations in  
 1970 winter (by 0.01–0.03 DU) but underestimated them in the other seasons (–0.05 to –0.001  
 1971 DU) (Fig. S23). Regarding NH<sub>3</sub>, the only primary alkaline gas in the atmosphere, the  
 1972 WRF<sub>-CMAQ</sub> and WRF<sub>-Chem</sub> models performed better in summer (R: 0.81–0.87; MB:  
 1973 –3.42 to 2.07 × 10<sup>15</sup> molecules cm<sup>-2</sup>) (Fig. S25). The NH<sub>3</sub> emissions from fertilizers and  
 1974 livestock have been substantially underestimated in China (Zhang et al., 2017), and the  
 1975 peak values were obtained in spring and summer (Huang et al., 2012). Additionally, the  
 1976 bidirectional exchanges of fertilizer-induced NH<sub>3</sub> were not considered in our simulations.  
 1977 Compared with the above column variables, WRF<sub>-CMAQ</sub>, WRF<sub>-Chem</sub>, and WRF<sub>-</sub>  
 1978 CHIMERE exhibited relatively poor performances (R: 0.68–0.79) in simulating the CO  
 1979 columns during spring, summer, and autumn, respectively, than in simulating them in the  
 1980 other seasons (Fig. S24). WRF<sub>-CMAQ</sub> and WRF<sub>-CHIMERE</sub> underestimated and  
 1981 overestimated the CO columns in the other seasons, respectively, except for summer and  
 1982 spring, with MBs of –3.29 to 0.31 × 10<sup>17</sup> and –0.62 to 2.09 × 10<sup>17</sup> molecules cm<sup>-2</sup>,  
 1983 respectively. WRF<sub>-Chem</sub> obtained positive MBs in summer and autumn (4.03–5.12 ×  
 1984 10<sup>17</sup> molecules cm<sup>-2</sup>) and negative ones in spring and winter (–3.15 to –2.10 × 10<sup>17</sup>  
 1985 molecules cm<sup>-2</sup>).

1986 Moreover, after comparing the performances of the models for each pollutant  
 1987 between Sections 4.1 and 4.2, the only disparity found between evaluations with  
 1988 ground-based observations and those with satellite-borne observations was for CO. The  
 1989 formation of CO via the oxidation of methane, an important source of CO emissions  
 1990 (Stein et al., 2014), was not considered in the three coupled models, and the methane  
 1991 emissions were not included in the MEIC inventory. Furthermore, the contribution of CO  
 1992 to atmospheric oxidation capacity (OH radicals) was nonnegligible (e.g., the values were  
 1993 approximately 20.54%–38.97% in Beijing (Liu et al., 2021) and 26%–31% in Shanghai  
 1994 (Zhu et al., 2020)). In addition, these discrepancies in the model performances in  
 1995 simulating AOD and column concentrations of gases can be explained by the differences  
 1996 in the representations of the aerosol species groups, Fast-JX photolysis scheme, and  
 1997 gas-phase mechanisms in the three coupled models. More detailed interpretations were  
 1998 grouped into four aspects: (1) AODs are calculated via the Mie theory using the refractive  
 1999 indices of different numbers (5, 6, and 10) of aerosol species groups in different coupled  
 2000 models (WRF<sub>-CMAQ</sub>, WRF<sub>-Chem</sub>, and WRF<sub>-CHIMERE</sub>) (Tables S5–S6); (2) seven  
 2001 (294.6, 303.2, 310.0, 316.4, 333.1, 382.0, and 607.7 nm), four (300, 400, 600, and 999  
 2002 nm), and five (200, 300, 400, 600, and 999 nm) effective wavelengths were used to  
 2003 calculate the actinic fluxes and photolysis rates in the Fast-JX photolysis modules of  
 2004 WRF<sub>-CMAQ</sub>, WRF<sub>-Chem</sub>, and WRF<sub>-CHIMERE</sub>, respectively; (3) different methods  
 2005 exist in the Fast-JX schemes of the three coupled models for calculating the aerosol and  
 2006 cloud optical properties (Tables S1 and S5–S6); (4) 77, 52, and 40 gas-phase species

**Deleted:** The seasonal NO<sub>2</sub> columns were generally underestimated in Generally, WRF-...CMAQ (-...-0.68 to ...)

**Deleted:** WRF

**Deleted:** (-1.31 to - ...)

**Deleted:** approximately 0.01–0.03 DU) but underestimated ...

**Deleted:** performance results performances of the models for ...

**Commented [Editor17]:** Remark: Starting a sentence with short conjunctions like “and,” “also,” “then,” and “but” lends a slightly informal tone to the writing. These words should preferably be replaced with formal alternatives like “further”/“moreover” (for “and”), “thereafter”/“afterward” (for “then”), and “however” (for “but”). Further, then is considered informal irrespective of its position in a sentence in academic writing. As a conjunction, it is preferably replaced by “thereafter,” “after which,” and “afterward.”

**Deleted:** addition

**Deleted:** ,

**Deleted:** for

**Deleted:** group groups in different coupled models ...

**Commented [Editor18]:** Remark: Numbers under 10 are spelt out, except for measurements with a unit (8 mmol/L) or lists with other numbers (11 dogs, 9 cats, 4 gerbils).

**Deleted:** 4four (300, 400, 600, and 999 nm), and 5...ive (200 ...)

2080 comprised 218, 132, and 120 gas-phase reactions under the CB6, CBMZ, and  
 2081 MELCHIOR2 mechanisms, respectively.

2082 When the three models enabled only the ARI effects, relatively limited  
 2083 improvements were observed in the annual AOD and NO<sub>2</sub> columns simulated by these  
 2084 models. The AOD simulations improved in spring and summer, but worsened in autumn  
 2085 and winter (Table 4 and Fig. 9). Larger ARI-induced variations in seasonal MBs of the  
 2086 NO<sub>2</sub> columns were observed in WRF-CMAQ (-0.18 to 0.13 petamolecules cm<sup>-2</sup>)  
 2087 compared with WRF-Chem and WRF-CHIMERE (0–0.01 petamolecules cm<sup>-2</sup>). When  
 2088 the ARI and ACI effects were enabled in WRF-Chem, the model performance for  
 2089 seasonal AOD simulations worsened considerably. The annual and seasonal NO<sub>2</sub>  
 2090 simulations by WRF-Chem became slightly worse, whereas those by WRF-CHIMERE  
 2091 became slightly better. Dissimilar to AOD and the NO<sub>2</sub> column concentrations, the  
 2092 improvements in the annual and seasonal column simulations of total ozone, PBL SO<sub>2</sub>,  
 2093 and NH<sub>3</sub> by all the two-way coupled models were limited when one or both of ARI and  
 2094 ACI were enabled.

2095 Table 5. Statistical metrics (R, MB, NMB, NGE, and RMSE) of the simulated and  
 2096 satellite-retrieved AOD, TCO, tropospheric column NO<sub>2</sub>, PBL column SO<sub>2</sub>, total column  
 2097 CO, and total column density of NH<sub>3</sub> in ECR. The best results are captured in bold fonts,  
 2098 and the annual mean simulations and observations are in italics.

Variables	Statistics	WRF-CMAQ_NO	WRF-CMAQ_ARI	WRF-Chem_NO	WRF-Chem_ARI	WRF-Chem_BOTH	WRF-CHIMERE_NO	WRF-CHIMERE_ARI	WRF-CHIMERE
AOD (0.27)	Mean_sim	<i>0.26</i>	<i>0.27</i>	<i>0.35</i>	<i>0.36</i>	<i>0.25</i>	<i>0.21</i>	<i>0.22</i>	<i>0.22</i>
	R	0.80	0.80	0.80	0.80	0.75	<b>0.87</b>	<b>0.87</b>	0.86
	MB	-0.01	-0.01	0.09	0.09	-0.01	-0.05	-0.05	-0.04
	NMB (%)	-3.99	<b>-2.93</b>	34.14	35.03	-4.92	-18.72	-17.37	-16.22
	NGE (%)	34.90	34.82	58.21	58.89	41.46	32.15	<b>32.11</b>	32.06
	RMSE	<b>0.09</b>	<b>0.09</b>	0.15	0.15	0.10	<b>0.09</b>	<b>0.09</b>	0.10
O <sub>3</sub>	Mean_sim	<i>306.15</i>	<i>306.15</i>	<i>300.77</i>	<i>300.73</i>	<i>300.46</i>	<i>307.69</i>	<i>307.47</i>	<i>307.75</i>
VCDs (212.07 DU)	R	<b>0.98</b>	<b>0.98</b>	0.97	0.97	0.97	0.65	0.65	0.65
	MB	-5.92	-5.92	-10.68	-10.72	-10.99	-3.69	-3.91	-3.63
	NMB (%)	-1.90	-1.90	-3.43	-3.44	-3.53	-1.19	-1.26	-1.17
	NGE (%)	<b>2.46</b>	<b>2.46</b>	25.02	25.02	25.08	10.95	10.89	10.93
	RMSE	<b>8.91</b>	<b>8.91</b>	83.72	83.73	83.94	39.88	39.71	39.73
Tropospheric NO <sub>2</sub> VCDs (2.71 × 10 <sup>15</sup> molecules cm <sup>-2</sup> )	Mean_sim	<i>3.80</i>	<i>3.91</i>	<i>3.07</i>	<i>3.08</i>	<i>3.06</i>	<i>2.62</i>	<i>2.63</i>	<i>2.63</i>
	R	0.85	0.85	<b>0.87</b>	<b>0.87</b>	<b>0.87</b>	<b>0.87</b>	<b>0.87</b>	<b>0.87</b>
	MB	1.09	1.21	0.62	0.63	0.61	0.28	0.29	0.29
	NMB (%)	40.35	44.64	25.27	25.52	24.89	<b>12.03</b>	12.47	12.42
	NGE (%)	52.80	55.08	46.01	46.05	<b>45.17</b>	46.06	46.31	46.24
	RMSE	3.18	3.33	2.27	2.27	2.27	<b>1.65</b>	1.67	1.68
PBL SO <sub>2</sub> VCDs (0.49 DU)	Mean_sim	<i>0.07</i>	<i>0.07</i>	<i>0.09</i>	<i>0.09</i>	<i>0.06</i>	<i>0.06</i>	<i>0.06</i>	<i>0.06</i>
	R	0.53	0.53	<b>0.56</b>	<b>0.56</b>	0.54	0.50	0.50	0.50
	MB	-0.03	-0.02	-0.03	-0.02	-0.03	-0.03	-0.02	-0.02

- Deleted: involve
- Deleted: in
- Deleted: all
- Deleted: just
- Deleted: in
- Deleted: were relatively limited.
- Deleted: ,
- Deleted: induced by ARI effects occurred
- Deleted: -
- Deleted: -
- Deleted: -
- Deleted: both
- Deleted: -
- Deleted: via
- Deleted: -
- Deleted: while
- Deleted: using
- Deleted: -
- Deleted: In contrast
- Deleted: via
- Deleted: total column ozone
- Deleted: eastern China.
- Deleted: , while
- Deleted: .
- Formatted: Font: Italic
- Formatted: Font: Italic
- Formatted: Font: Italic
- Formatted: Font: Italic
- Formatted: Font: Italic
- Formatted: Font: Italic
- Formatted: Font: Italic
- Formatted: Font: Italic

Total CO VCDs ( $21.60 \times 10^6$ ) molecules cm <sup>-2</sup>	NMB (%)	-27.32	-25.48	-32.50	<b>-21.50</b>	-35.08	-28.64	-27.31	-27.51
	NGE (%)	<b>57.45</b>	58.26	67.55	68.07	64.83	68.31	68.61	68.80
	RMSE	<b>0.07</b>	<b>0.07</b>	0.08	0.08	<b>0.07</b>	<b>0.07</b>	<b>0.07</b>	<b>0.07</b>
	Mean_sim	<i>20.34</i>	<i>20.35</i>	<i>22.20</i>	<i>22.20</i>	<i>22.21</i>	<i>22.34</i>	<i>22.36</i>	<i>22.35</i>
	R	0.83	0.83	<b>0.87</b>	<b>0.87</b>	<b>0.87</b>	0.86	0.86	0.86
	MB	-1.26	-1.24	0.93	0.93	0.94	1.19	1.21	1.19
	NMB (%)	-5.83	-5.75	<b>4.35</b>	4.37	4.44	5.64	5.70	5.65
	NGE (%)	9.33	<b>9.31</b>	10.30	10.28	10.32	11.02	11.06	11.10
	RMSE	<b>2.54</b>	<b>2.54</b>	2.69	2.68	2.69	2.57	2.58	2.58
	Total NH <sub>3</sub> VCDs ( $16.05 \times 10^6$ ) molecules cm <sup>-2</sup>	Mean_sim	<i>13.06</i>	<i>13.15</i>	<i>12.31</i>	<i>12.27</i>	<i>8.63</i>	<i>N/A</i>	<i>N/A</i>
R	<b>0.76</b>	<b>0.76</b>	0.73	0.73	0.76	<i>N/A</i>	<i>N/A</i>	<i>N/A</i>	
MB	-3.00	-2.90	-3.27	-3.32	-3.34	<i>N/A</i>	<i>N/A</i>	<i>N/A</i>	
NMB (%)	-18.66	<b>-18.08</b>	-21.01	-21.28	-21.41	<i>N/A</i>	<i>N/A</i>	<i>N/A</i>	
NGE (%)	<b>47.69</b>	48.09	50.84	50.80	50.99	<i>N/A</i>	<i>N/A</i>	<i>N/A</i>	
RMSE	<b>9.26</b>	9.47	9.48	9.46	9.61	<i>N/A</i>	<i>N/A</i>	<i>N/A</i>	

Formatted: Font: Italic

Formatted: Font: Italic

Formatted: Font: Italic

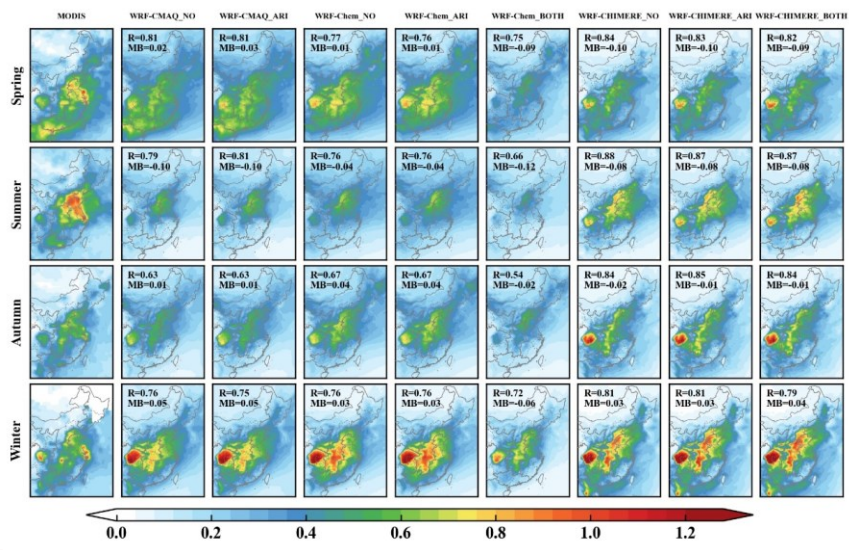
Formatted: Font: Italic

1223 N/A indicates that the outputs of the NH<sub>3</sub> column concentrations were not extracted from WRF-CHIMERE simulations  
1224 with/without aerosol feedbacks.

Deleted: -

Deleted: simulations.

Deleted:



1225  
1226 Figure 8. Spatial distributions of seasonal AOD between MODIS observations and simulations using  
1227 the WRF-CMAQ, WRF-Chem, and WRF-CHIMERE models with and without aerosol feedbacks in  
1228 ECR.  
1229

Deleted: from

Deleted: -

Deleted: -

Deleted: -

Deleted: feedbacks

Deleted: eastern China.



2139 4.3 Computational performance

2140 Table 5 presents a summary of the comparative results of the time consumption by  
 2141 the central processing unit (CPU) per simulation day using WRF\_CMAQ, WRF\_Chem,  
 2142 and WRF\_CHIMERE with and without aerosol feedbacks in 2017. The results indicated  
 2143 that WRF\_CMAQ consumed the shortest CPU time simulating one-day meteorology and  
 2144 air quality with or without enabling aerosol feedbacks. This CPU time consumption was  
 2145 followed by WRF\_CHIMERE and WRF\_Chem. Compared with the simulations without  
 2146 aerosol feedbacks, the processing time of WRF\_CMAQ with ARI increased by 0.22–0.34  
 2147 h per day. The increases in the running time of WRF\_Chem and WRF\_CHIMERE were  
 2148 insignificant (0.02–0.03 h per day). The CPU times for WRF\_Chem and WRF\_  
 2149 CHIMERE with the ARI and ACI effects enabled increased slightly, and the increase in  
 2150 the CPU time for the former (0.25 h per day) was higher than that for the latter (0.11 h  
 2151 per day). Compared with WRF\_CMAQ and WRF\_Chem, the CPU time consumed by  
 2152 WRF\_CHIMERE exhibited clear seasonal differences, with the CPU times in winter and  
 2153 spring being significantly longer than those in summer and autumn. These differences can  
 2154 be partially explained by the choice of the main configurations, including the model  
 2155 resolution, model version, and parametrization schemes (cloud microphysics, PBL,  
 2156 cumulus, surface layer, land surface, gas-phase chemistry, and aerosol mechanisms).

Deleted: summarizes presents a summary of the comparative

2157 Table 5. Summary of the running time for the different coupled models.

Month	WRF_CMAQ (h)		WRF_Chem (h)			WRF_CHIMERE (h)		
	NO	ARI	NO	ARI	BOTH	NO	ARI	BOTH
Jan.	0.37	0.59	0.69	0.71	0.96	0.67	0.70	0.77
Feb.	0.35	0.60	0.68	0.70	0.93	0.64	0.67	0.73
Mar.	0.39	0.65	0.70	0.72	1.00	0.59	0.62	0.72
Apr.	0.37	0.67	0.67	0.69	0.92	0.54	0.57	0.65
May	0.39	0.71	0.61	0.66	0.86	0.52	0.55	0.62
June	0.40	0.74	0.66	0.67	0.95	0.48	0.51	0.63
July	0.36	0.69	0.65	0.67	0.86	0.49	0.50	0.58
Aug.	0.38	0.68	0.66	0.68	0.90	0.49	0.52	0.61
Sept.	0.37	0.63	0.64	0.65	0.89	0.48	0.52	0.63
Oct.	0.38	0.62	0.66	0.68	0.94	0.53	0.56	0.69
Nov.	0.36	0.58	0.68	0.70	0.91	0.64	0.67	0.72
Dec.	0.35	0.57	0.63	0.66	0.87	0.67	0.70	0.74

Deleted: .

Deleted: --CMAQ (hour

Deleted: --Chem (hour

Deleted: --CHIMERE (hour

2158  
 2159 5 Conclusions

2160 Two-way coupled meteorology and air-quality models have been deployed in ECR  
 2161 in recent years. However, no study comprehensively assessed multiple coupled models in  
 2162 this region. To the best of our knowledge, this is the first study to perform comprehensive

Deleted: Applications of two

Deleted: quality models have been performed...employed in

Deleted: ;, Hh

Deleted: research focused on the comprehensive assessments of study comprehensively assessed multiple coupled models in

2232 ~~intercomparisons of~~ the open-sourced two-way coupled meteorology and air quality  
2233 models (WRF\_CMAQ, WRF\_Chem, and WRF\_CHIMERE). ~~Here, we~~ systemically  
2234 evaluated the hindcast simulations for 2017 and explored the impacts of ARI and/or ACI  
2235 on ~~the model performance~~ and computational ~~efficiency~~ in ~~ECR~~.

Deleted: inter-comparisons amongintercomparisons of the ...

2236 After detailed comparisons with ground-based and satellite-borne observations, the  
2237 evaluation results ~~revealed~~ that ~~the~~ three coupled models ~~performed~~ well for meteorology  
2238 and air quality, ~~particularly~~ for surface temperature (with ~~an R-value of~~ up to 0.97) and  
2239 PM<sub>2.5</sub> concentrations (with ~~an R-value of~~ up to 0.68). The effects of aerosol ~~feedbacks~~ on  
2240 ~~the model performance~~ varied ~~with~~ the two-way coupled models, variables, and time  
2241 scales. ~~The~~ computational time ~~increased by 20%–70%~~ when these two-way coupled  
2242 models enabled aerosol ~~feedbacks compared with when the simulations proceeded~~  
2243 without aerosol\_ radiation\_ cloud interactions. ~~Notably, the~~ three coupled models could  
2244 ~~effectively~~ reproduce the spatiotemporal distributions of ~~the~~ satellite-retrieved CO  
2245 column concentrations but not for ground-observed CO concentrations.

Deleted: s and their ...computational efficiencyperformance...

Deleted: eastern China

Deleted: showedrevealed that the three coupled models ...

2246 ~~The intercomparisons revealed~~ some uncertainty sources ~~in the evaluation of the~~  
2247 aerosol feedback effects. As numerous schemes can be combined ~~with the~~ configurations  
2248 of different coupled models, ~~we~~ only evaluated ~~the~~ simulations with specific settings.  
2249 Future ~~comparisons~~ considering more combinations of multiple schemes within the same  
2250 or different coupled models ~~are desired~~. Among the three coupled models, the numerical  
2251 representations for specific ~~variables in the same scheme~~ are diverse, e.g., ~~the~~ treatments  
2252 of cloud cover and cloud optical properties in the Fast-JX photolysis scheme. More  
2253 accurate representations of photolysis processes ~~must be considered~~ to reduce ~~evaluation~~  
2254 uncertainties. ~~Additionally, the~~ FDDA nudging technique can attenuate the ARI effects  
2255 during severe air ~~pollution~~ episodes, and optimal nudging coefficients among different  
2256 regions ~~must be determined~~. ~~Finally,~~ the actual mechanisms underlying ~~the~~ ACI effects  
2257 are still unclear, and the new advances in the measurements and parameterizations of  
2258 CCN/IN activations and ~~PREC must be duly~~ incorporated in coupled models.

Deleted: With inter-comparisons,The intercomparisons ...

#### 2260 Code availability

2261 The source codes of the two-way coupled WRF v4.1.1-CMAQ v5.3.1, WRF-Chem  
2262 v4.1.1, and WRF v3.7.1-CHIMERE v2020r1 models are obtained from  
2263 <https://github.com/USEPA/CMAQ>, <https://github.com/wrf-model/WRF>, and  
2264 <https://www.lmd.polytechnique.fr/chimere>, respectively (last access: November 2020).  
2265 The related source codes, configuration information, namelist files and automated run  
2266 scripts of these three two-way coupled models are archived at Zenodo with the associated  
2267 DOI: <https://doi.org/10.5281/zenodo.7901682> (Gao et al., 2023a; link:  
2268 <https://zenodo.org/record/7901682>).

#### 2270 Data availability

2271 The meteorological ICs and BCs used for three coupled models can be obtained at

2317 <https://doi.org/10.5281/zenodo.7925012> (Gao et al., 2023b; link:  
2318 <https://zenodo.org/record/7925012>). The Chemical ICs and BCs used for WRF-CMAQ,  
2319 WRF-Chem and WRF-CHIMERE are available at  
2320 <https://doi.org/10.5281/zenodo.7932390> (Gao et al., 2023c; link:  
2321 <https://zenodo.org/record/7932390>), <https://doi.org/10.5281/zenodo.7932936> (Gao et al.,  
2322 2023d; link: <https://zenodo.org/record/7932936>), and  
2323 <https://doi.org/10.5281/zenodo.7933641> (Gao et al., 2023e; link:  
2324 <https://zenodo.org/record/7933641>), respectively. The emission data used for  
2325 WRF-CMAQ, WRF-Chem and WRF-CHIMERE can be downloaded from  
2326 <https://doi.org/10.5281/zenodo.7932430> (Gao et al., 2023f; link:  
2327 <https://zenodo.org/record/7932430>), <https://doi.org/10.5281/zenodo.7932734> (Gao et al.,  
2328 2023g; link: <https://zenodo.org/record/7932734>), and  
2329 <https://doi.org/10.5281/zenodo.7931614> (Gao et al., 2023h; link:  
2330 <https://zenodo.org/record/7931614>), respectively. The DOIs and links regarding the  
2331 output data of each simulation scenario are presented in Table S9. All data used to create  
2332 figures and tables in this study are provided in an open repository on Zenodo  
2333 (<https://doi.org/10.5281/zenodo.7750907>, Gao et al., 2023i; link:  
2334 <https://zenodo.org/record/7750907>).

Formatted: Font: 小四

#### 2335 Author contributions

2336 CG, ZX, AX performed the majority of the source code configuration of  
2337 WRF-CMAQ, WRF-Chem and WRF-CHIMERE, designed the numerical simulations to  
2338 carry them out, related analysis, figure plotting, and paper writing. QT, HZ, SZ, GY, MZ  
2339 and XS were involved with the original research plan and made suggestions for the paper  
2340 writing.  
2341

2342

#### 2343 Competing interests

2344 The contact author has declared that neither they nor their co-authors have any  
2345 competing interests.  
2346

2347

#### 2348 Acknowledgements

2349 The authors are very grateful to David Wong, Chun Zhao and Laurent Menut who  
2350 provided detailed information on the two-way coupled WRF-CMAQ, WRF-Chem and  
2351 WRF-CHIMERE models, respectively.

2352

#### 2353 Financial support

2354 This study was financially sponsored by the National Natural Science Foundation of  
2355 China (grant nos. 42305171, 42371154 & 42171142), the Youth Innovation Promotion  
2356 Association of Chinese Academy of Sciences, China (grant nos. 2022230), the National

2356 Key Research and Development Program of China (grant nos. 2017YFC0212304 &  
2357 2019YFE0194500), the Talent Program of Chinese Academy of Sciences (Y8H1021001),  
2358 and the Natural Science Foundation of Jilin Province (YDZJ202201ZYTS476).

2359

## 2360 References

- 2361 Abdul-Razzak, H. and Ghan, S. J.: A parameterization of aerosol activation 3. Sectional representation,  
2362 *J. Geophys. Res. Atmos.*, 107, AAC-1, <https://doi.org/10.1029/2001JD000483>, 2002.
- 2363 Alapaty, K., Herwehe, J. A., Otte, T. L., Nolte, C. G., Bullock, O. R., Mallard, M. S., Kain, J. S., and  
2364 Dudhia, J.: Introducing subgrid-scale cloud feedbacks to radiation for regional meteorological  
2365 and climate modeling, *Geophys. Res. Lett.*, 39, 1–5, <https://doi.org/10.1029/2012GL054031>,  
2366 2012.
- 2367 Archer-Nicholls, S., Lowe, D., Utembe, S., Allan, J., Zaveri, R. A., Fast, J. D., Hodnebrog, Ø., Denier  
2368 Van Der Gon, H., and Mcfiggans, G.: Gaseous chemistry and aerosol mechanism developments  
2369 for version 3.5.1 of the online regional model, WRF-Chem, *Geosci. Model Dev.*, 7, 2557–2579,  
2370 <https://doi.org/10.5194/gmd-7-2557-2014>, 2014.
- 2371 Baklanov, A., Schlünzen, K., Suppan, P., Baldasano, J., Brunner, D., Aksoyoglu, S., Carmichael, G.,  
2372 Dourou, J., Flemming, J., and Forkel, R.: Online coupled regional meteorology chemistry models  
2373 in Europe: current status and prospects, *Atmos. Chem. Phys.*, 14, 317–398,  
2374 <https://doi.org/10.5194/acp-14-317-2014>, 2014.
- 2375 Balzarini Briant, R., Tuccella, P., Deroubaix, A., Khvorostyanov, D., Menut, L., Mailler, S., and  
2376 Turquety, S.: Aerosol-radiation interaction modelling using online coupling between the WRF  
2377 3.7.1 meteorological model and the CHIMERE 2016 chemistry-transport model, through the  
2378 OASIS3-MCT coupler, *Geosci. Model Dev.*, 10, 927–944,  
2379 <https://doi.org/10.5194/gmd-10-927-2017>, 2017.
- 2380 Briant, R., Tuccella, P., Deroubaix, A., Khvorostyanov, D., Menut, L., Mailler, S., and Turquety, S.:  
2381 Aerosol-radiation interaction modelling using online coupling between the WRF 3.7.1  
2382 meteorological model and the CHIMERE 2016 chemistry-transport model, through the  
2383 OASIS3-MCT coupler, *Geosci. Model Dev.*, 10, 927–944,  
2384 <https://doi.org/10.5194/gmd-10-927-2017>, 2017.
- 2385 Brunner, D., Savage, N., Jorba, O., Eder, B., Giordano, L., Badia, A., Balzarini, A., Baro, R., Bianconi,  
2386 R., and Chemel, C.: Comparative analysis of meteorological performance of coupled  
2387 chemistry-meteorology models in the context of AQMEII phase 2, *Atmos. Environ.*, 115, 470–  
2388 498, <https://doi.org/10.1016/j.atmosenv.2014.12.032>, 2015.
- 2389 Campbell, P., Zhang, Y., Wang, K., Leung, R., Fan, J., Zheng, B., Zhang, Q., and He, K.: Evaluation  
2390 of a multi-scale WRF-CAM5 simulation during the 2010 East Asian Summer Monsoon, *Atmos.*  
2391 *Environ.*, 169, 204–217, <https://doi.org/10.1016/j.atmosenv.2017.09.008>, 2017.
- 2392 Carslaw, K. S., Boucher, O., Spracklen, D. V., Mann, G. W., Rae, J. G. L., Woodward, S., and  
2393 Kulmala, M.: A review of natural aerosol interactions and feedbacks within the Earth system,  
2394 *Atmos. Chem. Phys.*, 10, 1701–1737, <https://doi.org/10.5194/acp-10-1701-2010>, 2010.
- 2395 Chapman, E. G., Jr, W. I. G., Easter, R. C., Barnard, J. C., Ghan, S. J., Pekour, M. S., and Fast, J. D.:  
2396 and Physics Coupling aerosol-cloud-radiative processes in the WRF-Chem model : Investigating

2397 the radiative impact of elevated point sources, 945–964, <https://doi.org/10.5194/acp-9-945-2009>,  
2398 2009.

2399 Chen, L., Gao, Y., Zhang, M., Fu, J. S., Zhu, J., Liao, H., Li, J., Huang, K., Ge, B., and Wang, X.:  
2400 MICS-Asia III: Multi-model comparison and evaluation of aerosol over East Asia, *Atmos. Chem.*  
2401 *Phys.*, 19, 11911–11937, <https://doi.org/10.5194/acp-19-11911-2019>, 2019.

2402 Ding, Q. J., Sun, J., Huang, X., Ding, A., Zou, J., Yang, X., and Fu, C.: Impacts of black carbon on the  
2403 formation of advection–radiation fog during a haze pollution episode in eastern China, *Atmos.*  
2404 *Chem. Phys.*, 19, 7759–7774, <https://doi.org/10.5194/acp-19-7759-2019>, 2019.

2405 Dionne, J., von Salzen, K., Cole, J., Mahmood, R., Leaitch, W. R., Lesins, G., Folkins, I., and Chang,  
2406 R. Y.-W.: Modelling the relationship between liquid water content and cloud droplet number  
2407 concentration observed in low clouds in the summer Arctic and its radiative effects, *Atmos.*  
2408 *Chem. Phys.*, 20, 29–43, <https://doi.org/10.5194/acp-20-29-2020>, 2020.

2409 Fan, J., Wang, Y., Rosenfeld, D., and Liu, X.: Review of aerosol-cloud interactions: Mechanisms,  
2410 significance, and challenges, *J. Atmos. Sci.*, 73, 4221–4252,  
2411 <https://doi.org/10.1175/JAS-D-16-0037.1>, 2016.

2412 Feng, X., Lin, H., Fu, T.-M., Sulprizio, M. P., Zhuang, J., Jacob, D. J., Tian, H., Ma, Y., Zhang, L.,  
2413 and Wang, X.: WRF-GC (v2.0): online two-way coupling of WRF (v3.9.1.1) and GEOS-Chem  
2414 (v12.7.2) for modeling regional atmospheric chemistry–meteorology interactions, *Geosci. Model*  
2415 *Dev.*, 14, 3741–3768, <https://doi.org/10.5194/gmd-14-3741-2021>, 2021.

2416 Forkel, R., Werhahn, J., Hansen, A. B., McKeen, S., Peckham, S., Grell, G., and Suppan, P.: Effect of  
2417 aerosol-radiation feedback on regional air quality—A case study with WRF/Chem, *Atmos.*  
2418 *Environ.*, 53, 202–211, <https://doi.org/10.1016/j.atmosenv.2011.10.009>,

2419 Gao, C., Zhang, X., Xiu, A., Huang, L., Zhao, H., Wang, K., and Tong, Q.: Spatiotemporal  
2420 distribution of biogenic volatile organic compounds emissions in China, *Acta Sci. Circumstantiae*,  
2421 39, 4140–4151, <https://doi.org/10.13671/j.hjkxxb.2019.0243>, 2019.

2422 Gao, C., Xiu, A., Zhang, X., Tong, Q., Zhao, H., Zhang, S., Yang, G., and Zhang, M.: Two-way  
2423 coupled meteorology and air quality models in Asia: a systematic review and meta-analysis of  
2424 impacts of aerosol feedbacks on meteorology and air quality, *Atmos. Chem. Phys.*, 22, 5265–  
2425 5329, <https://doi.org/10.5194/acp-22-5265-2022>, 2022.

2426 Gao, C., Xiu, A., Zhang, X.: Observational data for sfdda nudging analysis in WRF model over China  
2427 during 2017, Zenodo [Data set], <https://doi.org/10.5281/zenodo.6975602>, 2022.

2428 Gao, C., Xiu, A., Zhang, X., Tong, Q., Zhao, H., Zhang, S., Yang, G., Zhang, M., Xie, S.: Source  
2429 codes of WRF v4.1.1-CMAQ v5.3.1, WRF-Chem v4.1.1 and WRF  
2430 v3.7.1-CHIMERE v2020r1, Zenodo [software].  
2431 <https://doi.org/10.5281/zenodo.7901682>, 2023a.

2432 Gao, C., Xiu, A., Zhang, X., Tong, Q., Zhao, H., Zhang, S., Yang, G., Zhang, M., Xie, S.: FNL data  
2433 used for producing meteorological ICs/BCs of WRF v4.1.1-CMAQ v5.3.1,  
2434 WRF-Chem v4.1.1 and WRF v3.7.1-CHIMERE v2020r1, Zenodo [data set],  
2435 <https://doi.org/10.5281/zenodo.7925012>, 2023b.



2436 Gao, C., Xiu, A., Zhang, X., Tong, Q., Zhao, H., Zhang, S., Yang, G., Zhang, M., Xie, S.: Chemical  
2437 initial and boundary conditions for WRF-CMAQ, Zenodo [data set],  
2438 <https://doi.org/10.5281/zenodo.7932390>, 2023c.

2439 Gao, C., Xiu, A., Zhang, X., Tong, Q., Zhao, H., Zhang, S., Yang, G., Zhang, M., Xie, S.: Chemical  
2440 initial and boundary conditions for WRF-Chem. Zenodo [data set],  
2441 <https://doi.org/10.5281/zenodo.7932936>, 2023d.

2442 Gao, C., Xiu, A., Zhang, X., Tong, Q., Zhao, H., Zhang, S., Yang, G., Zhang, M., Xie, S.: Chemical  
2443 initial and boundary conditions for WRF-CHIMERE, Zenodo [data set],  
2444 <https://doi.org/10.5281/zenodo.7933641>, 2023e.

2445 Chao Gao, Xuelei Zhang, Aijun Xiu, Qingqing Tong, Hongmei Zhao, Shichun Zhang,  
2446 Guangyi Yang, Mengduo Zhang, Shengjin Xie: Emission input data for  
2447 WRF-CMAQ, Zenodo [data set], <https://doi.org/10.5281/zenodo.7932430>, 2023f.

2448 Gao, C., Xiu, A., Zhang, X., Tong, Q., Zhao, H., Zhang, S., Yang, G., Zhang, M., Xie, S.: Emission  
2449 input data for WRF-Chem, Zenodo [data set],  
2450 <https://doi.org/10.5281/zenodo.7932734>, 2023g.

2451 Gao, C., Xiu, A., Zhang, X., Tong, Q., Zhao, H., Zhang, S., Yang, G., Zhang, M., Xie, S.: Emission  
2452 input data for WRF-CHMIERE, Zenodo [data set],  
2453 <https://doi.org/10.5281/zenodo.7931614>, 2023h.

2454 Gao, C., Xiu, A., Zhang, X., Tong, Q., Zhao, H., Zhang, S., Yang, G., Zhang, M., Xie, S.: Data  
2455 used to create figures and tables in the GMD manuscript "Inter-comparison of  
2456 multiple two-way coupled meteorology and air quality models (WRF v4.1.1-CMAQ  
2457 v5.3.1, WRF-Chem v4.1.1 and WRF v3.7.1-CHIMERE v2020r1) in eastern China",  
2458 Zenodo [data set], <https://doi.org/10.5281/zenodo.7750907>, 2023i.

2459 Gao, J., Woodward, A., Vardoulakis, S., Kovats, S., Wilkinson, P., Li, L., Xu, L., Li, J., Yang, J., and  
2460 Cao, L.: Haze, public health and mitigation measures in China: A review of the current evidence  
2461 for further policy response, *Sci. Total Environ.*, 578, 148–157,  
2462 <https://doi.org/10.1016/j.scitotenv.2016.10.231>, 2017.

2463 Gao, M., Han, Z., Liu, Z., Li, M., Xin, J., Tao, Z., Li, J., Kang, J. E., Huang, K., Dong, X., Zhuang, B.,  
2464 Li, S., Ge, B., Wu, Q., Cheng, Y., Wang, Y., Lee, H. J., Kim, C. H., Fu, J. S., Wang, T., Chin, M.,  
2465 Woo, J. H., Zhang, Q., Wang, Z., and Carmichael, G. R.: Air quality and climate change, Topic 3  
2466 of the Model Inter-Comparison Study for Asia Phase III (MICS-Asia III)- Part 1: Overview and  
2467 model evaluation, *Atmos. Chem. Phys.*, 18, 4859–4884,  
2468 <https://doi.org/10.5194/acp-18-4859-2018>, 2018.

2469 Gao, M., Han, Z., Tao, Z., Li, J., Kang, J.-E., Huang, K., Dong, X., Zhuang, B., Li, S., and Ge, B.: Air  
2470 quality and climate change, Topic 3 of the Model Inter-Comparison Study for Asia Phase III  
2471 (MICS-Asia III)–Part 2: aerosol radiative effects and aerosol feedbacks, *Atmos. Chem. Phys.*, 20,  
2472 1147–1161, <https://doi.org/10.5194/acp-20-1147-2020>, 2020.

2473 Gao, Y., Zhang, M., Liu, Z., Wang, L., Wang, P., Xia, X., Tao, M., and Zhu, L.: Modeling the  
2474 feedback between aerosol and meteorological variables in the atmospheric boundary layer during  
2475 a severe fog-haze event over the North China Plain., *Atmos. Chem. Phys.*, 15, 4279–4295,  
2476 <https://doi.org/10.5194/acp-15-4279-2015>, 2015.

2477 Ge, B., Itahashi, S., Sato, K., Xu, D., Wang, J., Fan, F., Tan, Q., Fu, J. S., Wang, X., and Yamaji, K.:  
2478 Model Inter-Comparison Study for Asia (MICS-Asia) phase III: multimodel comparison of  
2479 reactive nitrogen deposition over China, *Atmos. Chem. Phys.*, 20, 10587–10610,  
2480 <https://doi.org/10.5194/acp-20-10587-2020>, 2020.

2481 Geng, G., Zheng, Y., Zhang, Q., Xue, T., Zhao, H., Tong, D., Zheng, B., Li, M., Liu, F., and Hong, C.:  
2482 Drivers of PM<sub>2.5</sub> air pollution deaths in China 2002–2017, *Nat. Geosci.*, 14, 645–650,  
2483 <https://doi.org/10.1038/s41561-021-00792-3>, 2021.

2484 Gillies, S., Ward, B., and Petersen, A. S.: Rasterio: Geospatial raster I/O for Python programmers,  
2485 URL <https://github.com/mapbox/rasterio>, 2013.

2486 Govardhan, G. R., Nanjundiah, R. S., Sathesh, S. K., Moorthy, K. K., and Takemura, T.:  
2487 Inter-comparison and performance evaluation of chemistry transport models over Indian region,  
2488 *Atmos. Environ.*, 125, 486–504, <https://doi.org/10.1016/j.atmosenv.2015.10.065>, 2016.

2489 Grell, G. and Baklanov, A.: Integrated modeling for forecasting weather and air quality: A call for  
2490 fully coupled approaches, *Atmos. Environ.*, 45, 6845–6851,  
2491 <https://doi.org/10.1016/j.atmosenv.2011.01.017>, 2011.

2492 Grell, G. A., Peckham, S. E., Schmitz, R., McKeen, S. A., Frost, G., Skamarock, W. C., and Eder, B.:  
2493 Fully coupled “online” chemistry within the WRF model, *Atmos. Environ.*, 39, 6957–6975,  
2494 <https://doi.org/10.1016/j.atmosenv.2005.04.027>, 2005.

2495 Guo, J., Li, Y., Cohen, J. B., Li, J., Chen, D., Xu, H., Liu, L., Yin, J., Hu, K., and Zhai, P.: Shift in the  
2496 temporal trend of boundary layer height in China using long-term (1979-2016) radiosonde data,  
2497 *Geophys. Res. Lett.*, 46, 6080–6089, <https://doi.org/10.1029/2019GL082666>, 2019.

2498 He, K., Huo, H., and Zhang, Q.: Urban air pollution in China: current status, characteristics, and  
2499 progress, *Annu. Rev. Environ. Resour.*, 27, 397,  
2500 <https://doi.org/10.1146/annurev.energy.27.122001.083421>, 2002.

2501 Hogrefe, C., Bash, J. O., Pleim, J. E., Schwede, D. B., Gilliam, R. C., Foley, K. M., Appel, K. W., and  
2502 Mathur, R.: An Analysis of CMAQ Gas Phase Dry Deposition over North America Through  
2503 Grid-Scale and Land-Use Specific Diagnostics in the Context of AQMEII4, *Atmos. Chem. Phys.*  
2504 *Discuss.*, 1–52, <https://doi.org/10.5194/acp-2023-10>, 2023.

2505 Hong, C., Zhang, Q., Zhang, Y., Tang, Y., Tong, D., and He, K.: Multi-year downscaling application  
2506 of two-way coupled WRF v3.4 and CMAQ v5.0.2 over east Asia for regional climate and air  
2507 quality modeling: model evaluation and aerosol direct effects., *Geosci. Model Dev.*, 10, 2447–  
2508 2470, <https://doi.org/10.5194/gmd-10-2447-2017>, 2017.

2509 Huang, D. and Gao, S.: Impact of different reanalysis data on WRF dynamical downscaling over  
2510 China, *Atmos. Res.*, 200, 25–35, <https://doi.org/10.1016/j.atmosres.2017.09.017>, 2018.

2511 Huang, X., Song, Y., Li, M., Li, J., Huo, Q., Cai, X., Zhu, T., Hu, M., and Zhang, H.: A  
2512 high-resolution ammonia emission inventory in China, *Global Biogeochem. Cycles*, 26,  
2513 <https://doi.org/10.1029/2011GB004161>, 2012.

2514 Iacono, M. J., Delamere, J. S., Mlawer, E. J., Shephard, M. W., Clough, S. A., and Collins, W. D.:  
2515 Radiative forcing by long - lived greenhouse gases: Calculations with the AER radiative transfer  
2516 models, *J. Geophys. Res. Atmos.*, 113, <https://doi.org/10.1029/2008JD009944>, 2008.

2517 Im, U., Bianconi, R., Solazzo, E., Kioutsioukis, I., Badia, A., Balzarini, A., Baró, R., Bellasio, R.,

2518 Brunner, D., and Chemel, C.: Evaluation of operational on-line-coupled regional air quality  
2519 models over Europe and North America in the context of AQMEII phase 2. Part I: Ozone, Atmos.  
2520 Environ., 115, 404–420, <https://doi.org/10.1016/j.atmosenv.2014.09.042>, 2015a.

2521 Im, U., Bianconi, R., Solazzo, E., Kioutsioukis, I., Badia, A., Balzarini, A., Baró, R., Bellasio, R.,  
2522 Brunner, D., and Chemel, C.: Evaluation of operational online-coupled regional air quality  
2523 models over Europe and North America in the context of AQMEII phase 2. Part II: Particulate  
2524 matter, Atmos. Environ., 115, 421–441, <https://doi.org/10.1016/j.atmosenv.2014.08.072>, 2015b.

2525 IPCC: Climate change 2007: Synthesis Report. Contribution of Working Groups I, II and III to the  
2526 Fourth Assessment Report of the Intergovernmental Panel on Climate Change, 2007.

2527 IPCC: Climate change 2021: Synthesis Report. Contribution of Working Groups I, II and III to the  
2528 Sixth Assessment Report of the Intergovernmental Panel on Climate Change., 2021.

2529 Itahashi, S., Ge, B., Sato, K., Fu, J. S., Wang, X., Yamaji, K., Nagashima, T., Li, J., Kajino, M., and  
2530 Liao, H.: MICS-Asia III: overview of model intercomparison and evaluation of acid deposition  
2531 over Asia, Atmos. Chem. Phys., 20, 2667–2693, <https://doi.org/10.5194/acp-20-2667-2020>,  
2532 2020.

2533 Jacobson, M. Z.: Developing, coupling, and applying a gas, aerosol, transport, and radiation model to  
2534 study urban and regional air pollution, 1994.

2535 Jacobson, M. Z.: Development and application of a new air pollution modeling system—Part III.  
2536 Aerosol-phase simulations, Atmos. Environ., 31, 587–608,  
2537 [https://doi.org/10.1016/S1352-2310\(96\)00201-4](https://doi.org/10.1016/S1352-2310(96)00201-4), 1997.

2538 Jacobson, M. Z.: Studying the effects of aerosols on vertical photolysis rate coefficient and  
2539 temperature profiles over an urban airshed, J. Geophys. Res. Atmos., 103, 10593–10604,  
2540 <https://doi.org/10.1029/98jd00287>, 1998.

2541 Jacobson, M. Z.: GATOR-GCMM: A global-through urban-scale air pollution and weather forecast  
2542 model: 1. Model design and treatment of subgrid soil, vegetation, roads, rooftops, water, sea ice,  
2543 and snow, J. Geophys. Res. Atmos., 106, 5385–5401, <https://doi.org/10.1029/2000JD900560>,  
2544 2001.

2545 Jacobson, M. Z.: Analysis of aerosol interactions with numerical techniques for solving coagulation,  
2546 nucleation, condensation, dissolution, and reversible chemistry among multiple size distributions,  
2547 J. Geophys. Res. Atmos., 107, AAC-2, <https://doi.org/10.1029/2001JD002044>, 2002.

2548 Keita, S. A., Girard, E., Raut, J.-C., Leriche, M., Blanchet, J.-P., Pelon, J., Onishi, T., and Cirisan, A.:  
2549 A new parameterization of ice heterogeneous nucleation coupled to aerosol chemistry in  
2550 WRF-Chem model version 3.5.1: evaluation through ISDAC measurements, Geosci. Model Dev.,  
2551 13, 5737–5755, <https://doi.org/10.5194/gmd-13-5737-2020>, 2020.

2552 Klein, S. A., McCoy, R. B., Morrison, H., Ackerman, A. S., Avramov, A., Boer, G. de, Chen, M.,  
2553 Cole, J. N. S., Del Genio, A. D., and Falk, M.: Intercomparison of model simulations of mixed-  
2554 phase clouds observed during the ARM Mixed-Phase Arctic Cloud Experiment. I: Single-layer  
2555 cloud, Q. J. R. Meteorol. Soc. A J. Atmos. Sci. Appl. Meteorol. Phys. Oceanogr., 135, 979–1002,  
2556 <https://doi.org/10.1002/qj.416>, 2009.

2557 Knote, C., Tuccella, P., Curci, G., Emmons, L., Orlando, J. J., Madronich, S., Baró, R.,  
2558 Jiménez-Guerrero, P., Lueken, D., and Hogrefe, C.: Influence of the choice of gas-phase

2559 mechanism on predictions of key gaseous pollutants during the AQMEII phase-2  
 2560 intercomparison, *Atmos. Environ.*, 115, 553–568,  
 2561 <https://doi.org/10.1016/j.atmosenv.2014.11.066>, 2015.

2562 Kong, L., Tang, X., Zhu, J., Wang, Z., Fu, J. S., Wang, X., Itahashi, S., Yamaji, K., Nagashima, T.,  
 2563 and Lee, H.-J.: Evaluation and uncertainty investigation of the NO<sub>2</sub>, CO and NH<sub>3</sub> modeling over  
 2564 China under the framework of MICS-Asia III, *Atmos. Chem. Phys.*, 20, 181–202,  
 2565 <https://doi.org/10.5194/acp-20-181-2020>, 2020.

2566 Li, J., Nagashima, T., Kong, L., Ge, B., Yamaji, K., Fu, J. S., Wang, X., Fan, Q., Itahashi, S., and  
 2567 Hyo-Jung, L.: Model evaluation and intercomparison of surface-level ozone and relevant species  
 2568 in East Asia in the context of MICS-Asia Phase III–Part 1: Overview, *Atmos. Chem. Phys.*, 19,  
 2569 12993–13015, <https://doi.org/10.5194/acp-19-12993-2019>, 2019.

2570 Li, M., Liu, H., Geng, G., Hong, C., Liu, F., Song, Y., Tong, D., Zheng, B., Cui, H., and Man, H.:  
 2571 Anthropogenic emission inventories in China: a review, *Natl. Sci. Rev.*, 4, 834–866,  
 2572 <https://doi.org/10.1093/nsr/nwx150>, 2017.

2573 Liu, Z., Wang, Y., Hu, B., Lu, K., Tang, G., Ji, D., Yang, X., Gao, W., Xie, Y., and Liu, J.:  
 2574 Elucidating the quantitative characterization of atmospheric oxidation capacity in Beijing, China,  
 2575 *Sci. Total Environ.*, 771, 145306, <https://doi.org/10.1016/j.scitotenv.2021.145306>, 2021.

2576 Ma, Y., Jin, Y., Zhang, M., Gong, W., Hong, J., Jin, S., Shi, Y., Zhang, Y., and Liu, B.: Aerosol  
 2577 optical properties of haze episodes in eastern China based on remote-sensing observations and  
 2578 WRF-Chem simulations, *Sci. Total Environ.*, 757, 143784,  
 2579 <https://doi.org/10.1016/j.scitotenv.2020.143784>, 2021.

2580 Mailler, S., Menut, L., Khvorostyanov, D., Valari, M., Couvidat, F., Siour, G., Turquety, S., Briant, R.,  
 2581 Tuccella, P., and Bessagnet, B.: CHIMERE-2017: from urban to hemispheric chemistry-transport  
 2582 modeling, *Geosci. Model Dev.*, 10, 2397–2423, <https://doi.org/10.5194/gmd-10-2397-2017>,  
 2583 2017.

2584 Makar, P. A., Gong, W., Milbrandt, J., Hogrefe, C., Zhang, Y., Curci, G., Žabkar, R., Im, U., Balzarini,  
 2585 A., Baró, R., Bianconi, R., Cheung, P., Forkel, R., Gravel, S., Hirtl, M., Honzak, L., Hou, A.,  
 2586 Jiménez-Guerrero, P., Langer, M., Moran, M. D., Pabla, B., Pérez, J. L., Pirovano, G., San José,  
 2587 R., Tuccella, P., Werhahn, J., Zhang, J., and Galmarini, S.: Feedbacks between air pollution and  
 2588 weather, Part 1: Effects on weather, *Atmos. Environ.*, 115, 442–469,  
 2589 <https://doi.org/10.1016/j.atmosenv.2014.12.003>, 2015a.

2590 Makar, P. A., Gong, W., Hogrefe, C., Zhang, Y., Curci, G., Žabkar, R., Milbrandt, J., Im, U., Balzarini,  
 2591 A., Baró, R., Bianconi, R., Cheung, P., Forkel, R., Gravel, S., Hirtl, M., Honzak, L., Hou, A.,  
 2592 Jiménez-Guerrero, P., Langer, M., Moran, M. D., Pabla, B., Pérez, J. L., Pirovano, G., San José,  
 2593 R., Tuccella, P., Werhahn, J., Zhang, J., and Galmarini, S.: Feedbacks between air pollution and  
 2594 weather, part 2: Effects on chemistry, *Atmos. Environ.*, 115, 499–526,  
 2595 <https://doi.org/10.1016/j.atmosenv.2014.10.021>, 2015b.

2596 Menut, L., Bessagnet, B., Khvorostyanov, D., Beekmann, M., Blond, N., Colette, A., Coll, I., Curci,  
 2597 G., Foret, G., and Hodzic, A.: CHIMERE 2013: a model for regional atmospheric composition  
 2598 modelling, *Geosci. Model Dev.*, 6, 981–1028, <https://doi.org/10.5194/gmd-6-981-2013>, 2013.

2599 Qu, Y., Voulgarakis, A., Wang, T., Kasoar, M., Wells, C., Yuan, C., Varma, S., and Mansfield, L.: A

2600 study of the effect of aerosols on surface ozone through meteorology feedbacks over China,  
 2601 Atmos. Chem. Phys., 21, 5705–5718, <https://doi.org/10.5194/acp-21-5705-2021>, 2021.  
 2602 Rosenfeld, D., Andreae, M. O., Asmi, A., Chin, M., de Leeuw, G., Donovan, D. P., Kahn, R., Kinne,  
 2603 S., Kivekäs, N., and Kulmala, M.: Global observations of aerosol-cloud-precipitation-climate  
 2604 interactions, Rev. Geophys., 52, 750–808, <https://doi.org/10.1002/2013RG000441>, 2014.  
 2605 Safieddine, S., Boynard, A., Coheur, P.-F., Hurtmans, D., Pfister, G., Quennehen, B., Thomas, J. L.,  
 2606 Raut, J.-C., Law, K. S., and Klimont, Z.: Summertime tropospheric ozone assessment over the  
 2607 Mediterranean region using the thermal infrared IASI/MetOp sounder and the WRF-Chem model,  
 2608 Atmos. Chem. Phys., 14, 10119–10131, <https://doi.org/10.5194/acp-14-10119-2014>, 2014.  
 2609 Stein, O., Schultz, M. G., Bouarar, I., Clark, H., Huijnen, V., Gaudel, A., George, M., and Clerbaux,  
 2610 C.: On the wintertime low bias of Northern Hemisphere carbon monoxide found in global model  
 2611 simulations, Atmos. Chem. Phys., 14, 9295–9316, <https://doi.org/10.5194/acp-14-9295-2014>,  
 2612 2014.  
 2613 Tang, W., Yang, K., Qin, J., Li, X., and Niu, X.: A 16-year dataset (2000–2015) of high-resolution (3  
 2614 h, 10 km) global surface solar radiation, Earth Syst. Sci. Data, 11, 1905–1915,  
 2615 <https://doi.org/10.5194/essd-11-1905-2019>, 2019.  
 2616 Tuccella, P., Menut, L., Briant, R., Deroubaix, A., Khvorostyanov, D., Mailler, S., Siour, G., and  
 2617 Turquety, S.: Implementation of aerosol-cloud interaction within WRF-CHIMERE online  
 2618 coupled model: Evaluation and investigation of the indirect radiative effect from anthropogenic  
 2619 emission reduction on the Benelux Union, Atmosphere (Basel), 10,  
 2620 <https://doi.org/10.3390/atmos10010020>, 2019.  
 2621 Wallace, J. M. and Hobbs, P. V.: Atmospheric science: an introductory survey, Elsevier, 2006.  
 2622 Wang, K., Zhang, Y., Yahya, K., Wu, S.-Y., and Grell, G.: Implementation and initial application of  
 2623 new chemistry-aerosol options in WRF/Chem for simulating secondary organic aerosols and  
 2624 aerosol indirect effects for regional air quality, Atmos. Environ., 115, 716–732,  
 2625 <https://doi.org/10.1016/j.atmosenv.2014.12.007>, 2015.  
 2626 Wang, K., Zhang, Y., Zhang, X., Fan, J., Leung, L. R., Zheng, B., Zhang, Q., and He, K.: Fine-scale  
 2627 application of WRF-CAM5 during a dust storm episode over East Asia: Sensitivity to grid  
 2628 resolutions and aerosol activation parameterizations, Atmos. Environ., 176, 1–20,  
 2629 <https://doi.org/10.1016/j.atmosenv.2017.12.014>, 2018.  
 2630 Wang, K., Zhang, Y., Yu, S., Wong, D. C., Pleim, J., Mathur, R., Kelly, J. T., and Bell, M.: A  
 2631 comparative study of two-way and offline coupled WRF v3.4 and CMAQ v5.0.2 over the  
 2632 contiguous US: performance evaluation and impacts of chemistry–meteorology feedbacks on air  
 2633 quality, Geosci. Model Dev., 14, 7189–7221, <https://doi.org/10.5194/gmd-14-7189-2021>, 2021.  
 2634 Wang, K., Gao, C., Wu, K., Liu, K., Wang, H., Dan, M., Ji, X., and Tong, Q.: ISAT v2. 0: an  
 2635 integrated tool for nested-domain configurations and model-ready emission inventories for  
 2636 WRF-AQM, Geosci. Model Dev., 16, 1961–1973, <https://doi.org/10.5194/gmd-16-1961-2023>,  
 2637 2023.  
 2638 Wang, S. and Hao, J.: Air quality management in China: Issues, challenges, and options, J. Environ.  
 2639 Sci., 24, 2–13, [https://doi.org/10.1016/S1001-0742\(11\)60724-9](https://doi.org/10.1016/S1001-0742(11)60724-9), 2012.  
 2640 Wang, Z., Wang, Z., Li, J., Zheng, H., Yan, P., and Li, J.: Development of a meteorology-chemistry



2641 two-way coupled numerical model (WRF-NAQPMS) and its application in a severe autumn haze  
 2642 simulation over the Beijing-Tianjin-Hebei area, China. *Clim. Environ. Res.*, 19, 153–163,  
 2643 <https://doi.org/10.3878/j.issn.1006-9585.2014.13231>, 2014.

2644 Wiedinmyer, C., Akagi, S. K., Yokelson, R. J., Emmons, L. K., Al-Saadi, J. A., Orlando, J. J., and  
 2645 Soja, A. J.: The Fire INventory from NCAR (FINN): A high resolution global model to estimate  
 2646 the emissions from open burning, *Geosci. Model Dev.*, 4, 625–641,  
 2647 <https://doi.org/10.5194/gmd-4-625-2011>, 2011.

2648 Wong, D. C., Pleim, J., Mathur, R., Binkowski, F., Otte, T., Gilliam, R., Pouliot, G., Xiu, A., Young, J.  
 2649 O., and Kang, D.: WRF-CMAQ two-way coupled system with aerosol feedback: software  
 2650 development and preliminary results, *Geosci. Model Dev.*, 5, 299–312,  
 2651 <https://doi.org/10.5194/gmd-5-299-2012>, 2012.

2652 Xing, J., Mathur, R., Pleim, J., Hogrefe, C., Wang, J., Gan, C.-M., Sarwar, G., Wong, D. C., and  
 2653 McKeen, S.: Representing the effects of stratosphere–troposphere exchange on 3-D O<sub>3</sub>  
 2654 distributions in chemistry transport models using a potential vorticity-based parameterization,  
 2655 *Atmos. Chem. Phys.*, 16, 10865–10877, <https://doi.org/10.5194/acp-16-10865-2016>, 2016.

2656 Xing, J., Wang, J., Mathur, R., Wang, S., Sarwar, G., Pleim, J., Hogrefe, C., Zhang, Y., Jiang, J., and  
 2657 Wong, D. C.: Impacts of aerosol direct effects on tropospheric ozone through changes in  
 2658 atmospheric dynamics and photolysis rates, *Atmos. Chem. Phys.*, 17, 9869–9883,  
 2659 <https://doi.org/10.5194/acp-17-9869-2017>, 2017.

2660 Xu, K.-M. and Randall, D. A.: A semiempirical cloudiness parameterization for use in climate models,  
 2661 *J. Atmos. Sci.*, 53, 3084–3102,  
 2662 [https://doi.org/10.1175/1520-0469\(1996\)053<3084:ASCPFU>2.0.CO;2](https://doi.org/10.1175/1520-0469(1996)053<3084:ASCPFU>2.0.CO;2), 1996.

2663 Zaveri, R. A., Easter, R. C., Fast, J. D., and Peters, L. K.: Model for simulating aerosol interactions  
 2664 and chemistry (MOSAIC), *J. Geophys. Res. Atmos.*, 113, <https://doi.org/10.1029/2007JD008782>,  
 2665 2008.

2666 Zhang, X., Wu, Y., Liu, X., Reis, S., Jin, J., Dragosits, U., Van Damme, M., Clarisse, L., Whitburn, S.,  
 2667 and Coheur, P.-F.: Ammonia emissions may be substantially underestimated in China, *Environ.*  
 2668 *Sci. Technol.*, 51, 12089–12096, <https://doi.org/10.1021/acs.est.7b02171>, 2017.

2669 Zhang, Y.: Online-coupled meteorology and chemistry models: history, current status, and outlook,  
 2670 *Atmos. Chem. Phys.*, 8, 2895–2932, <https://doi.org/10.5194/acp-8-2895-2008>, 2008.

2671 Zhang, Y., Zhang, X., Wang, K., Zhang, Q., Duan, F., and He, K.: Application of WRF/Chem over  
 2672 East Asia: Part II. Model improvement and sensitivity simulations, *Atmos. Environ.*, 124, 301–  
 2673 320, <https://doi.org/10.1016/j.atmosenv.2015.07.023>, 2016.

2674 Zhao, B., Liou, K., Gu, Y., Li, Q., Jiang, J. H., Su, H., He, C., Tseng, H.-L. R., Wang, S., and Liu, R.:  
 2675 Enhanced PM<sub>2.5</sub> pollution in China due to aerosol-cloud interactions, *Sci. Rep.*, 7, 1–11,  
 2676 <https://doi.org/10.1038/s41598-017-04096-8>, 2017.

2677 Zhou, C., Zhang, X., Gong, S., Wang, Y., and Xue, M.: Improving aerosol interaction with clouds and  
 2678 precipitation in a regional chemical weather modeling system, 16, 145–160,  
 2679 <https://doi.org/10.5194/acp-16-145-2016>, 2016.

2680 Zhu, J., Wang, S., Wang, H., Jing, S., Lou, S., Saiz-Lopez, A., and Zhou, B.: Observationally  
 2681 constrained modeling of atmospheric oxidation capacity and photochemical reactivity in

2682 Shanghai, China, Atmos. Chem. Phys., 20, 1217–1232,  
2683 <https://doi.org/10.5194/acp-20-1217-2020>, 2020.  
2684 Zhu, J., Chen, L., Liao, H., Yang, H., Yang, Y., and Yue, X.: Enhanced PM<sub>2.5</sub> decreases and O<sub>3</sub>  
2685 increases in China during COVID-19 lockdown by aerosol-radiation feedback, Geophys. Res.  
2686 Lett., 48, 1–11, <https://doi.org/10.1029/2020GL090260>, 2021.

1 Supplement

2 1 Evaluations of other meteorological variables

3 1.1 Ground-based observations

4 For Q2, RMSEs between WRF-CMAQ, WRF-Chem, and WRF-CHIMERE  
5 simulations and surface observation were consistently below  $3 \text{ g kg}^{-1}$ , as illustrated in  
6 Table S3 and Fig. S2. Most models exhibited a tendency to underestimate annual and  
7 seasonal Q2, with MBs ranging from  $-0.57$  to  $-0.18 \text{ g kg}^{-1}$  and  $-1.16$  to  $+0.20 \text{ g kg}^{-1}$   
8 in WRF-Chem and WRF-CHIMERE, respectively. The more obvious underestimations  
9 appeared in summer. In the MICS-Asia III project, Gao et al. (2018) reported that all  
10 the seven included two-way coupled models produced slightly positive values for Q2  
11 during January 2010 over the North China Plain, In contrast to simulations without  
12 enabling aerosol feedbacks, the negative biases in annual and seasonal Q2 simulated by  
13 WRF-CMAQ\_ARI and WRF-CHIMERE\_ARI were amplified, and the WRF-  
14 CMAQ\_ARI simulations exhibited bigger negative biases (see Fig. 3 and Table S3).  
15 The changes in annual, summer, and autumn MBs for WRF-Chem\_ARI were consistent  
16 with the trend of WRF-CMAQ\_ARI, except for spring and winter.

17 The annual and seasonal correlation coefficients of precipitation were 0.56–0.69,  
18 0.46–0.63, and 0.25–0.55 for WRF-CMAQ, WRF-Chem, and WRF-CHIMERE,  
19 respectively (Table S3 and Fig. S5). All simulated results presented the highest  
20 correlations in winter and the lowest in summer, and the possible reasons are due to the  
21 much more convective activities in summertime, which are not accurately captured in  
22 all coupled models, WRF-CMAQ and WRF-CHIMERE exhibited underestimation, and  
23 overestimation in annual and seasonal precipitation, respectively. At the annual and  
24 seasonal scales, WRF-Chem and WRF-CHIMERE overestimated the daily  
25 precipitation magnitude by more than  $1 \text{ mm day}^{-1}$ , and WRF-CMAQ underestimated it  
26 by approximately  $0.5 \text{ mm day}^{-1}$ . A similar conclusion was obtained for North America  
27 during 2010, with the magnitude of precipitation MBs being higher in WRF-Chem  
28 compared to WRF-CMAQ (refer to Fig. 11 in Makar et al., 2015). The largest  
29 precipitation MBs simulated by the three models occurred in summer and varied from  
30  $-0.70$  to  $+1.39 \text{ mm day}^{-1}$ . The RMSE was highest in WRF-CHIMERE, followed by  
31 WRF-Chem, and WRF-CMAQ, and all models had the largest ( $> 10 \text{ mm day}^{-1}$ ) and  
32 smallest (approximately  $2.5 \text{ mm day}^{-1}$ ) values in summer and winter, respectively.  
33 Considering the ARI effects, WRF-CMAQ\_ARI simulations amplified the  
34 underestimations of annual and seasonal precipitation in eastern China. In contrast,  
35 WRF-Chem ARI (except for autumn) and WRF-CHIMERE ARI simulations  
36 mitigated the overestimations of precipitation. The effects of ARI on summer MBs were  
37 larger in all three coupled models compared to other seasons. When ACI effects were  
38 further included, WRF-Chem\_BOTH demonstrated only marginal improvement in  
39 precipitation overestimation compared to WRF-Chem\_NO, while WRF-  
40 CHIMERE\_BOTH gave out certain enhancement of precipitation overestimation. This  
41 can be interpreted as follows: WRF-CHIMERE has the ability to simulate the activation  
42 of aerosol particles into cloud ice via heterogeneous ice nucleation and homogeneous  
43 freezing, whereas WRF-Chem jacks this capability.

44 Overall, the PBLH was not well simulated by any of the three coupled models.

Deleted: less than

Formatted: Not Superscript/ Subscript

Deleted: (...able S3 and Fig. S2)

Deleted: tended to ...nderestimate annual and seasonal Q2  
(... with MBs ranging from  $-0.57$  to  $-0.18 \text{ g kg}^{-1}$  and  $-1.16$   
to  $+0.20 \text{ g kg}^{-1}$  in WRF-Chem and WRF-CHIMERE,  
respectively), ... The more obvious and  
the ...nderestimations were most significant ...ppeared in  
summer. However, ...n the MICS-Asia III project, Gao et al.  
(2018) reported that all the seven multiple...ncluded ...wo-  
way coupled models produced slightly positive values for Q2  
during January 2010 over the North China Plain in the MICS-  
Asia III project (Gao et al., 2018)... Compared with

Deleted: that did not have...ithout enabling aerosol  
feedbacks enabled... the negative biases in annual and  
Q2 simulated by WRF-CMAQ\_ARI and WRF-  
CHIMERE\_ARI were increased ...mplifiedthe negative  
biases of annual and seasonal Q2... with ...nd the  
WRF-CMAQ\_ARI simulations being ...xhibitedmore  
significant

Deleted: had ...resented the highest correlations in winter  
and the lowest in summer, because...and the possible reasons  
are due to the much more convective activities in  
summertimey was enhanced in summer

Deleted: and ...hich are not accurately captured in all  
coupled modelsthe models *struggled* to effectively capture  
this... WRF-CMAQ and WRF-CHIMERE (WRF-Chem  
except for autumn) ...xhibited underestimation...and  
overestimation ined...annual and seasonal precipitation,  
respectively. At the annual and seasonal scales, WRF-Chem  
and WRF-CHIMERE overestimated the magnitude of ...aily  
precipitation magnitude by more than  $1 \text{ mm day}^{-1}$ ,  
while ...nd WRF-CMAQ underestimated it by approximately  
 $0.5 \text{ mm day}^{-1}$ . A similar picture ...onclusion emerged ...as  
obtained for North America during 2010, whereby ...ith the  
magnitude of precipitation MBs was ...eing higher in WRF-  
Chem than ...ompared toin...WRF-CMAQ (see ...efer to  
Fig. 11 in Makar et al., 2015). The largest precipitation MBs  
simulated by the three models occurred in summer and  
ranged ...aried from  $-0.70$  to  $+1.39 \text{ mm day}^{-1}$ . The RMSE  
was highest in WRF-CHIMERE, followed by WRF-Chem,  
and WRF-CMAQ, and all models had the largest ( $> 10 \text{ mm}$   
 $\text{day}^{-1}$ ) and smallest (approximately  $2.5 \text{ mm day}^{-1}$ ) values in

319 which may be a result of the adoption of low resolution sounding data in evaluations,  
320 (Brunner et al., 2015) and the different settings of Richardson number thresholds in the  
321 calculation of observed PBLH (Guo et al., 2016). At 08:00 and 20:00 local time (LT),  
322 the simulated PBLHs in WRF-CMAQ have lower correlations only ranging from 0.21  
323 to 0.40, and largest negative MBs varying from -400 to -133 m. These poor  
324 performances were mainly caused by: 1) different configurations of the PBL scheme  
325 were employed in this study, namely, WRF-CMAQ adopted the ACM2 scheme with  
326 hybrid local-nonlocal closure, while WRF-Chem and WRF-CHIMERE adopted the  
327 YSU scheme with non-local closure (Table 1); 2) Richardson number threshold was set  
328 to different values for unstable atmospheric conditions, i.e., the YSU and ACM2  
329 schemes using the thresholds of 0 and 0.25, respectively (Xie et al., 2012); 3) different  
330 to the YSU scheme, the ACM2 scheme considers the entrainment layer in the PBLH  
331 calculations (Xie et al., 2012).

332 Meanwhile, all correlations of PBLH simulated by the three coupled models at  
333 20:00 LT (R = 0.3-0.4) were better than those at 08:00 LT (R = 0.1-0.2), which  
334 indicated that the PBL schemes in these model were able to calculate PLBH after PBL  
335 collapsing a little better than before PBL developing and more observation with better  
336 spatiotemporal resolutions are needed to further evaluate the models' performance. In  
337 addition, the RMSEs of PBLH in autumn (369.89-388.79 m) and winter (347.48-  
338 392.38 m) were smaller than those in spring (405.61-622.37 m) and summer (348.80-  
339 570.16 m) for all three models.

340 As shown in Fig. 3 and Table S3, the changes of MB and RMSE of simulated  
341 PBLH induced by the effects of aerosol feedbacks were greater than those of R.  
342 Meanwhile, the MBs were further analyzed. For WRF-CMAQ, ARI effects induced an  
343 increase (-1.93 m) and decrease (+6.66 m) in the annual underestimations of PBLH at  
344 8:00 and 20:00 LT, respectively (Table S3). The negative MBs for WRF-Chem\_ARI  
345 and WRF-Chem\_BOTH showed an enhancement (08:00 LT: -25.25 m, 20:00 LT:  
346 -25.60 m) and reduction (08:00 LT: +19.65 m, 20:00 LT: +14.09 m) compared to those  
347 for WRF-Chem\_NO and WRF-Chem\_ARI, respectively. Both the ARI (-6.17 and  
348 -3.34 m) and ACI (-0.65 and -1.11 m) effects further underestimated annual PBLH at  
349 08:00 and 20:00 LT for WRF-CHIMERE. Note that the variations in MBs induced by  
350 aerosol feedbacks for the three coupled models at the annual scale were similar to those  
351 at the seasonal scale.

## 352 1.2 Satellite-borne observations

353 As indicated in Table 3, the three coupled models demonstrated good performance  
354 in simulating the shortwave radiation at the top of the atmosphere (SRTOA) and  
355 longwave radiation at the top of the atmosphere (LRTOA). The annual MBs for SRTOA  
356 and LRTOA are ranging from -4.40 to +5.42 W m<sup>-2</sup> and -2.14 to 0.66 W m<sup>-2</sup>,  
357 respectively. Seasonal SRTOA was also well simulated by all three models, especially  
358 in winter (Figure S10). For seasonal LRTOA, the WRF-CMAQ and WRF-Chem model  
359 performances were better than that of WRF-CHIMERE for all seasons except autumn  
360 (Figure S11). No matter whether ARI and/or ACI effects were enabled or not,  
361 simulations by WRF-CMAQ exhibited negative MBs in all seasons, and WRF-

**Deleted:** PBLH data were not well reproduced by any of the three coupled models..., which may be a result of the low resolution of the sounding data ...Brunner et al., 2015) and different settings of Richardson number thresholds in the calculation calculating ...f observed PBLH (Guo et al., 2016). At 08:00 and 20:00 local time (LT), the simulated annual and seasonal...PBLHs in WRF-CMAQ simulated by WRF-CMAQ had ...ave the highest ...ower correlations only (R = ...anging from 0.21 ...o 0.40)...and largest negative MBs (ranging...arying ...rom -400 to -133 m)... The ...hese poor performancesperformance...werewas...mainly caused 1) different configurations of the PBL scheme were employed in this study, namely, WRF-CMAQ adopted the ACM2 scheme with hybrid local-nonlocal closure, while WRF-Chem and WRF-CHIMERE adopted the YSU scheme with non-local closure (Table 1); 2) the settings of the ...richardson number threshold ...varied owing...as set ...o the ...iff...

**Deleted:** t...he ACM2 scheme considers the entrainment layer in the PBLH calculations was further considered in the ACM2 scheme for PBLH calculations ...Xie et al., 2012

**Deleted:** the ...hree coupled models at 20:00 LT (R = 0.3-0.4) were better than those at 08:00 LT (R = 0.1-0.2), ..., which indicated that the PBL schemes in these model were able to calculate PLBH after PBL collapsing a little better than before PBL developing and more observation with better spatiotemporal resolutions are needed to further evaluate the models' performance.because the gradient of the rapid

**Deleted:** the effects of aerosol feedbacks on MB and RMSE were larger than that on R

**Deleted:** Considering that the MBs of PBLH are important for the simulation of air quality, ...he MBs were further analyzed here... For WRF-CMAQ, ARI effects induced an increase (-1.93 m) and decrease (+6.66 m) in the annual underestimations of PBLH at 8:00 and 20:00 LT, respectively (Table S3). The negative MBs for WRF-Chem\_ARI and WRF-Chem\_BOTH showed an increase ...nhancement

**Deleted:** listed ...ndicated in Table 3, the three coupled models performed ...emonstrated good performance in simulating well for ...he shortwave radiation at the ...he top of the atmosphere (T...RTOA) and longwave radiation at the ...he top of the atmosphere (T...RTOA). The annual MBs of ...or T...RTOA and T...RTOA are ranging from -4.40 to +5.42 W m<sup>-2</sup> and -2.14 to 0.66 W m<sup>-2</sup>, respectively. Seasonal

542 CHIMERE displayed negative MBs in all seasons except for spring. For WRF-Chem,  
543 it produced underestimations and overestimations of SRTOA in spring–summer and  
544 autumn–winter, respectively.

## 546 2 Evaluations of other air quality variables,

547 According to the annual statistical results (Table 4 and Fig. S17), the NO<sub>2</sub>  
548 simulated by all three models had comparable correlations (0.50–0.60) with ground-  
549 based observations. WRF-CMAQ slightly overestimated NO<sub>2</sub> (MBs of +2.74 to +3.26  
550 μg m<sup>-3</sup>, and NMBs of +8.77% to +10.44%). In contrast, WRF-Chem (MBs of -10.03  
551 to -9.22 μg m<sup>-3</sup>, and NMBs of -32.14% to -29.55%) and WRF-CHIMERE (MBs of  
552 -9.35 to -8.96 μg m<sup>-3</sup>, and NMBs of -29.96% to -28.73%) tended to significantly  
553 underestimate NO<sub>2</sub> in eastern China. For seasonal variations (Fig. 7), WRF-CMAQ  
554 showed the best performance in winter, and generally overestimated NO<sub>2</sub> in all seasons  
555 with the NMBs ranging from -2.21% to 34.34%. Both WRF-Chem and WRF-  
556 CHIMERE had maximum R and NMB values (0.42 to 0.50 and -13.09% to -3.23%,  
557 respectively) in winter, and minimum values (0.57 to 0.62 and -41.57% to -38.05%,  
558 respectively) in summer. The annual and seasonal positive biases of WRF-CMAQ are  
559 partially caused by lack of incorporation of heterogeneous reactions of NO<sub>2</sub> that  
560 occurred on ground and aerosol surfaces (Spataro et al., 2013; Li et al., 2018; Liu et al.,  
561 2019). Recently, Zhang et al. (2021) addressed these gaps in CMAQ v5.3 but related  
562 modules had not been integrated into the latest officially released version (version 5.4).  
563 For WRF-Chem and WRF-CHIMERE, underestimations of NO<sub>2</sub> were consistent with  
564 overestimations of O<sub>3</sub>, as the NO<sub>x</sub> depletions were dominated by O<sub>3</sub> titrations. In  
565 addition, subtle differences existed in the default settings of reaction rate constants for  
566 specific chemical reactions referring to NO<sub>x</sub> in WRF-CMAQ, WRF-Chem, and WRF-  
567 CHIMERE. More detailed information can be found in the source code files of  
568 mech\_cb6r3\_ae6\_aq.def, module\_cbmz.F, and rates.F, respectively. With ARI  
569 feedbacks enabled, the annual and seasonal R values of NO<sub>2</sub> simulated by WRF-CMAQ  
570 improved, but the NMBs worsened. In contrast, both WRF-Chem and WRF-CHIMERE  
571 presented improvements. Our results showed that ARI effects tended to amplify NO<sub>2</sub>  
572 overestimations in WRF-CMAQ, and alleviate underestimations in WRF-Chem and  
573 WRF-CHIMERE. This can be explained by the ARI-induced NO<sub>2</sub> reductions being  
574 associated with slower photochemical reactions, strengthened atmospheric stability and  
575 O<sub>3</sub> titration, and vice versa. The inclusion of ACI effects in WRF-Chem and WRF-  
576 CHIMERE resulted in relatively limited improvements in model performances.

577 All models had the poorest performance in the annual and seasonal SO<sub>2</sub> and CO  
578 simulations over eastern China (Table 4 and Fig. 6). For SO<sub>2</sub>, annual correlations were  
579 comparable for all models ranging from 0.39 to 0.41. All three models underestimated  
580 SO<sub>2</sub>. WRF-CMAQ showed the smallest MB of -4.31 μg m<sup>-3</sup>, while WRF-Chem had  
581 the largest of -10.30 μg m<sup>-3</sup>. Gao et al. (2018) also demonstrated that all two-way  
582 coupled models, except the WRF-Chem version from the University of Iowa modelling  
583 group, tended to underestimate SO<sub>2</sub> (-54.77 to 4.50 μg m<sup>-3</sup>) over the North China Plain  
584 during January, 2013. The R values for all models were highest in autumn and winter  
585 (0.31–0.46) and lowest in spring and summer (0.16–0.38), while NMBs showed the

**Deleted:** had ...isplayed negative MBs in all seasons except for spring, and... For WRF-Chem, it produced underestimations and overestimations of T...RTOA in spring–summer and autumn–winter, respectively. ...

**Deleted:**

**Deleted:** (%), (...). In contrast, but ...RF-Chem (MBs of -10.03 to -9.22 μg m<sup>-3</sup>, and NMBs of -32.14% to -29.55%) and WRF-CHIMERE (MBs of -9.35 to -8.96 μg m<sup>-3</sup>, and NMBs of -29.96% to -28.73%) tended to largely ...ignificantly underestimate NO<sub>2</sub> in eastern China. For seasonal variations (Fig. 7), WRF-CMAQ had ...howed the best performance in winter, and generally overestimated NO<sub>2</sub> in all seasons (...ith the NMBs ranging fromof...-2.21% to 34.34%)... Both WRF-Chem and WRF-CHIMERE had maximum R and NMB values (0.42...to 0.50 and -13.09% to -3.23%, respectively) in winter, and minimum values (0.57...to 0.62 and -41.57% to -38.05%, respectively) in summer. The annual and seasonal positive biases of WRF-CMAQ are partially caused by not ...ack of incorporation of ing the ...

**Deleted:** These gaps had been filled by ...hang et al. (2021) addressed these gaps in CMAQ v5.3 but related modules had not been integratedincorporated...into the latest ...

**Deleted:** s... For WRF-Chem and WRF-CHIMERE, underestimations of NO<sub>2</sub> were consistent with overestimations of O<sub>3</sub>, because... as thee... ...

**Formatted:** Font: Not Italic, Font color: Auto

**Deleted:** were

**Formatted:** Font: Italic

**Formatted:** Font: Italic, Subscript

**Deleted:** ; ... Mm...re detailed information can be found in the source code files of mech\_cb6r3\_ae6\_aq.def, module\_cbmz.F, and rates.F, respectively. With ARI feedbacks enabled, the annual and seasonal R values of NO<sub>2</sub> ...

**Deleted:** performed ...he poorest performance in most poorly for ...he annual and seasonal SO<sub>2</sub> and CO simulations over eastern China (Table 4 and Fig. 6). For SO<sub>2</sub>, annual ...

**Deleted:** showed

**Formatted:** Font color: Auto

**Deleted:** ,...2013. The R values for all models were highest in autumn and winter (0.31–0.46), ... and lowest in spring and summer (0.16–0.38), but ...



738 opposite trend. As concluded by Liu et al. (2010), the larger underestimations of  
 739 seasonal SO<sub>2</sub> concentrations were caused by the weaker solar radiation and lower  
 740 amount of precipitation in winter compared to summer. These conditions slowed down  
 741 the photochemical conversion of SO<sub>2</sub> to SO<sub>4</sub><sup>2-</sup>, wet scavenging, and aqueous-phase  
 742 oxidation rates of SO<sub>2</sub>.

743 For CO (Table 4), WRF-CHIMERE (0.47–0.48) had higher correlation  
 744 coefficients than those of WRF-CMAQ (0.23–0.24) and WRF-Chem (0.21–0.22). All  
 745 three models underestimated CO concentrations, with MBs ranging from –0.52 to  
 746 –0.39 mg m<sup>-3</sup>. These underestimations were partly attributed to uncertainties in the  
 747 vertical allocation of CO emissions (He et al., 2017). WRF-CMAQ and WRF-Chem  
 748 both produced spring-minimum (0.15) and winter-maximum (0.36) seasonal cycles of  
 749 R values (Fig. 6), while WRF-CHIMERE presented high (0.47) and low (0.26)  
 750 correlations in winter and summer, respectively. Negative seasonal NMBs varied from  
 751 –56.94% to –33.18% in all coupled models. When ARI effects were considered, annual  
 752 and seasonal SO<sub>2</sub> and CO model performances in all three models showed slight  
 753 improvement (R increased, approximately 0.01, and NMB enhanced from 0.98% to  
 754 1.71%). Moreover, the enhancements in the simulation accuracies of SO<sub>2</sub> and CO for  
 755 the two-way coupled WRF-Chem and WRF-CHIMERE were dominated by ARI effects  
 756 rather than ACI effects.

#### 757 S1 Statistical metrics

758 The correlation coefficient (R), mean bias (MB), normalized mean bias (NMB),  
 759 normalized gross error (NGE) and root mean square error (RMSE) were adopted to  
 760 assess the accuracy of coupled models in simulating meteorological and air quality  
 761 parameters against the ground-based and satellite observations with the following  
 762 equations:  
 763  
 764

$$765 \quad R = \frac{\sum_{i=1}^N (p_i - \bar{p})(o_i - \bar{o})}{\sqrt{\sum_{i=1}^N (p_i - \bar{p})^2} \sqrt{\sum_{i=1}^N (o_i - \bar{o})^2}} \quad (1)$$

$$766 \quad MB = \frac{1}{N} \sum_{i=1}^N (p_i - o_i) \quad (2)$$

$$767 \quad NMB = \frac{\sum_{i=1}^N (p_i - o_i)}{\sum_{i=1}^N (o_i)} \quad (3)$$

$$768 \quad NGE = \frac{\sum_{i=1}^N |p_i - o_i|}{\sum_{i=1}^N (o_i)} \quad (4)$$

$$769 \quad RMSE = \left[ \frac{1}{N} \sum_{i=1}^N (p_i - o_i)^2 \right]^{1/2} \quad (5)$$

770 where p<sub>i</sub> and o<sub>i</sub> are the simulated and observed parameters, respectively, n is the  
 771 total number of the values used for evaluation, and  $\bar{p}$  and  $\bar{o}$  are the averages of the  
 772 simulation and observation, respectively.  
 773

Deleted: lesser

Deleted: with

Deleted: ,

Deleted: which

Deleted: caused by

Deleted: had

Deleted: (

Deleted: ) were present

Deleted: were

Deleted: ly

Deleted: d

Deleted: ed by

Deleted: ,

Deleted: increas

Deleted: ed by

Deleted: –

Deleted: )

Deleted: improvements

Deleted: C

Formatted: Indent: Left 0.5 ch, First line: 1.5 ch

Deleted: applied

Deleted: parameters

Deleted: pollutants

Deleted: validation

797 Table S1. Summary of representations of cloud cover and cloud optical properties in  
 798 the Fast-JX scheme for WRF-CMAQ, WRF-Chem and WRF-CHIMERE.

Model	Cloud clover	Cloud optical properties			
		Optical properties	Effective Wavelength	Hydrometeor types	Method
WRF-CMAQ	1. CF <sup>a</sup> from WRF and CF calculated using RH and RH thresholds 2. Exponential-random overlapping	Extinction, single scattering albedo and asymmetry factor	294.6, 303.2, 310.0, 316.4, 333.1, 382.0 and 607.7 nm	Cloud liquid water, rain, snow, graupel and ice	The parameterizations proposed by Hu and Stammes (1993) and Fu (1996)
WRF-Chem	1. CF=0 if CLWC <sup>b</sup> =0 2. CF=1 if CIC <sup>c</sup> >0	Cloud optical depth	300, 400, 600 and 999 nm	Cloud liquid water	Based on the empirical functions of relative humidity and cloud liquid water content
WRF-CHIMERE	1. CF=0 if CLWC or CIWC=0 2. CF=1 if CLWC or CIC>0	Cloud optical depth	200, 300, 400, 600, and 999 nm	Cloud liquid water and ice	Based on the functions of cloud effective radius and cloud liquid water

799 <sup>a</sup>CF is cloud fraction. <sup>b</sup>CLWC is cloud liquid water content. <sup>c</sup>CIC is cloud ice content.

800  
 801 Table S2. Summary of the treatments for aerosol size distributions and components in  
 802 each mode or bin for the coupled WRF-CMAQ, WRF-Chem and WRF-CHIMERE  
 803 models.

Model	Aerosol mechanism	Modal approach			
		Aitken	Accumulation	Coarse	
WRF-CMAQ	AERO6	BC, OC, sulfate, nitrate, ammonium, PMOTHR <sup>d</sup> , PNCOM <sup>e</sup> water, metals	BC, OC, sulfate, nitrate, ammonium, PMOTHR, PNCOM, water, metals, sea salt, dust	PMC <sup>f</sup> , sea salt, dust	
WRF-Chem	MOSAIC <sup>g</sup>	Bin 1 0.039–0.156 μm <i>Black carbon (BC)</i> , OC, sulfate, nitrate, sea salt <sup>h</sup>	Bin 2 0.156–0.625 μm BC, OC, sulfate, nitrate, sea salt	Bin 3 0.625–2.5 μm BC, OC, sulfate, nitrate, sea salt	Bin 4 2.5–10.0 μm <i>Dust</i> , sea salt, OIN <sup>i</sup>
WRF-CHIMERE	SAM <sup>g</sup>	Bin 1 0.039–0.078 μm BC, OC, sulfate, PPM <sup>f</sup>	Bin 2 0.078–0.156 μm BC, OC, sulfate, PPM	Bin 3 0.156–0.312 μm BC, OC, sulfate, PPM	Bin 4 0.312–0.625 μm BC, OC, sulfate, PPM

804 <sup>g</sup>MOSAIC is the Model for Simulating Aerosol Interactions and Chemistry, and the cbmz-mosaic emissions in "PNL" format (emiss\_inpt\_opt=101) was used in WRF-Chem simulations.

805 <sup>h</sup>SAM is the sectional aerosol mechanism.

806 <sup>i</sup>PPM is the primary particulate matter.

807 <sup>d</sup>PMOTHR is the remaining particulate matter that can not be speciated in fine mode, and more detailed information is at

808 [https://www.airqualitymodeling.org/index.php/CMAQv5.0\\_PM\\_emitted\\_species\\_list](https://www.airqualitymodeling.org/index.php/CMAQv5.0_PM_emitted_species_list).

809 <sup>e</sup>PNCOM is the primary non-carbon organic matter in fine mode and more detailed information is at [https://www.airqualitymodeling.org/index.php/CMAQv5.0\\_PM\\_emitted\\_species\\_list](https://www.airqualitymodeling.org/index.php/CMAQv5.0_PM_emitted_species_list).

810 <sup>f</sup>PMC is the primary particulate matter in coarse mode and more detailed information is at [https://www.airqualitymodeling.org/index.php/CMAQv5.0\\_PM\\_emitted\\_species\\_list](https://www.airqualitymodeling.org/index.php/CMAQv5.0_PM_emitted_species_list).

811 <sup>i</sup>OIN is the other inorganic matter.

812  
 813 Table S3. Statistical metrics (R, MB, NMB, NGE, and RMSE) between simulated and  
 814 observed annual SSR, T2, RH2, Q2, WS10, WD10, precipitation, and PBLH at 08:00  
 815 and 20:00 LT) in eastern China. The best results are in bold, while mean simulations  
 816 and observations are in italics.

Variables	Statistics	WRF-CMAQ_NO	WRF-CMAQ_ARI	WRF-Chem_NO	WRF-Chem_ARI	WRF-Chem_BOTH	WRF-CHIMERE_NO	WRF-CHIMERE_ARI	WRF-CHIMERE_BOTH
SSR ( <i>55.22</i> m <sup>-2</sup> )	Mean_sim	<i>191.12</i>	<i>171.14</i>	<i>194.52</i>	<i>180.04</i>	<i>191.71</i>	<i>197.88</i>	<i>188.63</i>	<i>189.54</i>
	R	0.88	<b>0.89</b>	0.88	<b>0.89</b>	0.88	0.85	0.85	0.85
	MB	35.89	15.91	39.30	24.82	36.48	42.65	33.41	34.32
	NMB (%)	23.12	<b>10.25</b>	25.32	15.99	23.50	27.48	21.52	22.11
	NGE (%)	206.62	170.85	202.41	<b>170.70</b>	208.05	242.53	221.67	226.29
	RMSE	133.05	<b>120.60</b>	134.16	123.94	134.45	154.71	147.73	148.57
T2 ( <i>13.68</i> °C)	Mean_sim	<i>12.81</i>	<i>12.61</i>	<i>12.99</i>	<i>12.84</i>	<i>12.96</i>	<i>11.84</i>	<i>11.68</i>	<i>11.69</i>
	R	<b>0.97</b>	<b>0.97</b>	<b>0.97</b>	<b>0.97</b>	<b>0.97</b>	0.96	0.96	0.96

	MB	-0.86	-1.06	-0.68	-0.83	-0.71	-1.83	-2.00	-1.98	
	NMB (%)	-6.33	-7.76	<b>-4.97</b>	-6.09	-5.21	-13.39	-14.60	-14.50	
	NGE (%)	<b>10.58</b>	10.76	10.79	10.95	10.86	17.00	17.65	17.60	
	RMSE	<b>2.88</b>	2.94	3.05	3.07	3.05	3.87	3.94	3.97	
Q2	Mean_sim	<i>8.69</i>	<i>8.51</i>	<i>8.57</i>	<i>8.54</i>	<i>8.58</i>	<i>8.35</i>	<i>8.30</i>	<i>8.30</i>	Formatted: Font: Italic
(8.87 g kg <sup>-1</sup> )	R	<b>0.90</b>	<b>0.90</b>	0.89	0.89	0.89	0.88	0.88	0.88	Formatted: Font: Italic
	MB	-0.18	-0.35	-0.30	-0.32	-0.28	-0.52	-0.57	-0.56	
	NMB (%)	<b>-2.00</b>	-3.98	-3.36	-3.66	-3.19	-5.84	-6.37	-6.35	
	NGE (%)	<b>16.80</b>	16.85	19.70	19.66	19.77	20.55	20.65	20.62	
	RMSE	<b>2.93</b>	2.95	3.09	3.09	3.10	3.17	3.18	3.18	
RH2	Mean_sim	<i>71.03</i>	<i>70.51</i>	<i>70.01</i>	<i>70.33</i>	<i>70.13</i>	<i>70.41</i>	<i>70.58</i>	<i>70.46</i>	Formatted: Font: Italic
(67.48 %)	R	<b>0.73</b>	<b>0.73</b>	0.68	0.68	0.68	0.65	0.65	0.65	Formatted: Font: Italic
	MB	3.55	3.03	2.53	2.85	2.64	2.93	3.10	2.97	
	NMB (%)	5.26	4.49	<b>3.74</b>	4.22	3.92	4.34	4.59	4.41	
	NGE (%)	<b>19.90</b>	19.91	23.45	23.71	23.71	24.77	24.88	24.90	
	RMSE	<b>18.92</b>	18.98	19.78	19.79	19.84	20.81	20.82	20.84	
WS10	Mean_sim	<i>3.27</i>	<i>3.23</i>	<i>3.30</i>	<i>3.29</i>	<i>3.30</i>	<i>3.85</i>	<i>3.83</i>	<i>3.83</i>	Formatted: Font: Italic
(2.81 m s <sup>-1</sup> )	R	<b>0.62</b>	0.61	0.60	0.59	0.59	0.47	0.47	0.47	Formatted: Font: Italic
	MB	0.45	0.42	0.49	0.48	0.49	1.04	1.02	1.02	
	NMB (%)	16.16	<b>14.98</b>	17.45	17.11	17.53	36.98	36.27	36.34	
	NGE (%)	96.20	<b>95.00</b>	100.16	100.09	100.55	136.55	135.59	135.75	
	RMSE	1.89	1.88	1.92	1.92	1.93	2.46	2.45	2.45	
WD10	Mean_sim	<i>177.13</i>	<i>176.62</i>	<i>177.87</i>	<i>177.82</i>	<i>178.11</i>	<i>171.97</i>	<i>171.53</i>	<i>171.68</i>	Formatted: Font: Italic
(175.27 °)	R	0.01	0.01	0.01	0.01	0.01	0.02	0.02	0.02	Formatted: Font: Italic
	MB	1.85	1.35	2.60	2.55	2.83	-3.31	-3.74	-3.60	
	NMB (%)	1.06	0.77	1.48	1.45	1.62	-1.89	-2.14	-2.05	
	NGE (%)	94.30	<b>94.00</b>	101.16	101.09	101.55	126.75	125.79	125.85	
	RMSE	149.57	149.45	149.45	149.38	149.57	148.70	148.47	148.71	
Precipitation	Mean_sim	<i>2.46</i>	<i>2.31</i>	<i>3.24</i>	<i>3.19</i>	<i>3.26</i>	<i>3.31</i>	<i>3.24</i>	<i>3.21</i>	Formatted: Font: Italic
(PREC)	R	<b>0.59</b>	<b>0.59</b>	0.50	0.50	0.50	0.35	0.34	0.34	
(2.72 mm d <sup>-1</sup> )	MB	-0.27	-0.42	0.51	0.46	0.53	0.59	0.52	0.48	Formatted: Font: Italic
	NMB (%)	<b>-9.80</b>	-15.35	18.86	16.83	19.43	21.46	18.96	17.63	
	NGE (%)	310.71	<b>283.10</b>	442.60	428.11	445.89	573.24	565.36	557.56	
	RMSE	8.03	<b>7.96</b>	10.32	10.26	10.33	10.87	10.85	10.93	
PBLH00	Mean_sim	<i>253.54</i>	<i>251.61</i>	<i>288.41</i>	<i>263.16</i>	<i>282.81</i>	<i>276.45</i>	<i>270.28</i>	<i>269.63</i>	Formatted: Font: Italic
(32.13 m)	R	<b>0.21</b>	<b>0.21</b>	0.17	0.17	0.17	0.17	0.17	0.17	Formatted: Font: Italic
	MB	-178.59	-180.52	-143.72	-168.97	-149.32	-155.68	-161.85	-162.50	
	NMB (%)	-41.33	-41.77	<b>-33.26</b>	-39.10	-34.55	-36.03	-37.45	-37.61	
	NGE (%)	58.89	58.75	<b>54.37</b>	56.96	54.51	57.20	57.63	57.28	
	RMSE	380.23	378.79	<b>371.27</b>	379.72	372.14	373.78	375.85	374.52	
PBLH12	Mean_sim	<i>230.14</i>	<i>236.80</i>	<i>358.05</i>	<i>332.45</i>	<i>346.54</i>	<i>363.47</i>	<i>360.13</i>	<i>359.03</i>	Formatted: Font: Italic
(547.02 m)	R	<b>0.40</b>	<b>0.40</b>	0.39	<b>0.40</b>	0.39	0.34	0.35	0.35	Formatted: Font: Italic
	MB	-316.88	-310.22	-188.97	-214.57	-200.48	-183.55	-186.89	-188.00	
	NMB (%)	-57.93	-56.71	-34.55	-39.22	-36.65	<b>-33.56</b>	-34.16	-34.37	

---

NGE (%)	65.84	65.23	59.55	59.05	59.49	59.65	<b>59.32</b>	59.66
RMSE	505.64	502.24	459.64	460.51	<b>459.50</b>	470.39	467.90	469.19

---

825

Table S4. Effects of aerosol feedbacks (ARI and/or ACI) considered in different coupled models on *statistical* metrics between annual and seasonal meteorological and air quality simulations and observations in eastern China.

Deleted: evaluation

Surface observations		WRF-CMAQ_ARI	WRF-Chem_ARI	WRF-Chem_ACI	WRF-Chem_BOTH	WRF-CHIMERE_ARI	WRF-CHIMERE_ACI	WRF-CHIMERE_BOTH
SSR	Annual	R(↑), MB(↓), RMSE(↓)	R(↑), MB(↓), RMSE(↓)	R(↓), MB(↑), RMSE(↑)	R(↑), MB(↓), RMSE(↓)	R(↑), MB(↓), RMSE(↓)	R(↓), MB(↑), RMSE(↑)	R(↑), MB(↓), RMSE(↓)
	Spring	R(↑), MB(↓), RMSE(↓)	R(↑), MB(↓), RMSE(↓)	R(↓), MB(↑), RMSE(↑)	R(↓), MB(↓), RMSE(↓)	R(↑), MB(↓), RMSE(↓)	R(↓), MB(↓), RMSE(↑)	R(↑), MB(↓), RMSE(↓)
	Summer	R(↑), MB(↓), RMSE(↓)	R(↑), MB(↓), RMSE(↓)	R(↓), MB(↑), RMSE(↑)	R(↑), MB(↓), RMSE(↓)	R(↑), MB(↓), RMSE(↓)	R(↑), MB(↑), RMSE(↓)	R(↑), MB(↓), RMSE(↓)
	Autumn	R(↑), MB(↓), RMSE(↓)	R(↑), MB(↓), RMSE(↓)	R(↓), MB(↑), RMSE(↑)	R(↓), MB(↓), RMSE(↓)	R(↑), MB(↓), RMSE(↓)	R(↓), MB(↑), RMSE(↑)	R(↑), MB(↓), RMSE(↓)
	Winter	R(↑), MB(↓), RMSE(↓)	R(↑), MB(↓), RMSE(↓)	R(↓), MB(↑), RMSE(↑)	R(↑), MB(↓), RMSE(↓)	R(↑), MB(↓), RMSE(↓)	R(↓), MB(↓), RMSE(↑)	R(↑), MB(↓), RMSE(↓)
T2	Annual	R(↓), MB(↓), RMSE(↑)	R(↑), MB(↓), RMSE(↑)	R(↓), MB(↑), RMSE(↓)	R(↑), MB(↓), RMSE(↑)	R(↑), MB(↓), RMSE(↑)	R(↓), MB(↑), RMSE(↑)	R(↓), MB(↓), RMSE(↑)
	Spring	R(↓), MB(↓), RMSE(↑)	R(↑), MB(↓), RMSE(↑)	R(↓), MB(↑), RMSE(↓)	R(↑), MB(↓), RMSE(↑)	R(↑), MB(↓), RMSE(↑)	R(↓), MB(↓), RMSE(↑)	R(↓), MB(↓), RMSE(↑)
	Summer	R(↓), MB(↓), RMSE(↑)	R(↑), MB(↓), RMSE(↓)	R(↓), MB(↑), RMSE(↓)	R(↑), MB(↑), RMSE(↓)	R(↓), MB(↓), RMSE(↑)	R(↑), MB(↑), RMSE(↓)	R(↑), MB(↓), RMSE(↑)
	Autumn	R(↓), MB(↓), RMSE(↑)	R(↑), MB(↓), RMSE(↑)	R(↓), MB(↑), RMSE(↓)	R(↑), MB(↓), RMSE(↓)	R(↑), MB(↓), RMSE(↑)	R(↓), MB(↑), RMSE(↓)	R(↓), MB(↓), RMSE(↑)
	Winter	R(↑), MB(↓), RMSE(↑)	R(↑), MB(↓), RMSE(↑)	R(↑), MB(↑), RMSE(↓)	R(↑), MB(↓), RMSE(↑)	R(↑), MB(↓), RMSE(↑)	R(↓), MB(↓), RMSE(↑)	R(↑), MB(↓), RMSE(↑)
SH2	Annual	R(↓), MB(↓), RMSE(↑)	R(↑), MB(↓), RMSE(↓)	R(↓), MB(↑), RMSE(↑)	R(↓), MB(↑), RMSE(↑)	R(↓), MB(↓), RMSE(↑)	R(↓), MB(↑), RMSE(↑)	R(↓), MB(↓), RMSE(↑)
	Spring	R(↓), MB(↓), RMSE(↑)	R(↑), MB(↓), RMSE(↑)	R(↓), MB(↑), RMSE(↑)	R(↓), MB(↑), RMSE(↑)	R(↑), MB(↓), RMSE(↑)	R(↓), MB(↑), RMSE(↓)	R(↓), MB(↓), RMSE(↑)
	Summer	R(↓), MB(↓), RMSE(↑)	R(↑), MB(↓), RMSE(↑)	R(↓), MB(↑), RMSE(↑)	R(↓), MB(↑), RMSE(↑)	R(↓), MB(↓), RMSE(↑)	R(↓), MB(↓), RMSE(↑)	R(↓), MB(↓), RMSE(↑)
	Autumn	R(↓), MB(↓), RMSE(↑)	R(↑), MB(↓), RMSE(↑)	R(↓), MB(↑), RMSE(↑)	R(↓), MB(↑), RMSE(↓)	R(↑), MB(↓), RMSE(↑)	R(↓), MB(↑), RMSE(↓)	R(↑), MB(↑), RMSE(↑)
	Winter	R(↓), MB(↓), RMSE(↑)	R(↓), MB(↓), RMSE(↑)	R(↑), MB(↑), RMSE(↑)	R(↓), MB(↓), RMSE(↑)	R(↓), MB(↓), RMSE(↑)	R(↓), MB(↓), RMSE(↑)	R(↓), MB(↓), RMSE(↑)
Q2	Annual	R(↓), MB(↓), RMSE(↑)	R(↓), MB(↑), RMSE(↑)	R(↓), MB(↓), RMSE(↑)	R(↓), MB(↑), RMSE(↑)	R(↓), MB(↑), RMSE(↑)	R(↓), MB(↓), RMSE(↑)	R(↓), MB(↑), RMSE(↑)
	Spring	R(↓), MB(↓), RMSE(↑)	R(↓), MB(↑), RMSE(↑)	R(↓), MB(↓), RMSE(↑)	R(↓), MB(↑), RMSE(↑)	R(↓), MB(↑), RMSE(↑)	R(↓), MB(↑), RMSE(↑)	R(↓), MB(↑), RMSE(↑)
	Summer	R(↓), MB(↓), RMSE(↑)	R(↓), MB(↑), RMSE(↓)	R(↓), MB(↓), RMSE(↑)	R(↑), MB(↓), RMSE(↓)	R(↓), MB(↑), RMSE(↑)	R(↑), MB(↓), RMSE(↓)	R(↓), MB(↓), RMSE(↓)
	Autumn	R(↓), MB(↓), RMSE(↑)	R(↓), MB(↑), RMSE(-)	R(↓), MB(↓), RMSE(↑)	R(↓), MB(↑), RMSE(↑)	R(↑), MB(↑), RMSE(↓)	R(↓), MB(↓), RMSE(↑)	R(↓), MB(↓), RMSE(↑)
	Winter	R(↓), MB(↓), RMSE(-)	R(↑), MB(↑), RMSE(↑)	R(↓), MB(↓), RMSE(↓)	R(↓), MB(↑), RMSE(↑)	R(↑), MB(↑), RMSE(↓)	R(↓), MB(↓), RMSE(↑)	R(↑), MB(↑), RMSE(↑)
WS10	Annual	R(↓), MB(↓), RMSE(↓)	R(↓), MB(↓), RMSE(↓)	R(↓), MB(↑), RMSE(↑)	R(↓), MB(↓), RMSE(↑)	R(↓), MB(↓), RMSE(↓)	R(↑), MB(↑), RMSE(↑)	R(↓), MB(↓), RMSE(↓)
	Spring	R(↓), MB(↓), RMSE(↓)	R(↓), MB(↓), RMSE(↑)	R(↓), MB(↑), RMSE(↓)	R(↓), MB(↓), RMSE(↑)	R(↑), MB(↓), RMSE(↓)	R(↓), MB(↓), RMSE(↑)	R(↓), MB(↓), RMSE(↑)
	Summer	R(↑), MB(↓), RMSE(↑)	R(↑), MB(↓), RMSE(↓)	R(↓), MB(↑), RMSE(↑)	R(↑), MB(↑), RMSE(↑)	R(↓), MB(↓), RMSE(↑)	R(↑), MB(↓), RMSE(↓)	R(↑), MB(↓), RMSE(↓)
	Autumn	R(↓), MB(↓), RMSE(↓)	R(↓), MB(↓), RMSE(↑)	R(↓), MB(↑), RMSE(↑)	R(↓), MB(↓), RMSE(↑)	R(↓), MB(↓), RMSE(↓)	R(↑), MB(↑), RMSE(↑)	R(↓), MB(↓), RMSE(↑)
	Winter	R(↑), MB(↓), RMSE(↓)	R(↓), MB(↓), RMSE(↑)	R(↑), MB(↑), RMSE(↑)	R(↓), MB(↓), RMSE(↑)	R(↑), MB(↓), RMSE(↓)	R(↓), MB(↑), RMSE(↑)	R(↓), MB(↓), RMSE(↓)











1 Table S5. Radiation variables used in the two-way coupled WRF-CMAQ, WRF-Chem  
 2 and WRF-CHIMERE models with only enabling ARI compared to without aerosol  
 3 feedbacks.

Model	SW/LW radiation schemes	Turning off feedback	Turning on ARI feedback	
			Direct effects	Semi-direct effects
WRF-CMAQ	RRTMG/RRTMG	Aerosol optical properties are not calculated	Aerosol extinction, single scattering albedo ( $\omega_0$ ), and asymmetry factor ( $g$ ) 14 shortwave bands and 5 longwave bands (Wong et al., 2012)	1. Solar uv and ir fluxes 2. Radiative heating rate for the tten1d variable
WRF-Chem	RRTMG/RRTMG	Aerosol optical properties are not calculated	$\omega_0$ (300 nm, 400 nm, 600 nm, 999 nm), $g$ (300 nm, 400 nm, 600 nm, 999 nm), AOD ( $\tau$ ) (300 nm, 400 nm, 600 nm, 999 nm, 16 bands 3400 nm to 55600 nm) (Zhao et al., 2011)	1. Solar uv and ir fluxes 2. Radiative heating rate for the tten1d variable
WRF-CHIMERE	RRTMG/RRTMG	Aerosol optical properties are not calculated	$\omega_0$ (400 nm, 600 nm), $g$ (400 nm, 600 nm), AOD (300 nm, 400 nm, 600 nm, 16 bands 3400 nm to 55600 nm) (Briant et al., 2017)	1. Solar uv and ir fluxes 2. Radiative heating rate for the tten1d variable

Formatted

Formatted: Justified

Formatted: Justified

Formatted: Justified

4

5 Table S6. Description of refractive indices and radiation schemes used in the WRF-  
 6 CMAQ, WRF-Chem and WRF-CHIMERE models.

Model	Refractive indices of aerosol species groups	
	SW	LW
WRF-CMAQ	1. Water (1.408+1.420 $\times 10^3$ , 1.324+1.577 $\times 10^3$ , 1.277+1.516 $\times 10^3$ , 1.302+1.159 $\times 10^3$ , 1.312+2.360 $\times 10^3$ , 1.321+1.713 $\times 10^3$ , 1.323+2.425 $\times 10^3$ , 1.327+3.125 $\times 10^3$ , 1.331+3.405 $\times 10^3$ , 1.334+1.639 $\times 10^3$ , 1.340+2.955 $\times 10^3$ , 1.349+1.635 $\times 10^3$ , 1.362+3.350 $\times 10^3$ , 1.260+6.220 $\times 10^3$ ) 2. Water-soluble (1.443+5.718 $\times 10^3$ , 1.420+1.777 $\times 10^3$ , 1.420+1.060 $\times 10^3$ , 1.420+8.368 $\times 10^3$ , 1.463+1.621 $\times 10^3$ , 1.510+2.198 $\times 10^3$ , 1.510+1.929 $\times 10^3$ , 1.520+1.564 $\times 10^3$ , 1.530+7.000 $\times 10^3$ , 1.530+5.666 $\times 10^3$ , 1.530+5.000 $\times 10^3$ , 1.530+8.440 $\times 10^3$ , 1.530+3.000 $\times 10^3$ , 1.710+1.100 $\times 10^3$ ) 3. BC (2.089+1.070i, 2.014+0.939i, 1.962+0.843i, 1.950+0.784i, 1.940+0.760i, 1.930+0.749i, 1.905+0.737i, 1.870+0.726i, 1.850+0.710i, 1.850+0.710i, 1.850+0.710i, 1.850+0.710i, 2.589+1.771i) 4. Insoluble (1.272+1.165 $\times 10^3$ , 1.168+1.073 $\times 10^3$ , 1.208+8.650 $\times 10^3$ , 1.253+8.092 $\times 10^3$ , 1.329+8.000 $\times 10^3$ , 1.418+8.000 $\times 10^3$ , 1.456+8.000 $\times 10^3$ , 1.518+8.000 $\times 10^3$ , 1.530+8.000 $\times 10^3$ , 1.530+8.000 $\times 10^3$ , 1.530+8.000 $\times 10^3$ , 1.530+8.440 $\times 10^3$ , 1.530+3.000 $\times 10^3$ , 1.470+9.000 $\times 10^3$ ) 5. Sea-salt (1.480+1.788 $\times 10^3$ , 1.534+7.462 $\times 10^3$ , 1.437+2.950 $\times 10^3$ , 1.448+1.276 $\times 10^3$ , 1.450+7.944 $\times 10^3$ , 1.462+5.382 $\times 10^3$ , 1.469+3.754 $\times 10^3$ , 1.470+1.498 $\times 10^3$ , 1.490+2.050 $\times 10^3$ , 1.500+1.184 $\times 10^3$ , 1.502+9.938 $\times 10^3$ , 1.510+2.060 $\times 10^3$ , 1.510+5.000 $\times 10^3$ , 1.510+1.000 $\times 10^3$ ) in terms of 14 wavelengths at 3.4615, 2.7885, 2.325, 2.046, 1.784, 1.4625, 1.2705, 1.0101, 0.7016, 0.53325, 0.38815, 0.299, 0.2316, 8.24 $\mu\text{m}$	1. Water (1.160+0.321i, 1.140+0.117i, 1.232+0.047i, 1.266+0.038i, 1.300+0.034i) 2. Water-soluble (1.570+0.069i, 1.700+0.055i, 1.890+0.128i, 2.233+0.334i, 1.220+0.066i) 3. BC (1.570+2.200i, 1.700+2.200i, 1.890+2.200i, 2.233+2.200i, 1.220+2.200i) 4. Insoluble (1.482+0.096i, 1.600+0.107i, 1.739+0.162i, 1.508+0.117i, 1.175+0.042i) 5. Sea-salt (1.410+0.019i, 1.490+0.014i, 1.560+0.017i, 1.600+0.029i, 1.402+0.012i) in terms of 5 thermal windows at 13.240, 11.20, 9.73, 8.870, 7.830 $\mu\text{m}$
WRF-Chem	1. Water (1.35+1.524 $\times 10^3$ , 1.34+2.494 $\times 10^3$ , 1.33+1.638 $\times 10^3$ , 1.33+3.128 $\times 10^3$ ) 2. Dust (1.53+0.003i, 1.550+0.003i, 1.550+0.003i, 1.550+0.003i) 3. BC (1.95+0.79i, 1.95+0.79i, 1.95+0.79i, 1.95+0.79i) 4. OC (1.45+0i, 1.45+0i, 1.45+0i, 1.45+0i) 5. Sea salt (1.51+8.66 $\times 10^3$ , 1.5+7.019 $\times 10^3$ , 1.5+1.184 $\times 10^3$ , 1.47+1.5 $\times 10^3$ ) 6. Sulfate (1.52+1.00 $\times 10^3$ , 1.52+1.00 $\times 10^3$ , 1.52+1.00 $\times 10^3$ , 1.52+1.75 $\times 10^3$ ) in terms of 4 spectral intervals in 0.25-0.35, 0.35-0.45, 0.55-0.65, 0.998-1.000 $\mu\text{m}$	1. Water (1.532+0.336i, 1.524+0.360i, 1.420+0.426i, 1.274+0.403i, 1.161+0.321i, 1.142+0.115i, 1.232+0.047i, 1.266+0.039i, 1.296+0.034i, 1.321+0.0344i, 1.342+0.092i, 1.315+0.012i, 1.330+0.013i, 1.339+0.011i, 1.350+0.0049i, 1.408+0.0142i) 2. Dust (2.34+0.7i, 2.904+0.857i, 1.748+0.462i, 1.508+0.263i, 1.911+0.319i, 1.822+0.26i, 2.917+0.65i, 1.557+0.373i, 1.242+0.093i, 1.447+0.105i, 1.432+0.061i, 1.473+0.0245i, 1.495+0.011i, 1.5+0.008i) 3. BC (1.95+0.79i, 1.95+0.79i, 1.95+0.79i, 1.95+0.79i, 1.95+0.79i, 1.95+0.79i, 1.95+0.79i, 1.95+0.79i, 1.95+0.79i, 1.95+0.79i, 1.95+0.79i, 1.95+0.79i, 1.95+0.79i, 1.95+0.79i, 1.95+0.79i) 4. OC (1.86+0.5i, 1.91+0.268i, 1.988+0.185i, 1.439+0.198i, 1.606+0.059i, 1.7+0.0488i, 1.888+0.11i, 2.489+0.3345i, 1.219+0.065i, 1.419+0.058i, 1.426+0.0261i, 1.446+0.0142i, 1.457+0.013i, 1.458+0.01i) 5. Sea salt (1.74+0.1978i, 1.76+0.1978i, 1.78+0.129i, 1.456+0.038i, 1.41+0.019i, 1.48+0.014i, 1.56+0.016i, 1.63+0.03i, 1.4+0.012i, 1.43+0.0064i, 1.56+0.0196i, 1.45+0.0029i, 1.485+0.0017i, 1.486+0.0014i) 6. Sulfate (1.89+0.22i, 1.91+0.152i, 1.93+0.0846i, 1.586+0.2225i, 1.678+0.195i, 1.758+0.441i, 1.855+0.696i, 1.597+0.695i, 1.15+0.459i, 1.26+0.161i, 1.42+0.172i, 1.35+0.14i, 1.379+0.12i, 1.385+0.122i) in terms of 16 spectral intervals in 10-350, 350-500, 500-630, 630-700, 700-820, 820-980, 980-1080, 1080-1180, 1180-1390, 1390-1480, 1480-1800, 1800-2080, 2080-2250, 2250-2390, 2390-2600, 2600-3250 $\text{cm}^{-1}$
WRF-CHIMERE	1. Water (1.35+2.0 $\times 10^3$ , 1.34+2.0 $\times 10^3$ , 1.34+1.8 $\times 10^3$ , 1.33+3.4 $\times 10^3$ , 1.33+3.9 $\times 10^3$ ) 2. Dust (1.53+0.005i, 1.53+0.005i, 1.53+0.0024i, 1.53+8.94i, 1.53+7.6-4i) 3. BC (1.95+0.79i, 1.95+0.79i, 1.95+0.79i, 1.95+0.79i, 1.95+0.79i) 4. OC (1.53+0.09i, 1.53+0.008i, 1.53+0.005i, 1.53+0.0063i, 1.52+0.016i) 5. Sea salt (1.38+8.7 $\times 10^3$ , 1.38+3.5 $\times 10^3$ , 1.37+6.6 $\times 10^3$ , 1.36+1.2 $\times 10^3$ , 1.35+2.6 $\times 10^3$ ) 6. PPM (1.53+0.008i, 1.52+0.008i, 1.52+0.008i, 1.51+0.008i, 1.5+0.008i) 7. SOA (1.56+0.003i, 1.56+0.003i, 1.56+0.003i, 1.56+0.003i, 1.56+0.003i) 8. H <sub>2</sub> SO <sub>4</sub> (1.5+1.0 $\times 10^3$ , 1.47+1.0 $\times 10^3$ , 1.44+1.0 $\times 10^3$ , 1.43+1.3 $\times 10^3$ , 1.42+1.2 $\times 10^3$ ) 9. HNO <sub>3</sub> (1.53+0.006i, 1.53+0.006i, 1.53+0.006i, 1.53+0.006i, 1.53+0.006i) 10. NH <sub>3</sub> (1.53+0.0005i, 1.52+0.0005i, 1.52+0.0005i, 1.52+0.0005i, 1.52+0.0005i) in terms of 5 wavelengths at 0.2, 0.3, 0.4, 0.6, 0.999 $\mu\text{m}$	1. Water (1.42+0.02i, 1.35+0.0047i, 1.34+0.0088i, 1.33+0.015i, 1.32+0.01i, 1.32+0.13i, 1.32+0.032i, 1.3+0.034i, 1.27+0.039i, 1.23+0.047i, 1.15+0.1i, 1.16+0.32i, 1.27+0.4i, 1.41+0.43i, 1.52+0.37i, 1.65+0.55i) 2. BC (1.95+0.79i, 1.95+0.79i, 1.95+0.79i, 1.95+0.79i, 1.95+0.79i, 1.95+0.79i, 1.95+0.79i, 1.95+0.79i, 1.95+0.79i, 1.95+0.79i, 1.95+0.79i, 1.95+0.79i, 1.95+0.79i, 1.95+0.79i, 1.95+0.79i) 3. OC (1.43+1.42i, 1.46+1.43i, 1.46+1.25i, 1.46+2.67i, 1.45+1.89i, 1.42+1.71i, 1.43+1.71i, 1.25+0.007i, 2.67+0.005i, 1.89+0.01i, 1.71+0.013i, 1.43+0.014i, 1.46+0.025i, 1.46+0.062i, 1.46+0.064i, 1.45+0.031i) 4. Salt (1.43+0.019i, 1.37+0.0043i, 1.36+0.0084i, 1.36+0.011i, 1.34+0.01i, 1.35+0.083i, 1.34+0.029i, 1.31+0.03i, 1.33+0.037i, 1.29+0.042i, 1.2+0.09i, 1.2+0.27i, 1.3+0.34i, 1.47+0.37i, 1.56+0.03i, 1.51+0.09i) 5. PPM (1.45+0.01i, 1.45+0.01i, 1.45+0.01i, 1.45+0.01i, 1.45+0.01i, 1.45+0.05i, 1.45+0.05i, 1+0.5i, 1+0.2i, 2.6+0.2i, 1.7+0.2i, 1.7+0.2i, 1.7+0.2i, 1.7+0.2i, 1.7+0.2i, 1.7+0.2i) 6. SOA (1.56+0.003i, 1.56+0.003i, 1.56+0.003i, 1.56+0.003i, 1.56+0.003i, 1.56+0.003i, 1.56+0.003i, 1.56+0.003i, 1.56+0.003i, 1.56+0.003i, 1.56+0.003i, 1.56+0.003i, 1.56+0.003i, 1.56+0.003i, 1.56+0.003i)

Deleted:

7. H<sub>2</sub>SO<sub>4</sub> (1.35±0.16i, 1.4±0.13i, 1.39±0.12i, 1.38±0.12i, 1.35±0.15i, 1.42±0.18i, 1.26±0.16i, 1.15±0.44i, 1.57±0.73i, 1.83±0.7i, 1.71±0.46i, 1.68±0.2i, 1.59±0.21i, 1.87±0.48i, 1.89±0.27i, 1.86±0.31i)  
 8. HNO<sub>3</sub> (1.45±0.01i, 1.45±0.01i, 1.45±0.01i, 1.45±0.01i, 1.45±0.01i, 1.45±0.01i, 1.45±0.01i, 1.45±0.05i, 1±0.5i, 1±0.2i, 2.6±0.2i, 1.7±0.2i, 1.7±0.2i, 1.7±0.2i, 1.7±0.2i, 1.7±0.2i, 1.7±0.2i)  
 9. NH<sub>3</sub> (1.45±0.01i, 1.45±0.01i, 1.45±0.01i, 1.45±0.01i, 1.45±0.01i, 1.45±0.01i, 1.45±0.05i, 1±0.5i, 1±0.2i, 2.6±0.2i, 1.7±0.2i, 1.7±0.2i, 1.7±0.2i, 1.7±0.2i, 1.7±0.2i) in term of 16 wavelengths at 3.4, 4.4, 4.3, 4.6, 5.2, 6.1, 7.0, 7.8, 8.8, 9.7, 11.1, 13.2, 15.0, 17.7, 23.5, 55.6 μm

1

2 Table S7. Microphysics variables used in the two-way coupled WRF-CMAQ, WRF-  
 3 Chem and WRF-CHIMERE models with enabling ACI effects compared to *those*  
 4 without aerosol feedbacks.

Formatted: Font color: Auto

Model	Microphysics scheme	Turning off feedback	Turning on ACI feedback	
			First indirect effects	Second indirect effects
WRF-CMAQ	Morrison	1. Prescribed constant CDNC value of 250 cm <sup>-3</sup>	None	None
WRF-Chem	Morrison	1. Prescribed constant CDNC value of 250 cm <sup>-3</sup> 2. Constant cloud droplet effective radius with 10 μm 3. Cloud droplet extinction coefficient, single scattering albedo, and asymmetry factor 4. Prescribed ice nucleating particle (INP) concentration based on empirical formula (Rasmussen et al., 2002)	1. Hygroscopicity 2. Prognostic CDNC based on Köhler theory 3. Prognostic cloud droplet effective radius 4. Prognostic cloud droplet extinction coefficient, single scattering albedo, and asymmetry factor 5. Prescribed INP	1. Prognostic cloud-to-rain autoconversion rate
WRF-CHIMERE	Thompson	1. Prescribed constant CDNC values of 300 cm <sup>-3</sup> 2. Prescribed INP from heterogeneous ice nucleation in iceDeMott subroutine module mp_thompson.F file using climatological dust concentration (dimeters > 0.5 μm) (DeMott et al., 2015) and homogeneous freezing (Thompson and Eidhammer, 2014) with climatological hygroscopic aerosol concentrations (dimeters > 0.1 μm) generated by QNWFA_QNIFA_Monthly_GFS file 3. Prescribed cloud droplet and ice effective radius 4. Prescribed extinction coefficient, single scattering albedo, and asymmetry factor of cloud droplet and ice	1. Hygroscopicity 2. Prognostic CDNC based on Köhler theory 3. Prognostic INP from heterogeneous ice nucleation based on online dust calculation (dimeters > 0.5 μm) and homogeneous freezing with prognostic hygroscopic aerosol concentrations (dimeters > 0.1 μm) (Tuccella et al., 2019) 4. Prognostic cloud droplet and ice effective radius 5. Prognostic extinction coefficient, single scattering albedo, and asymmetry factor of cloud droplet and ice	1. Prognostic cloud-to-rain autoconversion rate

Deleted: based on Eqs. (2)-(4)

Deleted:

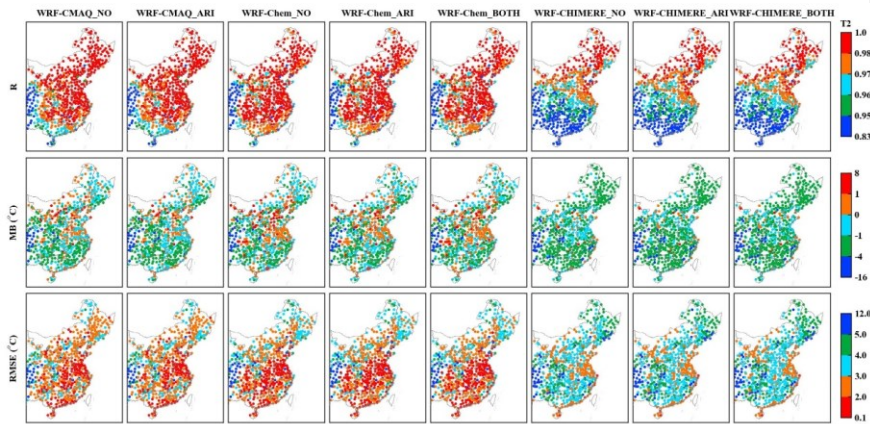
5

6 Table S8. Summary of download information on model output of each simulation  
 7 scenario.

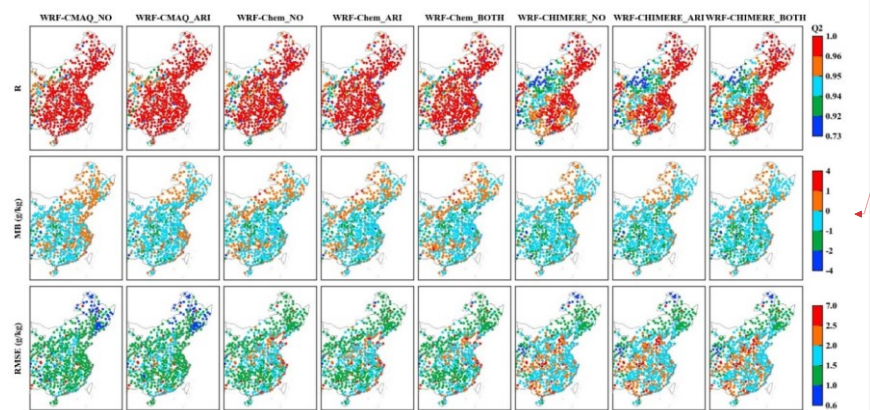
Formatted: Normal

Scenario	DOI	Link	Reference
WRF-CMAQ_NO	<a href="https://doi.org/10.5281/zenodo.7951404">https://doi.org/10.5281/zenodo.7951404</a>	<a href="https://zenodo.org/record/7951404">https://zenodo.org/record/7951404</a>	Gao et al., 2023i_part1
	<a href="https://doi.org/10.5281/zenodo.7951467">https://doi.org/10.5281/zenodo.7951467</a>	<a href="https://zenodo.org/record/7951467">https://zenodo.org/record/7951467</a>	Gao et al., 2023i_part2
	<a href="https://doi.org/10.5281/zenodo.7951475">https://doi.org/10.5281/zenodo.7951475</a>	<a href="https://zenodo.org/record/7951475">https://zenodo.org/record/7951475</a>	Gao et al., 2023i_part3
WRF-CMAQ_ARI	<a href="https://doi.org/10.5281/zenodo.7949895">https://doi.org/10.5281/zenodo.7949895</a>	<a href="https://zenodo.org/record/7949895">https://zenodo.org/record/7949895</a>	Gao et al., 2023j_part1
	<a href="https://doi.org/10.5281/zenodo.7950644">https://doi.org/10.5281/zenodo.7950644</a>	<a href="https://zenodo.org/record/7950644">https://zenodo.org/record/7950644</a>	Gao et al., 2023j_part2
	<a href="https://doi.org/10.5281/zenodo.7950830">https://doi.org/10.5281/zenodo.7950830</a>	<a href="https://zenodo.org/record/7950830">https://zenodo.org/record/7950830</a>	Gao et al., 2023j_part3
WRF-Chem_NO	<a href="https://doi.org/10.5281/zenodo.7943804">https://doi.org/10.5281/zenodo.7943804</a>	<a href="https://zenodo.org/record/7943804">https://zenodo.org/record/7943804</a>	Gao et al., 2023k_part1
	<a href="https://doi.org/10.5281/zenodo.7945383">https://doi.org/10.5281/zenodo.7945383</a>	<a href="https://zenodo.org/record/7945383">https://zenodo.org/record/7945383</a>	Gao et al., 2023k_part2
	<a href="https://doi.org/10.5281/zenodo.7946944">https://doi.org/10.5281/zenodo.7946944</a>	<a href="https://zenodo.org/record/7946944">https://zenodo.org/record/7946944</a>	Gao et al., 2023k_part3
WRF-Chem_ARI	<a href="https://doi.org/10.5281/zenodo.7947169">https://doi.org/10.5281/zenodo.7947169</a>	<a href="https://zenodo.org/record/7947169">https://zenodo.org/record/7947169</a>	Gao et al., 2023k_part4
	<a href="https://doi.org/10.5281/zenodo.7947050">https://doi.org/10.5281/zenodo.7947050</a>	<a href="https://zenodo.org/record/7947050">https://zenodo.org/record/7947050</a>	Gao et al., 2023l_part1
	<a href="https://doi.org/10.5281/zenodo.7948216">https://doi.org/10.5281/zenodo.7948216</a>	<a href="https://zenodo.org/record/7948216">https://zenodo.org/record/7948216</a>	Gao et al., 2023l_part2
WRF-Chem_BOTH	<a href="https://doi.org/10.5281/zenodo.7949410">https://doi.org/10.5281/zenodo.7949410</a>	<a href="https://zenodo.org/record/7949410">https://zenodo.org/record/7949410</a>	Gao et al., 2023l_part3
	<a href="https://doi.org/10.5281/zenodo.7949561">https://doi.org/10.5281/zenodo.7949561</a>	<a href="https://zenodo.org/record/7949561">https://zenodo.org/record/7949561</a>	Gao et al., 2023l_part4
	<a href="https://doi.org/10.5281/zenodo.7939221">https://doi.org/10.5281/zenodo.7939221</a>	<a href="https://zenodo.org/record/7939221">https://zenodo.org/record/7939221</a>	Gao et al. 2023m_part1
WRF-CHIMERE_NO	<a href="https://doi.org/10.5281/zenodo.7943002">https://doi.org/10.5281/zenodo.7943002</a>	<a href="https://zenodo.org/record/7943002">https://zenodo.org/record/7943002</a>	Gao et al. 2023m_part2
	<a href="https://doi.org/10.5281/zenodo.7943079">https://doi.org/10.5281/zenodo.7943079</a>	<a href="https://zenodo.org/record/7943079">https://zenodo.org/record/7943079</a>	Gao et al. 2023m_part3
	<a href="https://doi.org/10.5281/zenodo.7943323">https://doi.org/10.5281/zenodo.7943323</a>	<a href="https://zenodo.org/record/7943323">https://zenodo.org/record/7943323</a>	Gao et al. 2023m_part4
WRF-CHIMERE_ARI	<a href="https://doi.org/10.5281/zenodo.7951775">https://doi.org/10.5281/zenodo.7951775</a>	<a href="https://zenodo.org/record/7951775">https://zenodo.org/record/7951775</a>	Gao et al. 2023n_part1
	<a href="https://doi.org/10.5281/zenodo.7951779">https://doi.org/10.5281/zenodo.7951779</a>	<a href="https://zenodo.org/record/7951779">https://zenodo.org/record/7951779</a>	Gao et al. 2023n_part2
	<a href="https://doi.org/10.5281/zenodo.7951791">https://doi.org/10.5281/zenodo.7951791</a>	<a href="https://zenodo.org/record/7951791">https://zenodo.org/record/7951791</a>	Gao et al. 2023n_part3
WRF-CHIMERE_BOTH	<a href="https://doi.org/10.5281/zenodo.7951793">https://doi.org/10.5281/zenodo.7951793</a>	<a href="https://zenodo.org/record/7951793">https://zenodo.org/record/7951793</a>	Gao et al. 2023n_part4
	<a href="https://doi.org/10.5281/zenodo.7952838">https://doi.org/10.5281/zenodo.7952838</a>	<a href="https://zenodo.org/record/7952838">https://zenodo.org/record/7952838</a>	Gao et al. 2023o_part1
	<a href="https://doi.org/10.5281/zenodo.7952840">https://doi.org/10.5281/zenodo.7952840</a>	<a href="https://zenodo.org/record/7952840">https://zenodo.org/record/7952840</a>	Gao et al. 2023o_part2
WRF-CHIMERE_BOTH	<a href="https://doi.org/10.5281/zenodo.7952842">https://doi.org/10.5281/zenodo.7952842</a>	<a href="https://zenodo.org/record/7952842">https://zenodo.org/record/7952842</a>	Gao et al. 2023o_part3
	<a href="https://doi.org/10.5281/zenodo.7952844">https://doi.org/10.5281/zenodo.7952844</a>	<a href="https://zenodo.org/record/7952844">https://zenodo.org/record/7952844</a>	Gao et al. 2023o_part4
	<a href="https://doi.org/10.5281/zenodo.7952859">https://doi.org/10.5281/zenodo.7952859</a>	<a href="https://zenodo.org/record/7952859">https://zenodo.org/record/7952859</a>	Gao et al. 2023p_part1
WRF-CHIMERE_BOTH	<a href="https://doi.org/10.5281/zenodo.7952863">https://doi.org/10.5281/zenodo.7952863</a>	<a href="https://zenodo.org/record/7952863">https://zenodo.org/record/7952863</a>	Gao et al. 2023p_part2
	<a href="https://doi.org/10.5281/zenodo.7952865">https://doi.org/10.5281/zenodo.7952865</a>	<a href="https://zenodo.org/record/7952865">https://zenodo.org/record/7952865</a>	Gao et al. 2023p_part3
	<a href="https://doi.org/10.5281/zenodo.7952867">https://doi.org/10.5281/zenodo.7952867</a>	<a href="https://zenodo.org/record/7952867">https://zenodo.org/record/7952867</a>	Gao et al. 2023p_part4

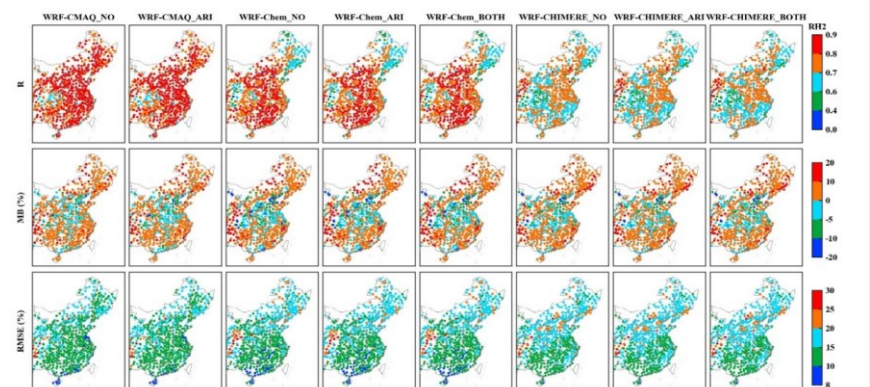




1  
2 Figure S1. Statistical metrics (R, MB and RMSE) between simulated and observed  
3 annual T2 in eastern China.



5  
6 Figure S2. The same as Fig. S1 but for Q2.



8  
9 Figure S3. The same as Fig. S1 but for RH2.

Deleted: s

Formatted: Normal

Formatted: Centered

Formatted: Justified

Formatted: Normal, Left

Formatted: Justified

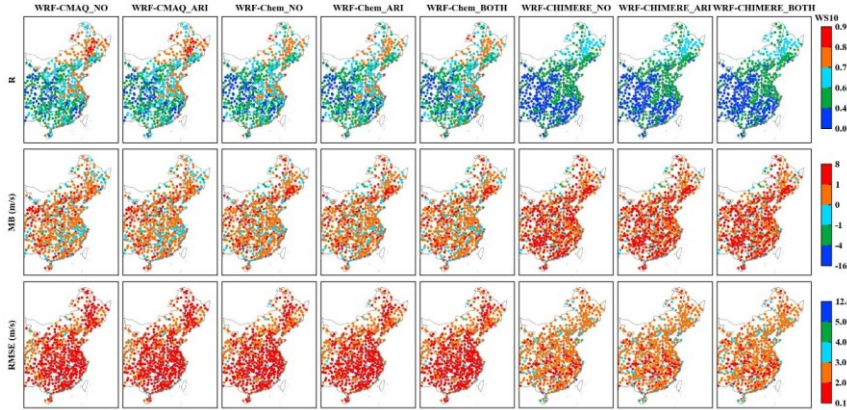


Figure S4. The same as Fig. S1 but for WS10.

Formatted: Justified

Formatted: Normal, Left

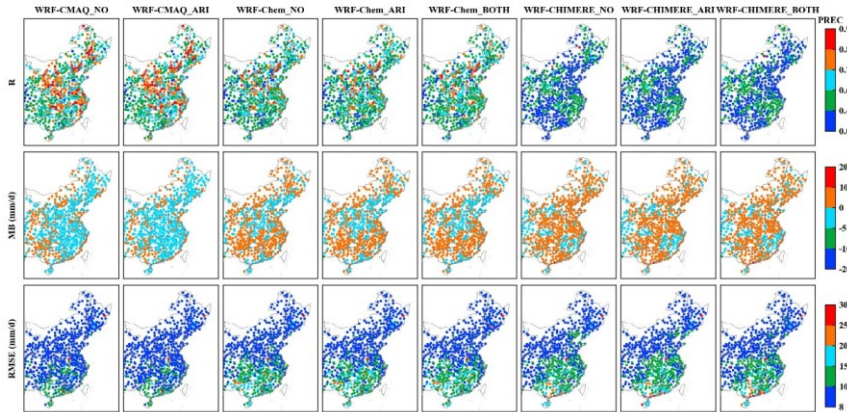


Figure S5. The same as Fig. S1 but for PREC.

Formatted: Justified

Formatted: Normal, Left

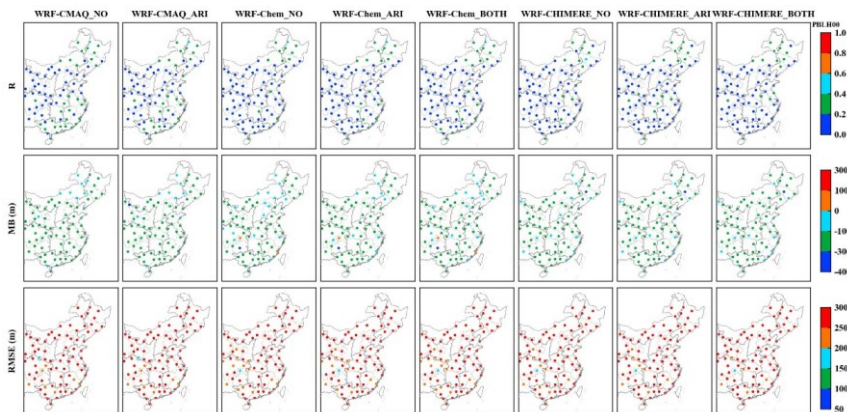


Figure S6. The same as Fig. S1 but for PBLH at 08:00 LT.

Deleted: 00

Formatted: Justified

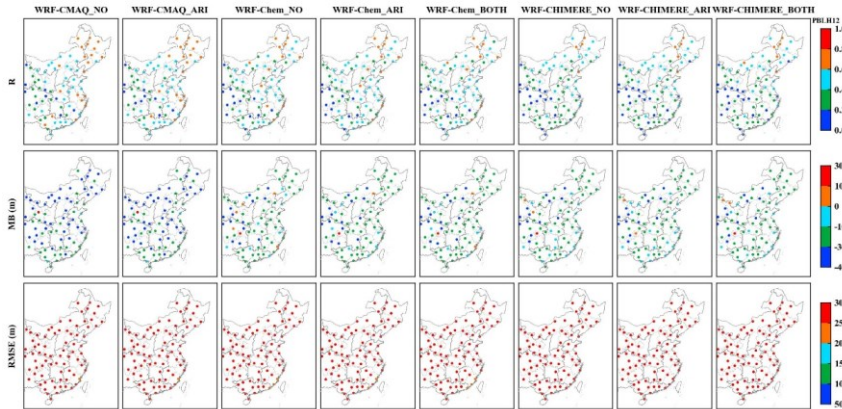


Figure S7. The same as Fig. S1 but for PBLH at 20:00 LT.

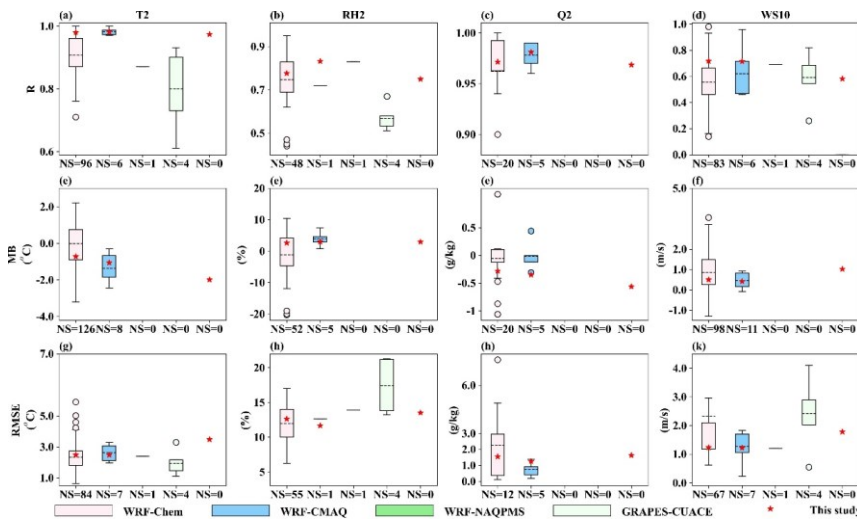


Figure S8. Comparisons of model capacities between our study (red stars) and previous literature (box plots) in terms of the surface T2, RH2, Q2, and WS10 in eastern China. Note that red stars in the fifth column of each subgraph represent the statistical metrics of WRF-CHIMERE in this study.

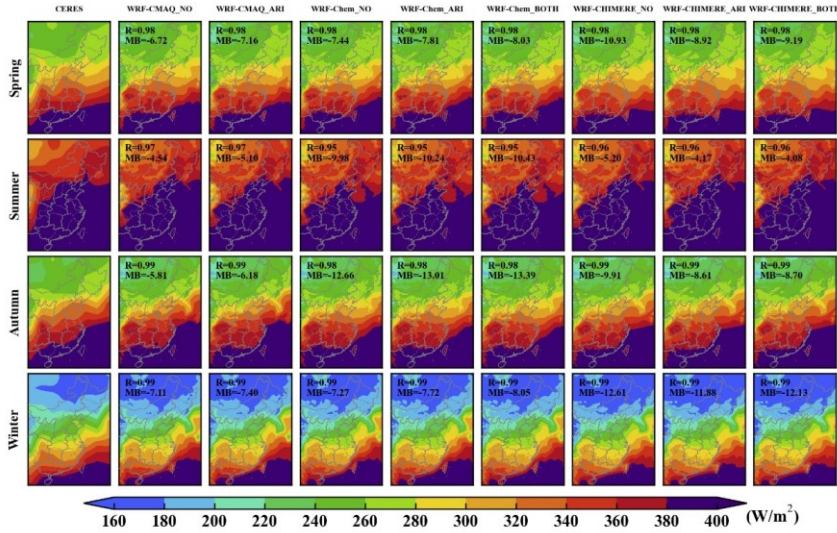
Formatted: Centered

Deleted: 12

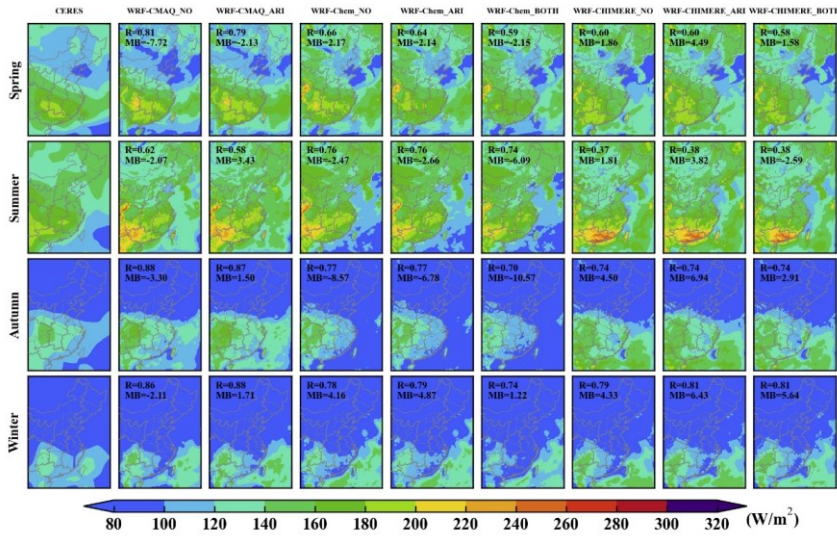
Formatted: Justified

Formatted: Centered





1  
2 Figure S9. Spatial distributions of seasonal SLR between CERES observations and  
3 simulations from WRF-CMAQ, WRF-Chem, and WRF-CHIMERE with and without  
4 aerosol feedbacks in eastern China.  
5



6  
7 Figure S10. The same as Fig. S9 but for SRTOA.  
8

Formatted: Normal

Deleted: TOA shortwave radiation

Formatted: Justified

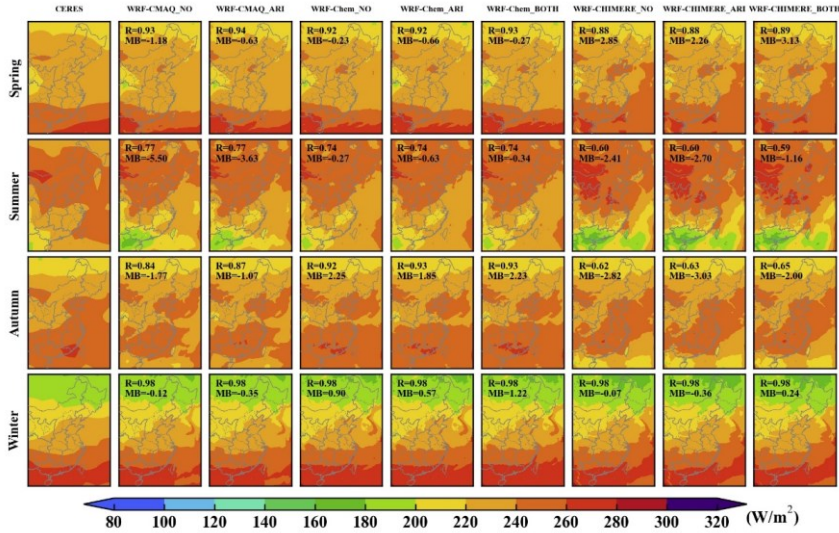


Figure S11. The same as Fig. S9 but for LRTOA.

Deleted: TOA longwave radiation

Formatted: Normal, Left

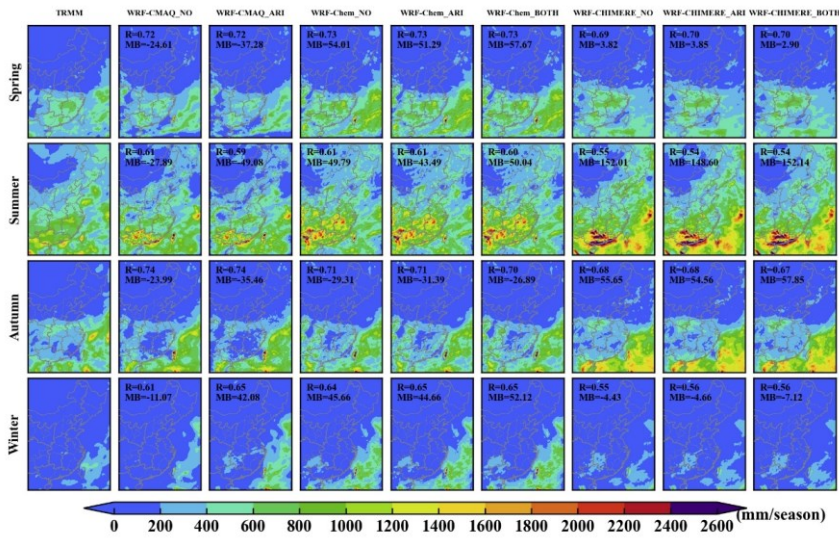


Figure S12. The same as Fig. S9 but for precipitation.

Formatted: Justified



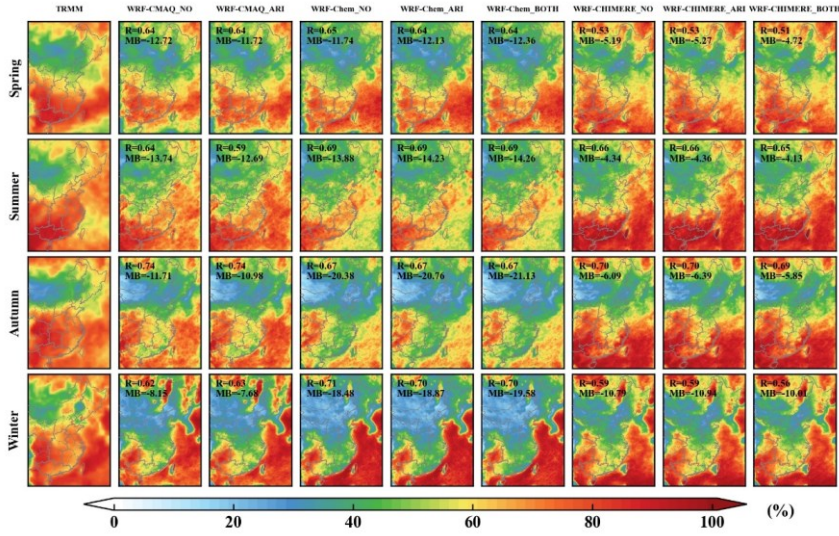


Figure S13. The same as Fig. S9 but for cloud fraction.

Formatted: Normal, Left

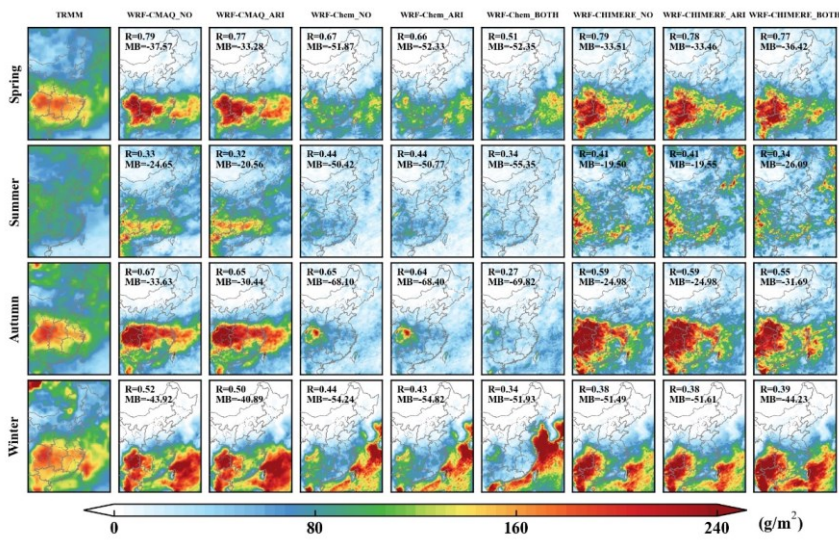
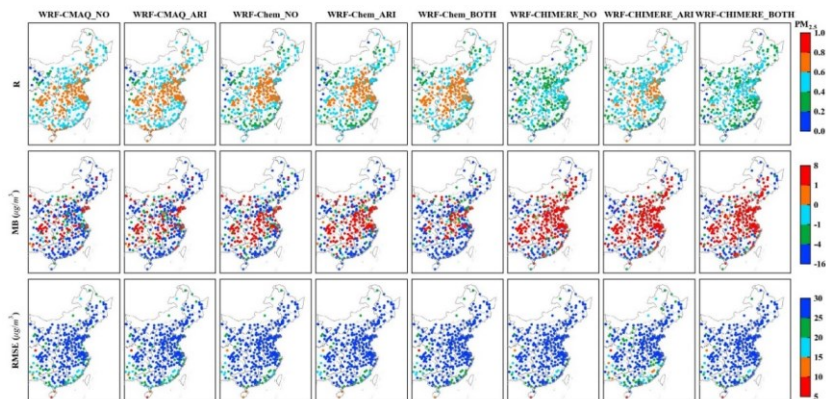


Figure S14. The same as Fig. S9 but for liquid water path.

Formatted: Justified

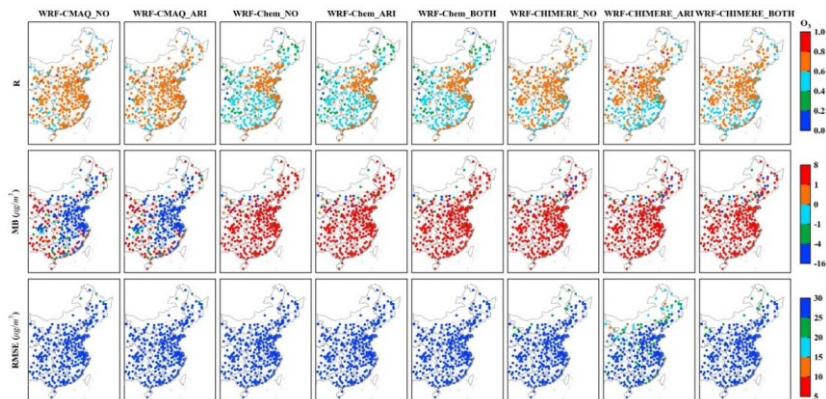




1  
2  
3  
4  
Figure S15. Statistical metrics (R, MB and RMSE) between simulated and observed annual  $PM_{2.5}$  concentrations in eastern China.

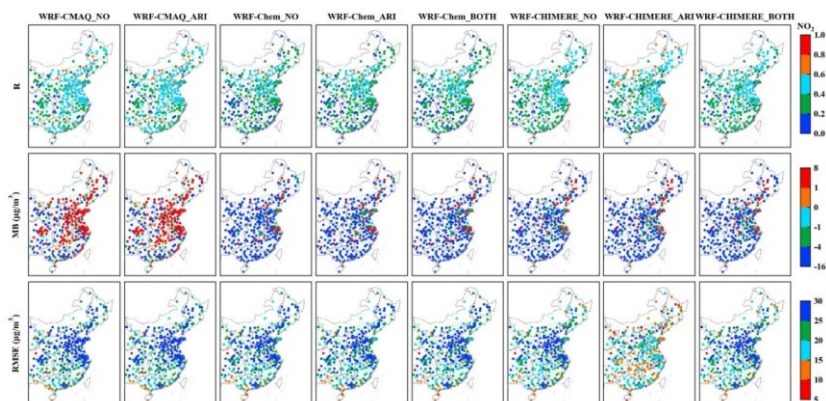
Deleted: s

Formatted: Normal



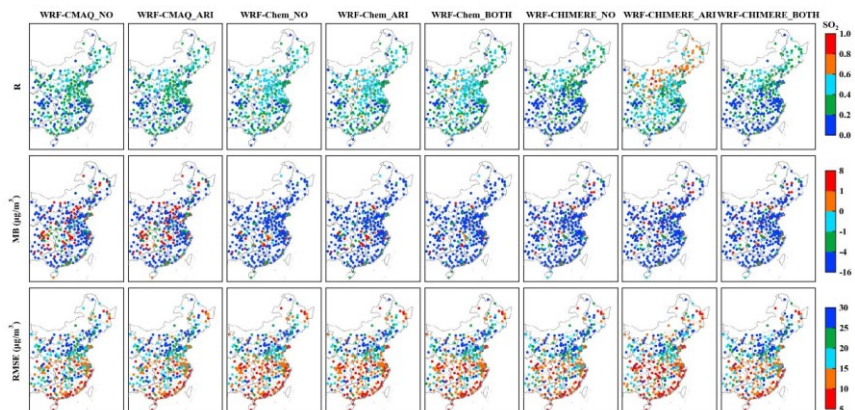
5  
6  
7  
Figure S16. The same as Fig. S15 but for  $O_3$ .

Formatted: Normal, Left



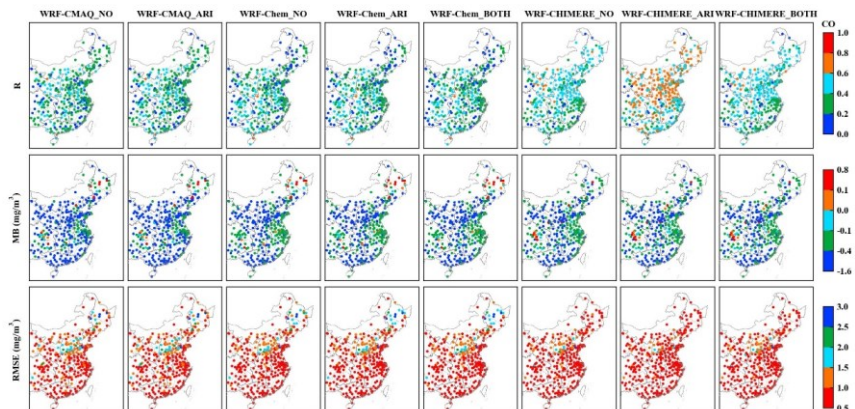
8  
9  
10  
Figure S17. The same as Fig. S15 but for  $NO_2$ .

Formatted: Justified



1  
2  
3 Figure S18. The same as Fig. S15 but for SO<sub>2</sub>.

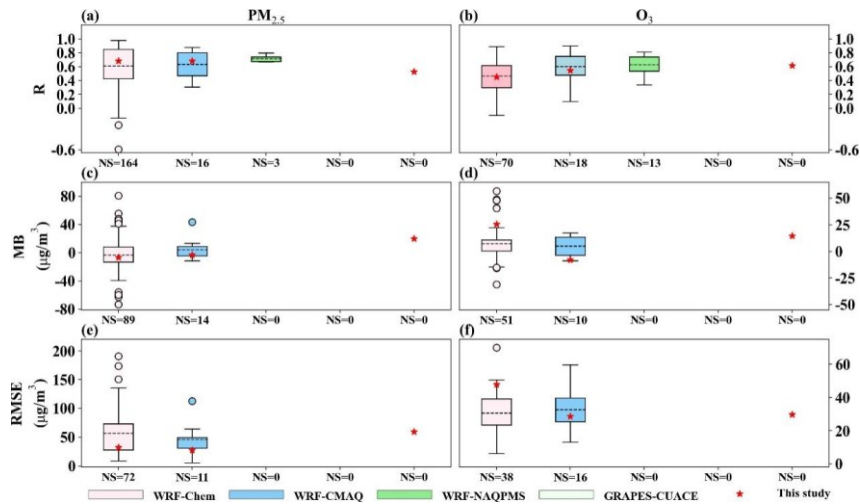
Formatted: Normal, Left



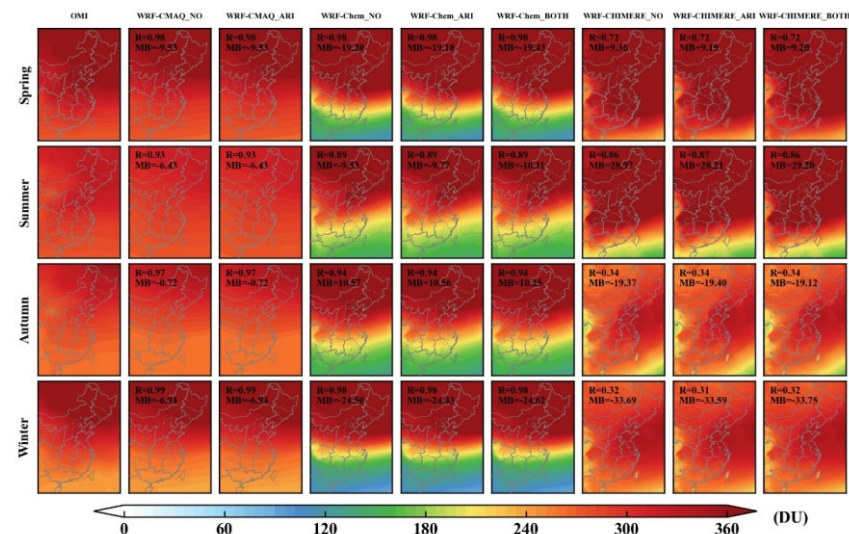
4  
5  
6  
7  
8  
9  
10  
11  
12  
13  
14  
15  
16  
17  
18 Figure S19. The same as Fig. S15 but for CO.

Formatted: Justified

Formatted: Normal, Left



1  
2 Figure S20. Comparisons of model capacities between our study (red stars) and  
3 previous literature (box plots) in terms of surface  $PM_{2.5}$  and  $O_3$  concentrations in eastern  
4 China. Note that red stars in the fifth column of each subgraph represent the statistical  
5 metrics of WRF-CHIMERE in this study.  
6



7  
8 Figure S21. Spatial distributions of seasonal total column ozone between OMI  
9 observations and simulations from WRF-CMAQ, WRF-Chem and WRF-CHIMERE  
10 with and without aerosol feedbacks in eastern China.  
11

Formatted: Centered



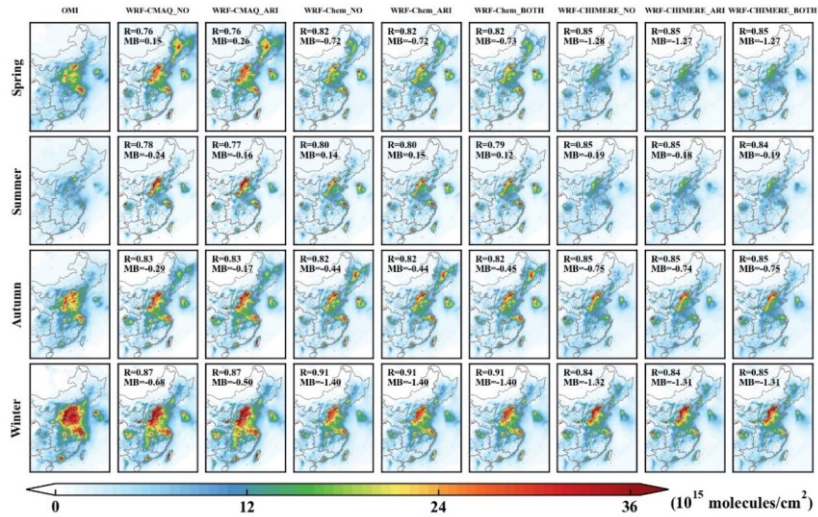


Figure S22. The same as Fig. S21 but for tropospheric NO<sub>2</sub> column.

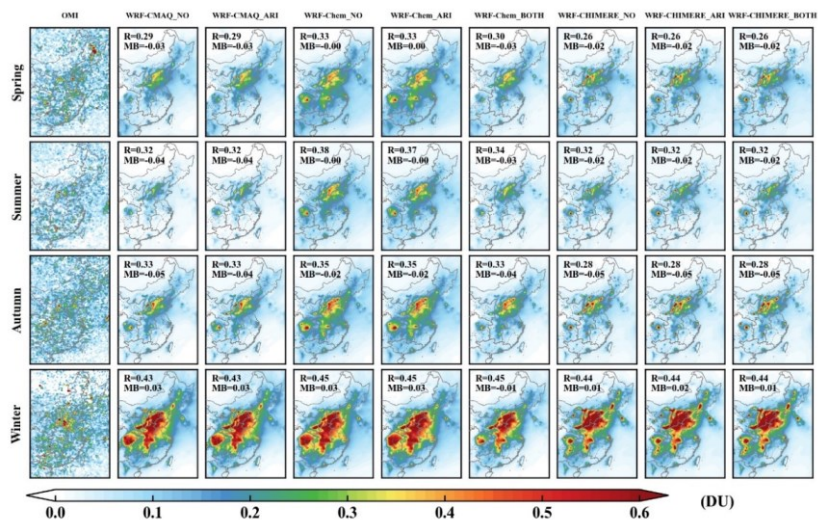


Figure S23. The same as Fig. S21 but for PBL SO<sub>2</sub> column.

Deleted:

Formatted: Justified

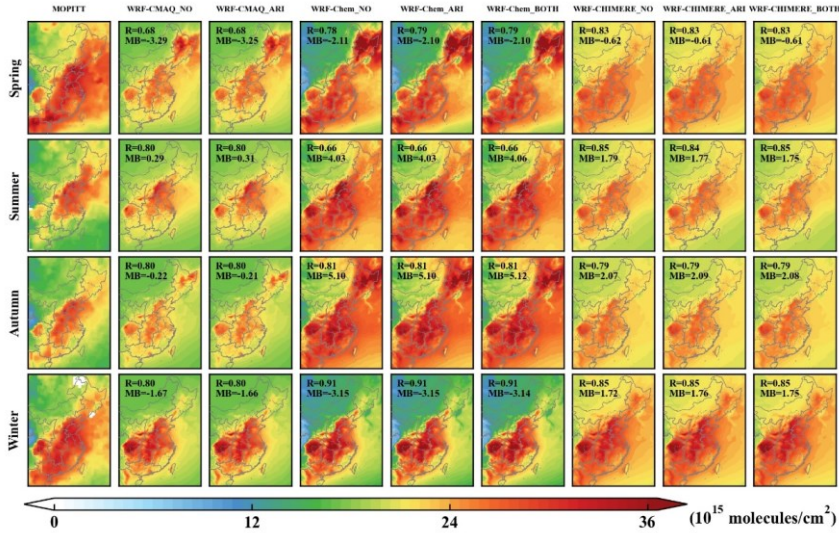


Figure S24. The same as Fig. S21 but for total CO column concentrations.

Formatted: Justified

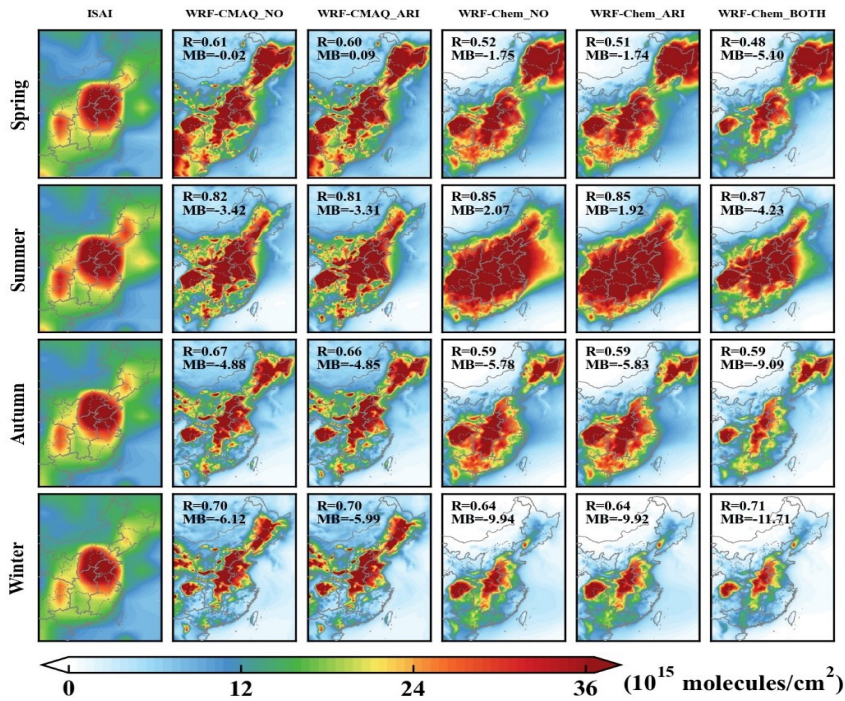


Figure S25. Spatial distributions of seasonal total NH<sub>3</sub> column between MOPITT observations and simulations from WRF-CMAQ and WRF-Chem with and without aerosol feedbacks in eastern China.

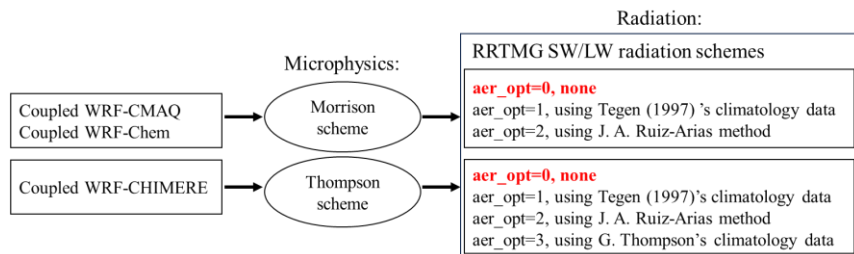


Figure S26. Summary of the selected options of radiation and microphysics schemes in coupled WRF-CMAQ, WRF-Chem and WRF-CHIMERE in this study.

### Reference

- Briant, R., Tuccella, P., Deroubaix, A., Khvorostyanov, D., Menut, L., Mailler, S., and Turquet, S.: *Aerosol-radiation interaction modelling using online coupling between the WRF 3.7.1 meteorological model and the CHIMERE 2016 chemistry-transport model, through the OASIS3-MCT coupler, Geoscientific Model Development*, 10, 927–944, <https://doi.org/10.5194/gmd-10-927-2017>, 2017.
- Brunner, D., Savage, N., Jorba, O., Eder, B., Giordano, L., Badia, A., Balzarini, A., Baro, R., Bianconi, R., and Chemel, C.: *Comparative analysis of meteorological performance of coupled chemistry-meteorology models in the context of AQMEII phase 2, Atmos. Environ.*, 115, 470–498, <https://doi.org/10.1016/j.atmosenv.2014.12.032>, 2015.
- Chao Gao, Xuelei Zhang, Aijun Xiu, Qingqing Tong, Hongmei Zhao, Shichun Zhang, Guangyi Yang, Mengduo Zhang, Shengjin Xie: Simulation results from WRF-CMAQ without aerosol feedbacks in eastern China for January-April 2017, Zenodo [data set], <https://doi.org/10.5281/zenodo.7951404>, 2023i\_part1.
- Chao Gao, Xuelei Zhang, Aijun Xiu, Qingqing Tong, Hongmei Zhao, Shichun Zhang, Guangyi Yang, Mengduo Zhang, Shengjin Xie: Simulation results from WRF-CMAQ without aerosol feedbacks in eastern China for May-August 2017, Zenodo [data set], <https://doi.org/10.5281/zenodo.7951467>, 2023i\_part2.
- Chao Gao, Xuelei Zhang, Aijun Xiu, Qingqing Tong, Hongmei Zhao, Shichun Zhang, Guangyi Yang, Mengduo Zhang, Shengjin Xie: Simulation results from WRF-CMAQ without aerosol feedbacks in eastern China for September-December 2017, Zenodo [data set], <https://doi.org/10.5281/zenodo.7951475>, 2023i\_part3.
- Chao Gao, Xuelei Zhang, Aijun Xiu, Qingqing Tong, Hongmei Zhao, Shichun Zhang, Guangyi Yang, Mengduo Zhang, Shengjin Xie: Simulation results from WRF-CMAQ with enabling aerosol-radiation interactions in eastern China for January-April 2017, Zenodo [data set], <https://doi.org/10.5281/zenodo.7949895>, 2023j\_part1.
- Chao Gao, Xuelei Zhang, Aijun Xiu, Qingqing Tong, Hongmei Zhao, Shichun Zhang, Guangyi Yang, Mengduo Zhang, Shengjin Xie: Simulation results from WRF-CMAQ with enabling aerosol-radiation interactions in eastern China for May-August 2017, Zenodo [data set], <https://doi.org/10.5281/zenodo.7950644>, 2023j\_part2.
- Chao Gao, Xuelei Zhang, Aijun Xiu, Qingqing Tong, Hongmei Zhao, Shichun Zhang, Guangyi Yang, Mengduo Zhang, Shengjin Xie: Simulation results from WRF-CMAQ with enabling aerosol-radiation interactions in eastern China for September-December 2017, Zenodo [data set], <https://doi.org/10.5281/zenodo.7950830>, 2023j\_part3.

Formatted: Indent: Left: 0 cm, Hanging: 2 ch, First line: -2 ch

Deleted: Briant R, Tuccella P, Deroubaix A, et al. Aerosol-radiation interaction modelling using online coupling between the WRF 3.7.1 meteorological model and the CHIMERE 2016 chemistry-transport model, through the OASIS3-MCT coupler[J]. Geoscientific Model Development, 2017, 10(2): 927-944.

Formatted: Font: 小四, Italic, Font color: Auto

Deleted:



- 1 Chao Gao, Xuelei Zhang, Aijun Xiu, Qingqing Tong, Hongmei Zhao, Shichun Zhang,  
2 Guangyi Yang, Mengduo Zhang, Shengjin Xie: Simulation results from WRF-  
3 Chem without aerosol feedbacks in eastern China for January-March 2017,  
4 Zenodo [data set], <https://doi.org/10.5281/zenodo.7943804>, 2023k\_part1.
- 5 Chao Gao, Xuelei Zhang, Aijun Xiu, Qingqing Tong, Hongmei Zhao, Shichun Zhang,  
6 Guangyi Yang, Mengduo Zhang, Shengjin Xie: Simulation results from WRF-  
7 Chem without aerosol feedbacks in eastern China for April-June 2017, Zenodo  
8 [data set], <https://doi.org/10.5281/zenodo.7945383>, 2023k\_part2.
- 9 Chao Gao, Xuelei Zhang, Aijun Xiu, Qingqing Tong, Hongmei Zhao, Shichun Zhang,  
10 Guangyi Yang, Mengduo Zhang, Shengjin Xie: Simulation results from WRF-  
11 Chem without aerosol feedbacks in eastern China for July-September 2017,  
12 Zenodo [data set], <https://doi.org/10.5281/zenodo.7946944>, 2023k\_part3.
- 13 Chao Gao, Xuelei Zhang, Aijun Xiu, Qingqing Tong, Hongmei Zhao, Shichun Zhang,  
14 Guangyi Yang, Mengduo Zhang, Shengjin Xie: Simulation results from WRF-  
15 Chem without aerosol feedbacks in eastern China for October-December 2017,  
16 Zenodo [data set], <https://doi.org/10.5281/zenodo.7947169>, 2023k\_part4.
- 17 Chao Gao, Xuelei Zhang, Aijun Xiu, Qingqing Tong, Hongmei Zhao, Shichun Zhang,  
18 Guangyi Yang, Mengduo Zhang, Shengjin Xie: Simulation results from WRF-  
19 Chem with enabling aerosol-radiation interactions in eastern China for January-  
20 March 2017, Zenodo [data set], <https://doi.org/10.5281/zenodo.7947050>,  
21 2023l\_part1.
- 22 Chao Gao, Xuelei Zhang, Aijun Xiu, Qingqing Tong, Hongmei Zhao, Shichun Zhang,  
23 Guangyi Yang, Mengduo Zhang, Shengjin Xie: Simulation results from WRF-  
24 Chem with enabling aerosol-radiation interactions in eastern China for April-June  
25 2017, Zenodo [data set], <https://doi.org/10.5281/zenodo.7948216>, 2023l\_part2.
- 26 Chao Gao, Xuelei Zhang, Aijun Xiu, Qingqing Tong, Hongmei Zhao, Shichun Zhang,  
27 Guangyi Yang, Mengduo Zhang, Shengjin Xie: Simulation results from WRF-  
28 Chem with enabling aerosol-radiation interactions in eastern China for July-  
29 September 2017, Zenodo [data set], <https://doi.org/10.5281/zenodo.7949410>,  
30 2023l\_part3.
- 31 Chao Gao, Xuelei Zhang, Aijun Xiu, Qingqing Tong, Hongmei Zhao, Shichun Zhang,  
32 Guangyi Yang, Mengduo Zhang, Shengjin Xie: Simulation results from WRF-  
33 Chem with enabling aerosol-radiation interactions in eastern China for October-  
34 December 2017, Zenodo [data set], <https://doi.org/10.5281/zenodo.7949561>,  
35 2023l\_part4.
- 36 Chao Gao, Xuelei Zhang, Aijun Xiu, Qingqing Tong, Hongmei Zhao, Shichun Zhang,  
37 Guangyi Yang, Mengduo Zhang, Shengjin Xie: Simulation results from WRF-  
38 Chem with enabling aerosol-radiation interactions and aerosol-cloud interactions  
39 in eastern China for January-March 2017, Zenodo [data set],  
40 <https://doi.org/10.5281/zenodo.7939221>, 2023m\_part1.
- 41 Chao Gao, Xuelei Zhang, Aijun Xiu, Qingqing Tong, Hongmei Zhao, Shichun Zhang,  
42 Guangyi Yang, Mengduo Zhang, Shengjin Xie: Simulation results from WRF-  
43 Chem with enabling aerosol-radiation interactions and aerosol-cloud interactions  
44 in eastern China for April-June 2017, Zenodo [data set],  
45 <https://doi.org/10.5281/zenodo.7943002>, 2023m\_part2.
- 46 Chao Gao, Xuelei Zhang, Aijun Xiu, Qingqing Tong, Hongmei Zhao, Shichun Zhang,  
47 Guangyi Yang, Mengduo Zhang, Shengjin Xie: Simulation results from WRF-  
48 Chem with enabling aerosol-radiation interactions and aerosol-cloud interactions  
49 in eastern China for July-September 2017, Zenodo [data set],  
50 <https://doi.org/10.5281/zenodo.7943079>, 2023m\_part3.

- 1 Chao Gao, Xuelei Zhang, Aijun Xiu, Qingqing Tong, Hongmei Zhao, Shichun Zhang,  
2 Guangyi Yang, Mengduo Zhang, Shengjin Xie: Simulation results from WRF-  
3 Chem with enabling aerosol-radiation interactions and aerosol-cloud interactions  
4 in eastern China for October-December 2017, Zenodo [data set],  
5 <https://doi.org/10.5281/zenodo.7943323>, 2023m\_part4.
- 6 Chao Gao, Xuelei Zhang, Aijun Xiu, Qingqing Tong, Hongmei Zhao, Shichun Zhang,  
7 Guangyi Yang, Mengduo Zhang, Shengjin Xie: Simulation results from WRF-  
8 CHIMERE without aerosol feedbacks in eastern China for January-March 2017,  
9 Zenodo [data set], <https://doi.org/10.5281/zenodo.7951775>, 2023n\_part1.
- 10 Chao Gao, Xuelei Zhang, Aijun Xiu, Qingqing Tong, Hongmei Zhao, Shichun Zhang,  
11 Guangyi Yang, Mengduo Zhang, Shengjin Xie: Simulation results from WRF-  
12 CHIMERE without aerosol feedbacks in eastern China for April-June 2017,  
13 Zenodo [data set], <https://doi.org/10.5281/zenodo.7951779>, 2023n\_part2.
- 14 Chao Gao, Xuelei Zhang, Aijun Xiu, Qingqing Tong, Hongmei Zhao, Shichun Zhang,  
15 Guangyi Yang, Mengduo Zhang, Shengjin Xie: Simulation results from WRF-  
16 CHIMERE without aerosol feedbacks in eastern China for July-September 2017,  
17 Zenodo [data set], <https://doi.org/10.5281/zenodo.7951791>, 2023n\_part3.
- 18 Chao Gao, Xuelei Zhang, Aijun Xiu, Qingqing Tong, Hongmei Zhao, Shichun Zhang,  
19 Guangyi Yang, Mengduo Zhang, Shengjin Xie: Simulation results from WRF-  
20 CHIMERE without aerosol feedbacks in eastern China for October-December  
21 2017, Zenodo [data set], <https://doi.org/10.5281/zenodo.7951793>, 2023n\_part4.
- 22 Chao Gao, Xuelei Zhang, Aijun Xiu, Qingqing Tong, Hongmei Zhao, Shichun Zhang,  
23 Guangyi Yang, Mengduo Zhang, Shengjin Xie: Simulation results from WRF-  
24 CHIMERE with enabling aerosol-radiation interactions in eastern China for  
25 January-March 2017, Zenodo [data set], <https://doi.org/10.5281/zenodo.7952838>,  
26 2023o\_part1.
- 27 Chao Gao, Xuelei Zhang, Aijun Xiu, Qingqing Tong, Hongmei Zhao, Shichun Zhang,  
28 Guangyi Yang, Mengduo Zhang, Shengjin Xie: Simulation results from WRF-  
29 CHIMERE with enabling aerosol-radiation interactions in eastern China for April-  
30 June 2017, Zenodo [data set], <https://doi.org/10.5281/zenodo.7952840>,  
31 2023o\_part2.
- 32 Chao Gao, Xuelei Zhang, Aijun Xiu, Qingqing Tong, Hongmei Zhao, Shichun Zhang,  
33 Guangyi Yang, Mengduo Zhang, Shengjin Xie: Simulation results from WRF-  
34 CHIMERE with enabling aerosol-radiation interactions in eastern China for July-  
35 September 2017, Zenodo [data set], <https://doi.org/10.5281/zenodo.7952842>,  
36 2023o\_part3.
- 37 Chao Gao, Xuelei Zhang, Aijun Xiu, Qingqing Tong, Hongmei Zhao, Shichun Zhang,  
38 Guangyi Yang, Mengduo Zhang, Shengjin Xie: Simulation results from WRF-  
39 CHIMERE with enabling aerosol-radiation interactions in eastern China for  
40 October-December 2017, Zenodo [data set],  
41 <https://doi.org/10.5281/zenodo.7952844>, 2023o\_part4.
- 42 Chao Gao, Xuelei Zhang, Aijun Xiu, Qingqing Tong, Hongmei Zhao, Shichun Zhang,  
43 Guangyi Yang, Mengduo Zhang, Shengjin Xie: Simulation results from WRF-  
44 CHIMERE with enabling aerosol-radiation interactions and aerosol-cloud  
45 interactions in eastern China for January-March 2017, Zenodo [data set],  
46 <https://doi.org/10.5281/zenodo.7952859>, 2023p\_part1.
- 47 Chao Gao, Xuelei Zhang, Aijun Xiu, Qingqing Tong, Hongmei Zhao, Shichun Zhang,  
48 Guangyi Yang, Mengduo Zhang, Shengjin Xie: Simulation results from WRF-  
49 CHIMERE with enabling aerosol-radiation interactions and aerosol-cloud

1 interactions in eastern China for April-June 2017, Zenodo [data set],  
2 <https://doi.org/10.5281/zenodo.7952863>, 2023p\_part2.

3 Chao Gao, Xuelei Zhang, Aijun Xiu, Qingqing Tong, Hongmei Zhao, Shichun Zhang,  
4 Guangyi Yang, Mengduo Zhang, Shengjin Xie: Simulation results from WRF-  
5 CHIMERE with enabling aerosol-radiation interactions and aerosol-cloud  
6 interactions in eastern China for July-September 2017, Zenodo [data set],  
7 <https://doi.org/10.5281/zenodo.7952865>, 2023p\_part3.

8 Chao Gao, Xuelei Zhang, Aijun Xiu, Qingqing Tong, Hongmei Zhao, Shichun Zhang,  
9 Guangyi Yang, Mengduo Zhang, Shengjin Xie: Simulation results from WRF-  
10 CHIMERE with enabling aerosol-radiation interactions and aerosol-cloud  
11 interactions in eastern China for October-December 2017, Zenodo [data set],  
12 <https://doi.org/10.5281/zenodo.7952867>, 2023p\_part4.

13 *DeMott, P. J., Prenni, A. J., McMeeking, G. R., Sullivan, R. C., Petters, M. D., Tobo,*  
14 *Y., Niemand, M., Möhler, O., Snider, J. R., Wang, Z., and Kreidenweis, S. M.:*  
15 *Integrating laboratory and field data to quantify the immersion freezing ice*  
16 *nucleation activity of mineral dust particles, Atmos. Chem. Phys., 15, 393–409,*  
17 *<https://doi.org/10.5194/acp-15-393-2015>, 2015.*

18 *Fu, Q.: An accurate parameterization of the solar radiative properties of cirrus clouds*  
19 *for climate models, Journal of climate, 9, 2058–2082,*  
20 *[https://doi.org/10.1175/1520-0442\(1996\)009<2058:AAPOTS>2.0.CO;2](https://doi.org/10.1175/1520-0442(1996)009<2058:AAPOTS>2.0.CO;2), 1996.*

21 Gao, M., Han, Z., Liu, Z., Li, M., Xin, J., Tao, Z., Li, J., Kang, J. E., Huang, K., Dong,  
22 X., Zhuang, B., Li, S., Ge, B., Wu, Q., Cheng, Y., Wang, Y., Lee, H. J., Kim, C.  
23 H., Fu, J. S., Wang, T., Chin, M., Woo, J. H., Zhang, Q., Wang, Z., and Carmichael,  
24 G. R.: Air quality and climate change, Topic 3 of the Model Inter-Comparison  
25 Study for Asia Phase III (MICS-Asia III)- Part 1: Overview and model evaluation,  
26 Atmos. Chem. Phys., 18, 4859–4884, <https://doi.org/10.5194/acp-18-4859-2018>,  
27 2018.

28 *Guo, J., Miao, Y., Zhang, Y., Liu, H., Li, Z., Zhang, W., He, J., Lou, M., Yan, Y., and*  
29 *Bian, L.: The climatology of planetary boundary layer height in China derived*  
30 *from radiosonde and reanalysis data, Atmos. Chem. Phys., 16, 13309–13319,*  
31 *<https://doi.org/10.5194/acp-16-13309-2016>, 2016.*

32 *Hu, Y. X. and Stamnes, K.: An accurate parameterization of the radiative properties of*  
33 *water clouds suitable for use in climate models, Journal of climate, 6, 728–742,*  
34 *[https://doi.org/10.1175/1520-0442\(1993\)006<0728:AAPOTR>2.0.CO;2](https://doi.org/10.1175/1520-0442(1993)006<0728:AAPOTR>2.0.CO;2), 1993.*

35 Li, D., Xue, L., Wen, L., Wang, X., Chen, T., Mellouki, A., Chen, J., and Wang, W.:  
36 Characteristics and sources of nitrous acid in an urban atmosphere of northern  
37 China: Results from 1-yr continuous observations, Atmos. Environ., 182, 296–306,  
38 <https://doi.org/10.1016/j.atmosenv.2018.03.033>, 2018.

39 Liu, X.-H., Zhang, Y., Cheng, S.-H., Xing, J., Zhang, Q., Streets, D. G., Jang, C., Wang,  
40 W.-X., and Hao, J.-M.: Understanding of regional air pollution over China using  
41 CMAQ, part I performance evaluation and seasonal variation, Atmos. Environ.,  
42 44, 2415–2426, <https://doi.org/10.1016/j.atmosenv.2010.03.035>, 2010.

43 Liu, Y., Lu, K., Li, X., Dong, H., Tan, Z., Wang, H., Zou, Q., Wu, Y., Zeng, L., and  
44 Hu, M.: A comprehensive model test of the HONO sources constrained to field  
45 measurements at rural North China Plain, Environ. Sci. Technol., 53, 3517–3525,  
46 <https://doi.org/10.1021/acs.est.8b06367>, 2019.

47 Makar, P. A., Gong, W., Milbrandt, J., Hogrefe, C., Zhang, Y., Curci, G., Žabkar, R.,  
48 Im, U., Balzarini, A., Baró, R., Bianconi, R., Cheung, P., Forkel, R., Gravel, S.,  
49 Hirtl, M., Honzak, L., Hou, A., Jiménez-Guerrero, P., Langer, M., Moran, M. D.,  
50 Pabla, B., Pérez, J. L., Pirovano, G., San José, R., Tuccella, P., Werhahn, J., Zhang,

Formatted: Font color: Auto

Deleted: Möhler

Formatted: Font color: Auto

Deleted: Fu Q. An accurate parameterization of the solar radiative properties of cirrus clouds for climate models[J]. Journal of climate, 1996, 9(9): 2058-2082.

Formatted: Font: 小四, Italic, Font color: Auto, Check spelling and grammar

Formatted: Font color: Auto

Deleted: Hu Y X, Stamnes K. An accurate parameterization of the radiative properties of water clouds suitable for use in climate models[J]. Journal of climate, 1993, 6(4): 728-742.

Formatted: Font color: Auto

Deleted:

Formatted: Font color: Auto

J., and Galmarini, S.: Feedbacks between air pollution and weather, Part 1: Effects on weather, *Atmos. Environ.*, 115, 442–469, <https://doi.org/10.1016/j.atmosenv.2014.12.003>, 2015.

*Rasmussen, R. M., Geresdi, I., Thompson, G., Manning, K., and Karplus, E.: Freezing drizzle formation in stably stratified layer clouds: The role of radiative cooling of cloud droplets, cloud condensation nuclei, and ice initiation, Journal of the atmospheric sciences*, 59, 837–860, [https://doi.org/10.1175/1520-0469\(2002\)059<0837:FDFISS>2.0.CO;2](https://doi.org/10.1175/1520-0469(2002)059<0837:FDFISS>2.0.CO;2), 2002.

Spataro, F., Ianniello, A., Esposito, G., Allegrini, I., Zhu, T., and Hu, M.: Occurrence of atmospheric nitrous acid in the urban area of Beijing (China), *Sci. Total Environ.*, 447, 210–224, <https://doi.org/10.1016/j.scitotenv.2012.12.065>, 2013.

*Thompson, G. and Eidhammer, T.: A study of aerosol impacts on clouds and precipitation development in a large winter cyclone, Journal of the atmospheric sciences*, 71, 3636–3658, <https://doi.org/10.1175/JAS-D-13-0305.1>, 2014.

*Tuccella, P., Menut, L., Briant, R., Deroubaix, A., Khvorostyanov, D., Mailler, S., Siour, G., and Turquety, S.: Implementation of Aerosol-Cloud Interaction within WRF-CHIMERE Online Coupled Model: Evaluation and Investigation of the Indirect Radiative Effect from Anthropogenic Emission Reduction on the Benelux Union, Atmosphere*, 10, 20, <https://doi.org/10.3390/atmos10010020>, 2019.

*Wong, D. C., Pleim, J., Mathur, R., Binkowski, F., Otte, T., Gilliam, R., Pouliot, G., Xiu, A., Young, J. O., and Kang, D.: WRF-CMAQ two-way coupled system with aerosol feedback: software development and preliminary results, Geoscientific Model Development*, 5, 299–312, <https://doi.org/10.5194/gmd-5-299-2012>, 2012.

*Xie, B., Fung, J. C. H., Chan, A., and Lau, A.: Evaluation of nonlocal and local planetary boundary layer schemes in the WRF model, J. Geophys. Res. Atmos.*, 117, <https://doi.org/10.1029/2011JD017080>, 2012.

Zhang, S., Sarwar, G., Xing, J., Chu, B., Xue, C., Sarav, A., Ding, D., Zheng, H., Mu, Y., and Duan, F.: Improving the representation of HONO chemistry in CMAQ and examining its impact on haze over China, *Atmos. Chem. Phys.*, 21, 15809–15826, <https://doi.org/10.5194/acp-21-15809-2021>, 2021.

*Zhao, C., Liu, X., Ruby Leung, L., and Hagos, S.: Radiative impact of mineral dust on monsoon precipitation variability over West Africa, Atmospheric Chemistry and Physics*, 11, 1879–1893, <https://doi.org/10.5194/acp-11-1879-2011>, 2011.

**Deleted:** Rasmussen R M, Geresdi I, Thompson G, et al. Freezing drizzle formation in stably stratified layer clouds: The role of radiative cooling of cloud droplets, cloud condensation nuclei, and ice initiation[J]. *Journal of the atmospheric sciences*, 2002, 59(4): 837-860.

**Formatted:** Font color: Auto

**Deleted:** Thompson G, Eidhammer T. A study of aerosol impacts on clouds and precipitation development in a large winter cyclone[J]. *Journal of the atmospheric sciences*, 2014, 71(10): 3636-3658.

**Formatted:** Font color: Auto

**Deleted:** Tuccella P, Menut L, Briant R, et al. Implementation of aerosol-cloud interaction within WRF-CHIMERE online coupled model: evaluation and investigation of the indirect radiative effect from anthropogenic emission reduction on the Benelux Union[J]. *Atmosphere*, 2019, 10(1): 20.

**Formatted:** Font color: Auto

**Deleted:** Wong D C, Pleim J, Mathur R, et al. WRF-CMAQ two-way coupled system with aerosol feedback: software development and preliminary results[J]. *Geoscientific Model Development Discussions*, 2011, 4(3): 2417-2450.

**Formatted:** Font color: Auto

**Formatted:** Font: 小四, Italic, Font color: Auto

**Deleted:**

**Deleted:** Zhao C, Liu X, Ruby Leung L, et al. Radiative impact of mineral dust on monsoon precipitation variability over West Africa[J]. *Atmospheric Chemistry and Physics*, 2011, 11(5): 1879-1893.